GL Garrad Hassan

BLADED MULTIBODY VALIDATION

Document No	1042/BR/01
Issue	B
Status	Final
Classification	Published
Date	22 February 2011

Authors: D Witcher, R Lupton, E Nim, E Bossanyi, J Nichols, Y Sun

Checked by: D Witcher

Approved by: E Bossanyi

Garrad Hassan & Partners Ltd

St Vincent's Works, Silverthorne Lane, Bristol BS2 0QD, UK Tel: +44 (0)117 972 9900, Registered in England 1878456

KEY TO DOCUMENT CLASSIFICATION

Strictly Confidential	:	For disclosure only to named individuals within the Client's organisation.
Private and Confidential	:	For disclosure only to individuals directly concerned with the subject matter of the Report within the Client's organisation.
Commercial in Confidence	:	Not to be disclosed outside the Client's organisation
GH only	:	Not to be disclosed to non GH staff
Client's Discretion	:	Distribution for information only at the discretion of the Client (subject to the above Important Notice and Disclaimer).
Published	:	Available for information only to the general public (subject to the above Important Notice and Disclaimer and Disclaimer).

REVISION HISTORY

Issue	Issue date	Summary
A	29.10.10	Original issue
B	22.02.10	Correction to pitch friction and tower shadow

CONTENTS

1 INTRODUCTION

Version 4.0 of the Bladed software includes a major update to the way in which the structural dynamics are modelled. A multibody formulation has been introduced, replacing the existing structural dynamics model. This has several key advantages:

- The coupling between different structural components is now completely self consistent and formulated at run-time rather than in explicit pre-defined equations, leading to a much more rigorous treatment of the structural dynamics.
- Further development and maintenance of the structural model including the addition of new structural features is now relatively easy.
- Rotor modes have now been replaced by individual blade modes, meaning simulations involving different pitch angles or transitioning from fine to feathered pitch can now be modelled correctly.
- Blade mass, frequency and mode shape can now be specified separately meaning loading due to icing on some but not all blades can now be analysed correctly.
- Blades now have six degrees of freedom, meaning blade torsion can now be modelled correctly and axial and shear stiffness can be included if desired.

In order to gain confidence with the new structural model, several different types of testing and validation have been carried out, a summary of which is presented in this document. These include comparison against hand calculations for simple features, comparison against known results, comparison against the previous version of Bladed for both individual structural features and complete load sets with full wind turbine models, comparison against other wind turbine simulation codes, comparison against ANSYS models and comparison against measured data.

The theory for the new multibody structural dynamics has been documented in the Bladed Theory manual [1].

2 SIMPLE COMPARISONS AGAINST KNOWN RESULTS

This section presents comparison against hand calculations and simulations carried out using existing Bladed for which the set up was simple enough for the results to be known, either in terms of the absolute values of various outputs or in terms of the expected dynamic behaviour or pattern of results. For all of the tests in this section the four combinations of an upwind/downwind turbine and clockwise/anticlockwise rotor direction were tested. For clarity in the examples below, when these four cases are the same, only the clockwise upwind case is shown.

In this section, the term "Old Bladed" refers to the pre-Multibody version of Bladed, which is used as a reference (where appropriate) in these tests. The new, Multibody, version of Bladed is referred to as "MB Bladed".

2.1 Blade

Mass axis

A series of tests with a simple blade with mass offset compared against hand calculations: on a uniform cylindrical blade, the centre of mass is moved along & perpendicular to the chord. With the blade fixed vertically upwards, this can be seen in the blade root bending moments, in this case for movement along the chord.

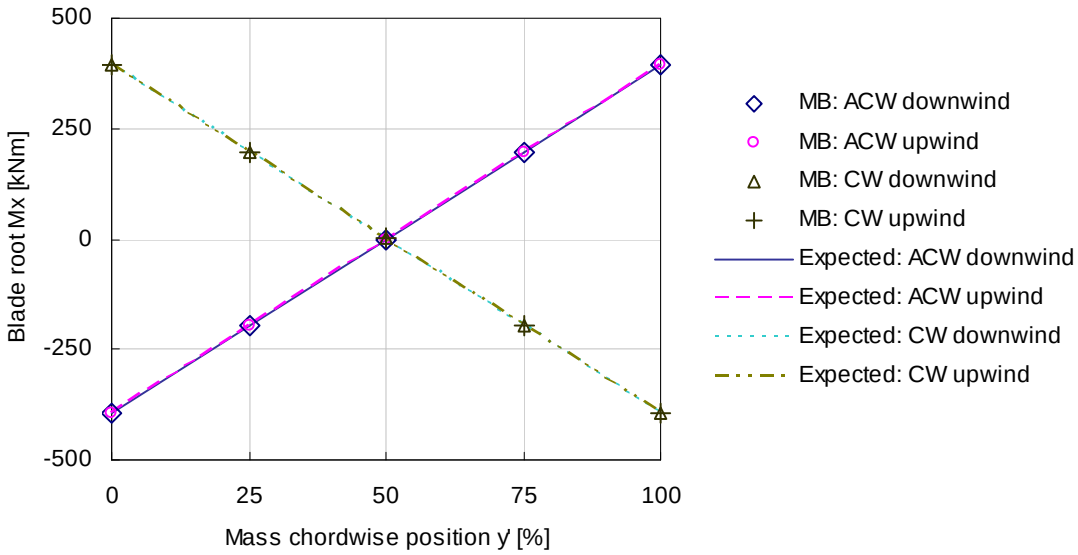

The effect on loading of the blade mass was tested by pitching the blade and looking at the blade root shear force, shown below:

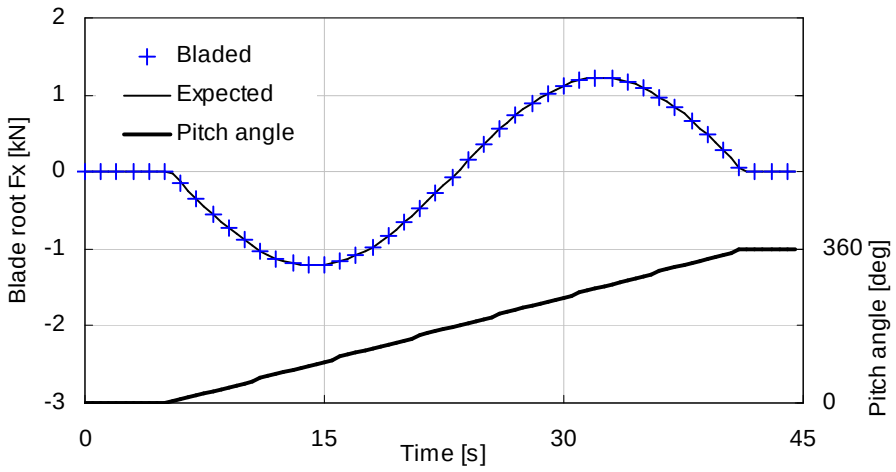

Neutral axis

The blade loads are output on the neutral axis. This was tested in a similar manner to the mass axis location, by parking the blade vertically and checking the blade root bending moments as the neutral axis was moved through the blade.

Point masses

Both rotating and parked blades with point masses at various locations were compared against both old Bladed and hand calculations.

Here a cylindrical uniform blade is rotating at constant rotor speed. A point mass is present at radius r = R/4, and the combined centrifugal force of the point mass and distributed blade mass is correct:

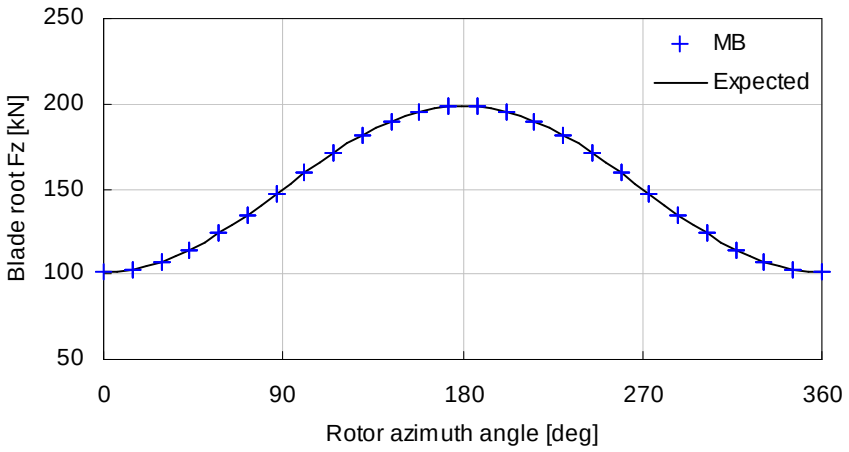

In a similar manner to checking the distributed mass, the loads due to different point mass locations in the blade cross-section were also checked.

Pre-bent blade

A parked case with wind loading (drag) only was run to check deflections, with the wind speed increasing up to a steady value. There are slight differences between the two versions of Bladed, probably due to the improved modal representation in MB Bladed, but the overall behaviour is similar.

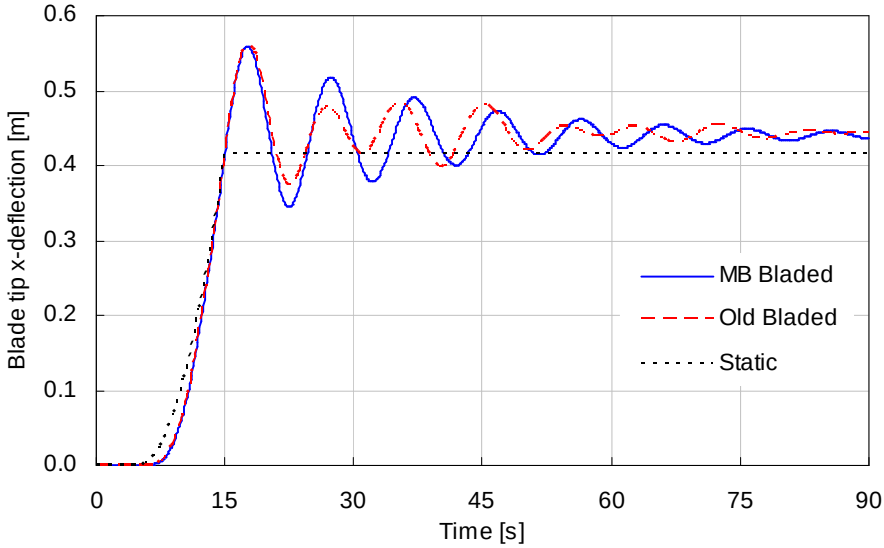

A rotating case with no wind loading or gravity was run to check centrifugal loads and deflections.

Mounting angles: precone and sweep

Pre-cone is the mounting angle of the blade in the out-of-plane direction. This was tested by looking at the blade root My of a vertically parked blade, due to gravity, for various pre-cone angles. The graph below shows differences between MB and Old Bladed; this is due to a change in the modelling of pre-cone.

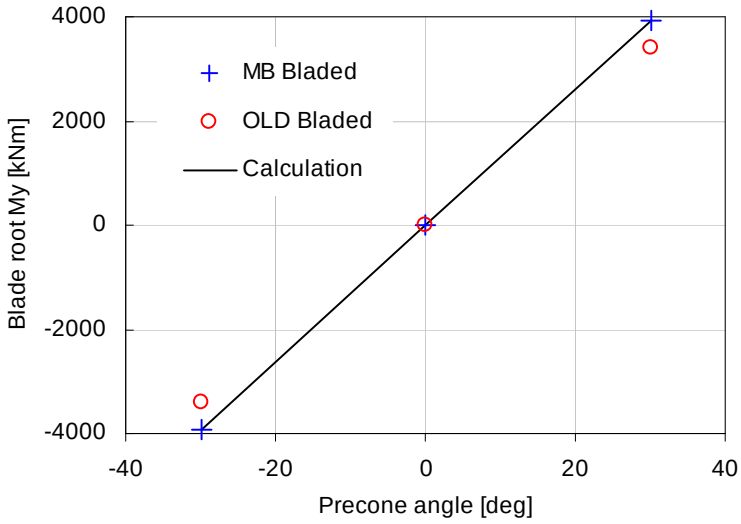

Sweep angle was tested in a similar way. Here is shown the blade root flapwise bending moment for two different sweep angles, as the wind drag loading increases. This demonstrates a minor issue with old Bladed, whereby the second-order effect of sweep angle on flapwise bending moment was not taken into account.

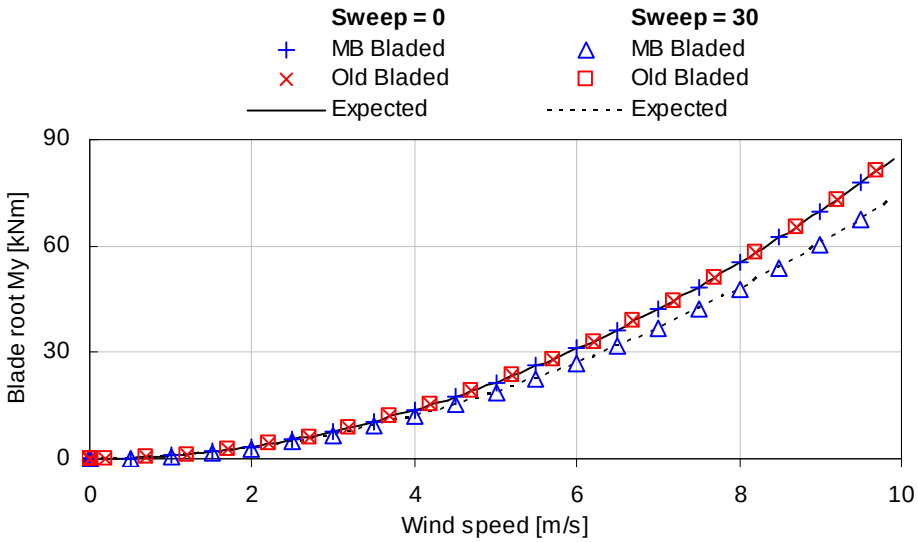

Axial stiffness

With the blade parked vertically, the blade tip extension due to gravity against uniform axial stiffness is checked:

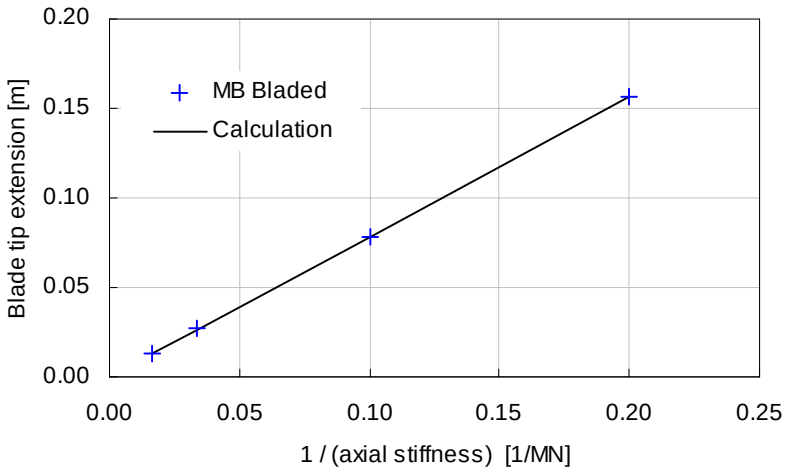

Old Bladed did not allow this effect to be modelled at all.

Encrypted blade

Bladed offers the possibility to encrypt the blade data. An encrypted blade was compared against results from old Bladed to make sure the interpretation of the encrypted data was correct.

Aerodynamic Loads

Comparisons were made with old Bladed of aerodynamic loading along the blade, and blade root total loading, for a real blade in the parked case.

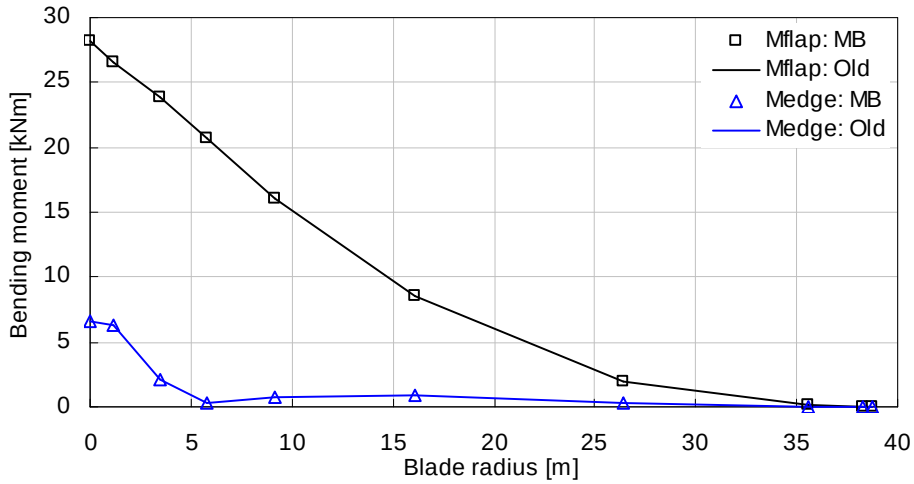

The loads were also compared for a rotor rotating at fixed speed in steady wind.

Deflection

It was confirmed that the blade deflections and absolute positions are in global coordinates, and do not vary as a uniform symmetric blade was twisted and pitched in steady wind.

Pitch bearing located outboard of blade root

A parked simulation with pitching was carried out. Blade forces on the inboard section of the blade, at the pitch bearing and on the outboard section of the blade were checked. The angle of attack was compared against old Bladed at all three locations.

2.2 Rotor

Tilt

A simulation with the rotor parked under gravity and drag loading was carried out, and the loads at the blade root and at the yaw bearing were checked.

Cone

A simulation with constant rotor speed, with and without cone, was carried out. Only the load due to gravity was considered here. The blade root thrust force is shown below (for cone = 10deg).

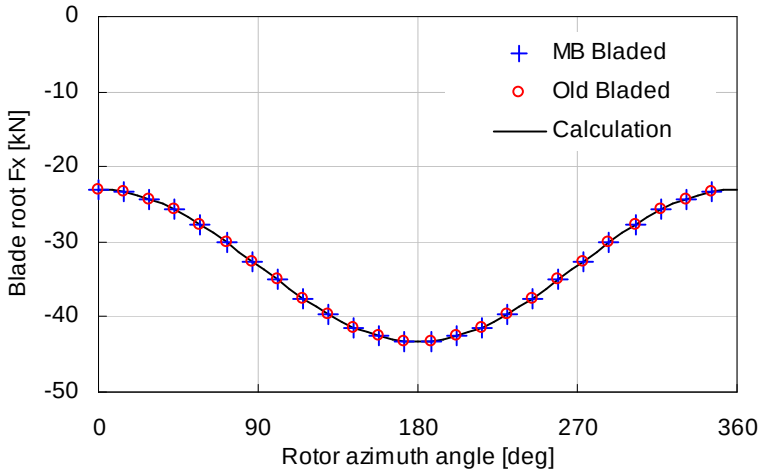

Overhang

The influence of overhang on the yaw bearing loads due to gravity was checked.

Lateral offset

The gravity loading at the yaw bearing was checked, for different lateral offset positions.

Hub mass

The effect of the hub mass location on gravitational and inertial contributions to the hub loads was checked. Similarly, the effect of a rotor mass imbalance was checked. For example, here the hub torque is plotted for three imbalance cases: imbalance lying on the axis, and at 1m radius at an azimuth angle of 0 and 70deg (the CW results are shown here; ACW torques will have the opposite sense).

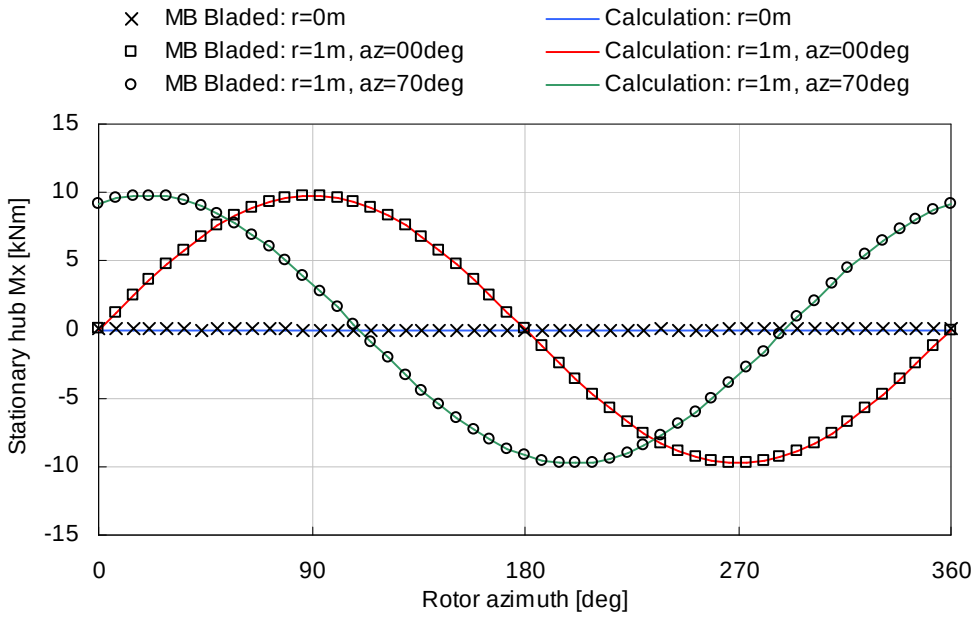

Set angle

The effect of set angle and set angle error on the output coordinates and blade angle of attack was tested, both for a parked and for a rotating rotor. For example, here the flapwise shear force due to drag on a parked blade is shown, for each blade, when a set angle error is applied to each blade in turn. It can be seen that the force drops by the appropriate amount.

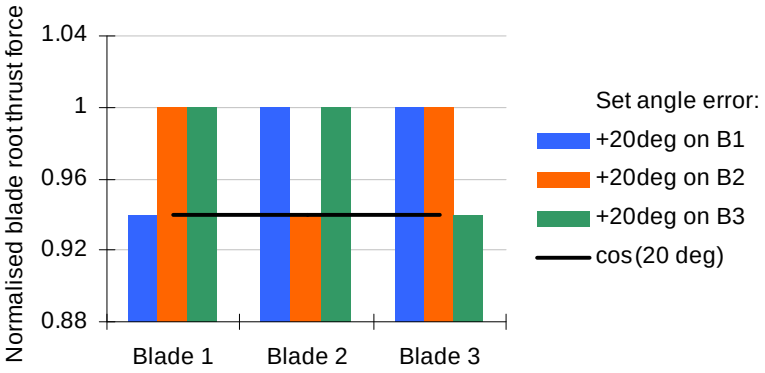

Azimthal blade imbalance

The azimuthal blade mounting imbalance was checked by looking at the blade tip position of each blade when an azimuthal imbalance was applied.

Teeter

Teeter movement was tested by rotating the blade through a sheared wind field. The movement was much slower than the teeter natural frequency, so in this case the quasi-static behaviour was tested.

Pitch-teeter coupling (PTC) was tested on a parked rotor subject to wind drag (again, non-uniform due to wind shear). The static movement of the blade tip is shown here for different δ_3 angles:

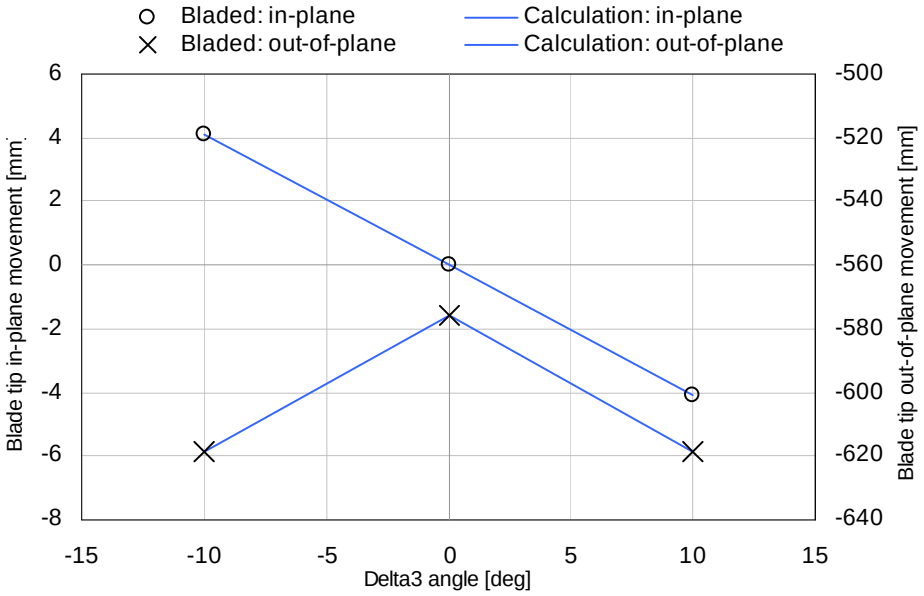

The teeter behaviour without a restraint present was also checked, including the stabilising effects of rotor rotation.

The behaviour when the teeter hinge is offset upwind or downwind from the rotor centre was tested for a parked rotor subject to gravity loading (a positive teeter offset places the hinge downwind of the rotor centre; a positive teeter restraint torque acts to push the top of the rotor upwind).

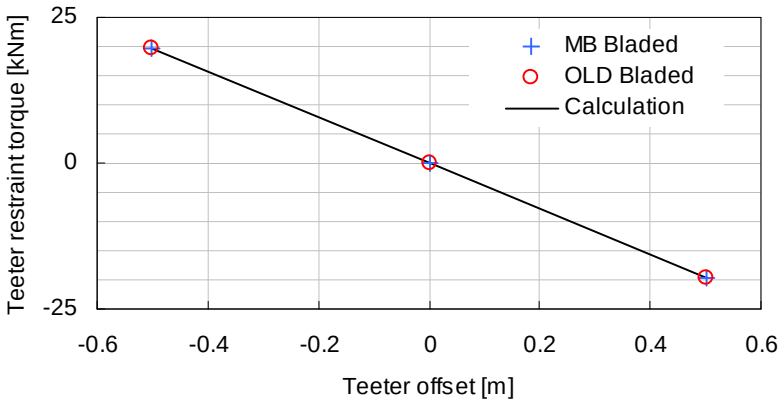

One-bladed rotors

The effect of a counterweight was checked for a 1-bladed rotor.

Teeter was also checked in a simple situation.

2.3 Nacelle

Nacelle mass

The change in yaw bearing loads when the nacelle mass was turned on and off was checked.

Nacelle drag

The yaw bearing loads due to nacelle drag were checked, using a rotor with zero drag coefficient, for a range of wind directions.

Yaw dynamics

The geometry of yawing motion was checked, for example by examining the angle of attack on a vertical blade as the nacelle yaws:

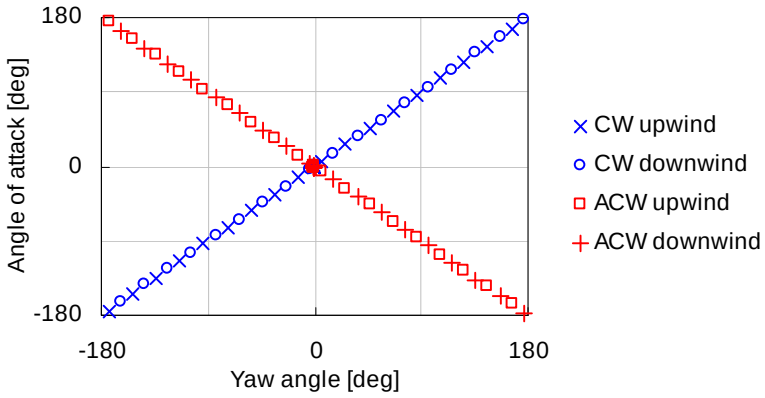

The behaviour with the yaw bearing represented by a spring and damper was tested by applying a step change in yaw moment.

In the “rigid” configuration, an applied yawing moment is resisted by friction until the limiting friction is reached, then the yaw actuator supplies the required remaining resisting moment:

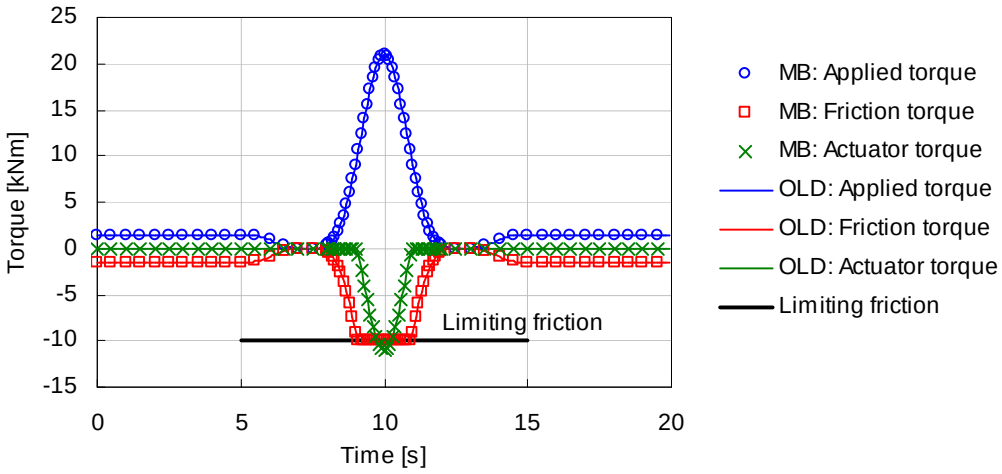

The next possibility for the yaw model is a “flexible” configuration. This includes both friction and stiction, and possibly a spring between the actuator position and the yaw bearing position.

This graph demonstrates the friction & stiction when the yaw bearing slips due to an applied yawing moment (which increases and then decreases over the simulation). The bearing initially sticks, then slips for a time before returning to rest.

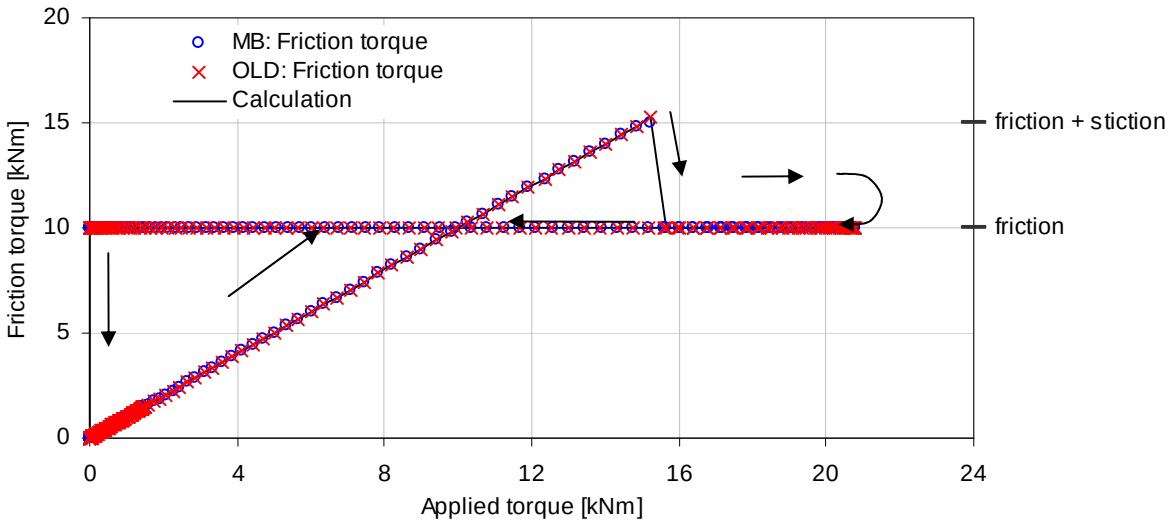

The next test added a yaw actuator, connected via a spring to the yaw bearing. Here the actuator is yawing at constant angular velocity, and the yaw bearing stick-slips.

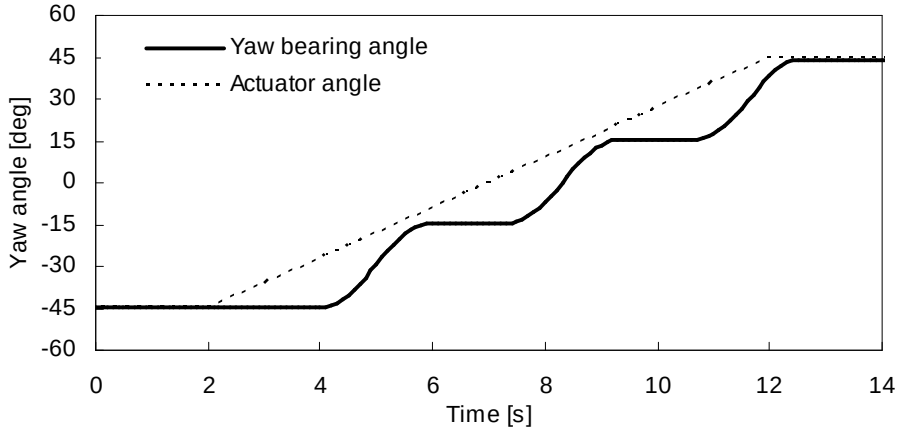

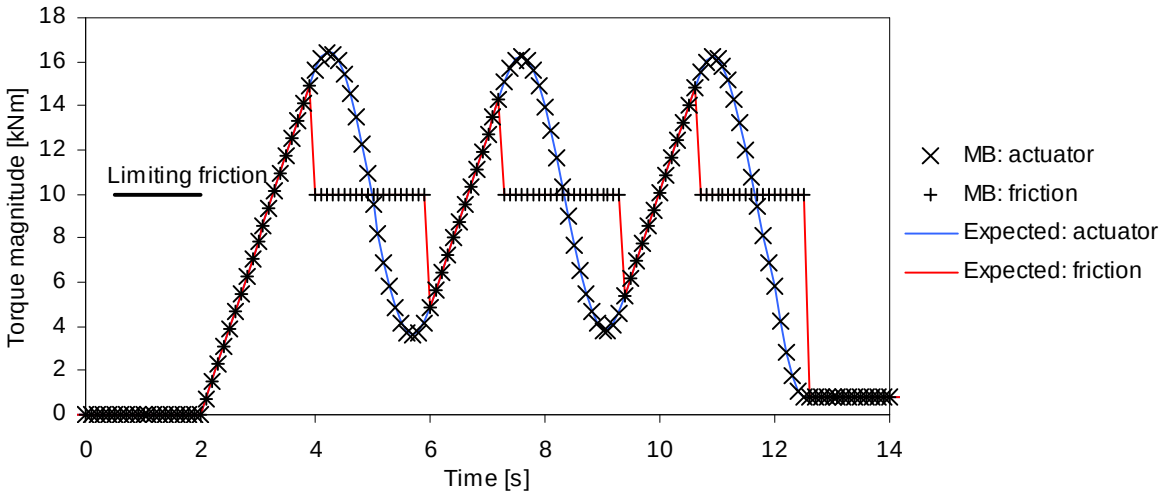

General yaw bearing loads

A few tests checked the consistency of loads at the rotor and nacelle with the loads at the yaw bearing. The yaw bearing loads resulting from various rotor loads for different tilts were checked. Also, it was confirmed that when the yaw bearing rotates, the yaw bearing loads are aligned with the nacelle, while the tower top loads do not rotate.

2.4 Drive train

Coordinate systems

It was confirmed that drive train outputs are measured with positive in the direction of normal rotation – i.e. the relationship between drive train outputs and global coordinates is opposite for CW and ACW rotors.

LSS flexibility

The low-speed shaft (LSS) flexibility was tested by applying a brake to the generator side of the LSS, and increasing the rotor torque while observing the rotor rotation. The LSS motion is damped, and the motion is correct.

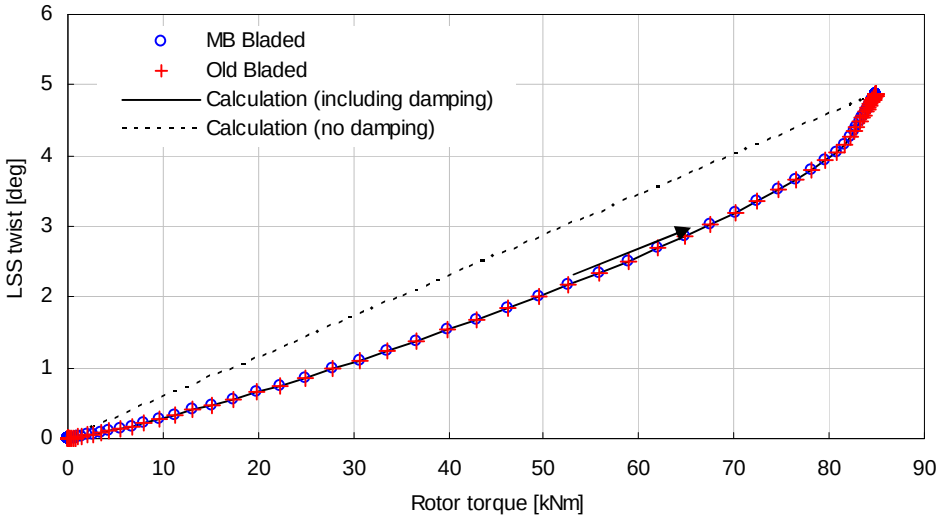

HSS flexibility

The HSS flexibility was tested in a similar manner to the LSS flexibility. The brake was not applied, so only the generator inertia resisted the applied rotor torque.

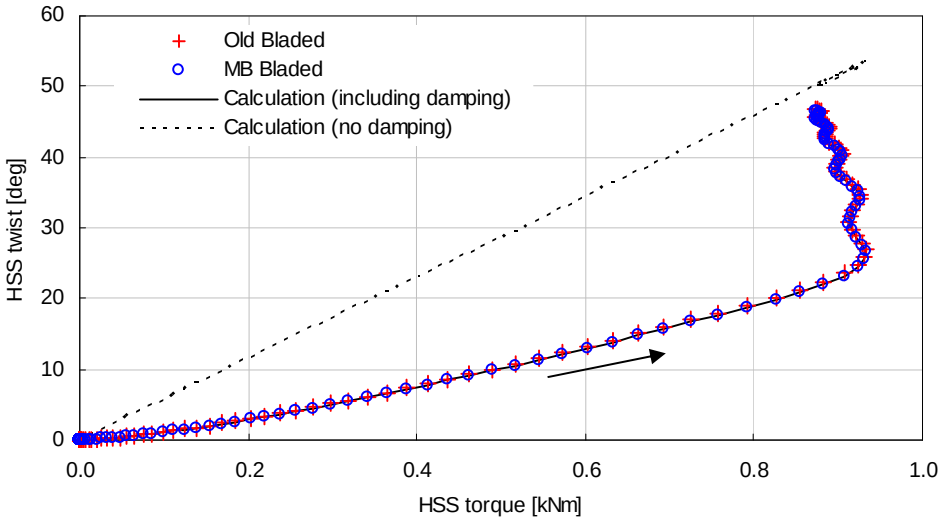

Drive train mounting

Here the drive train and rotor was locked by engaging a brake on the low speed shaft, and a step change in rotor torque was applied. The whole drive train was mounted on a stiffness and damping, and the resulting loads and motion checked.

Note that in this case, the "expected" loads shown below are calculated based on other MB Bladed outputs, as the situation is too complicated to calculate from first principles. The "spring torque" load is calculated from the drive train deflection angle and velocity based on the output stiffness and damping. The "mounting loading" is calculated based on the output hub torque, accounting for drive train inertias. In effect these two loads are calculated from opposite ends of the drive train, so it is a good check that they agree.

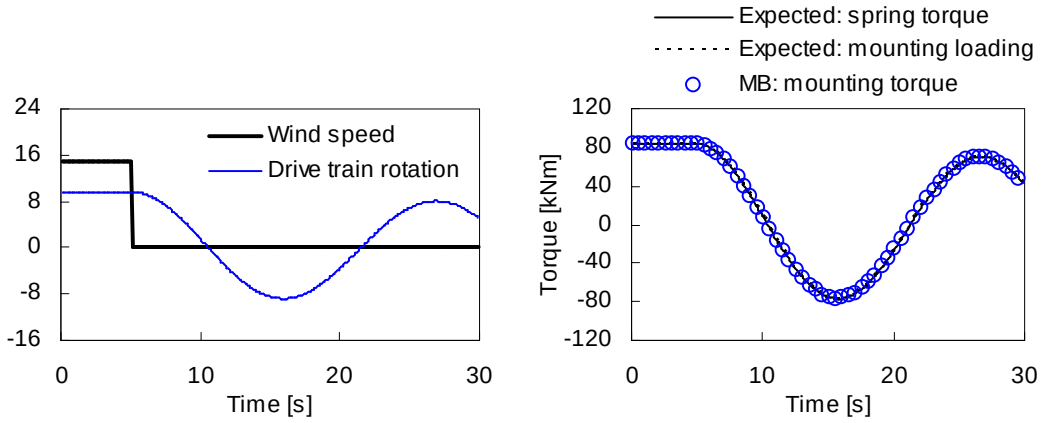

Gearbox mounting

The gearbox mounting degree of freedom was checked in a similar way to the drive train mounting. In Multibody Bladed, the drive train brake is attached to the gearbox, above the gearbox mounting, while in existing old Bladed, the brake is attached to the main frame below the gearbox mounting. Therefore, the results could not be compared between the two Bladed versions with the brake applied. An alternative test used a very large generator inertia instead of a brake.

Brakes

Firstly the stick-slip behaviour of the brakes was tested, with the brakes constantly engaged and a variable rotor torque. This was checked on both the low- and high-speed shafts. For example, the graph below shows the brake slipping on the low-speed shaft, once the hub torque reaches 20 kNm. While the brake is slipping, the brake reaction torque remains at 20 kNm, while the hub torque also includes the inertial torque associated with the generator inertia starting to move. Once the brake comes to rest, the torques fall back to the applied value.

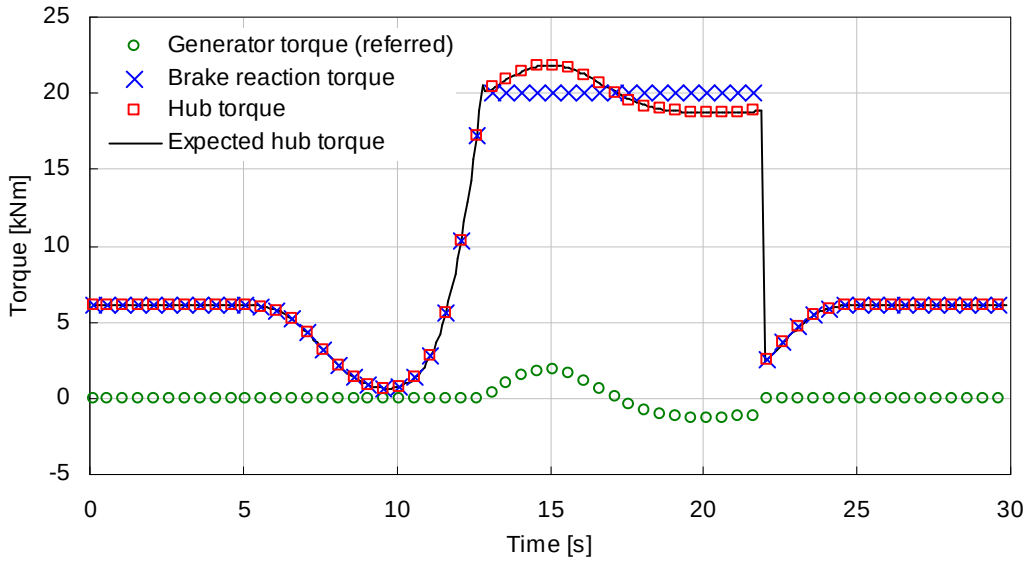

The behaviour during a stop was also tested, again for the LSS and HSS. This test was repeated for 3 simulation types: parked, idling and power production.

Up to 3 different brakes may be defined; the braking torques produced when each brake in turn is applied were checked.

Slipping clutch

To test the slipping clutch in the HSS, the generator inertia was made very large so that it is effectively fixed. A gust increases the rotor loading enough for the clutch to slip for some time. Inertial loads are visible. Static clutch friction is 400Nm, while the dynamic friction is 300Nm.

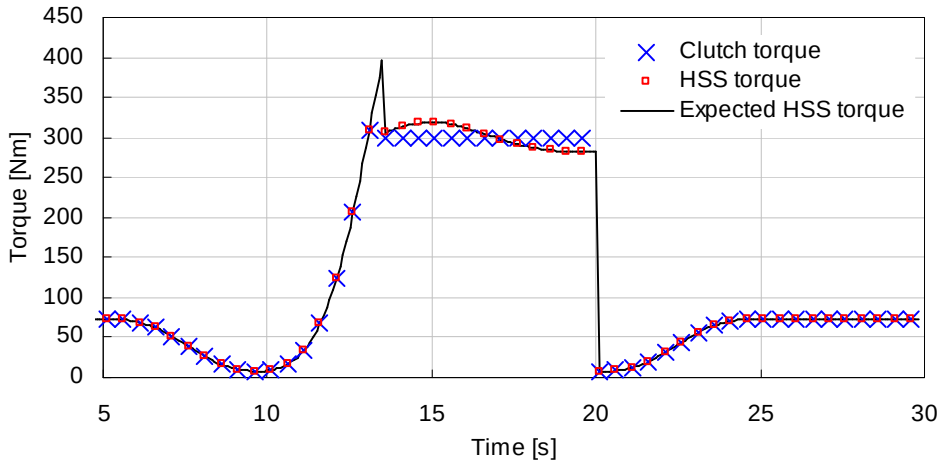

Losses

The mechanical losses, specified by a lookup table, were checked. Four combinations were considered: with the losses applied on the low- or high-speed shaft, and with the losses defined as torques or powers. For example, the results for a loss torque on the LSS are shown below:

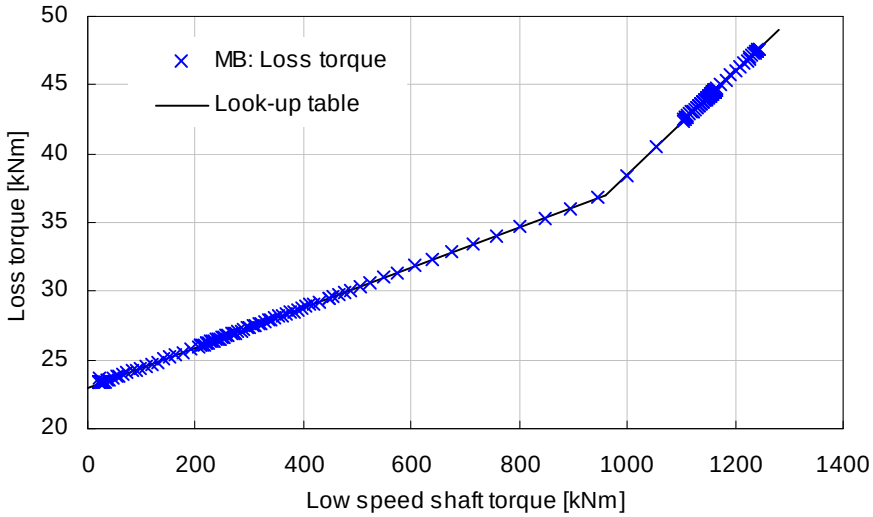

Here is the case for a loss defined in terms of power, again on the LSS:

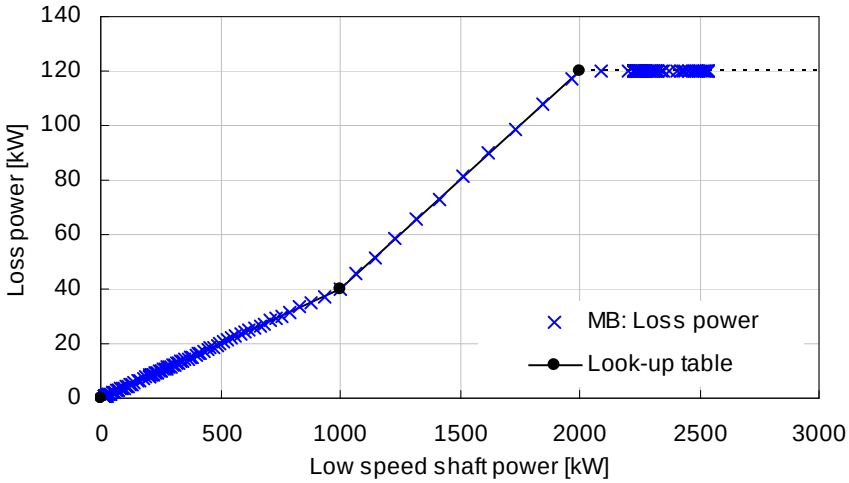

Electrical losses can be defined as a linear relationship, or by a lookup table, as shown below:

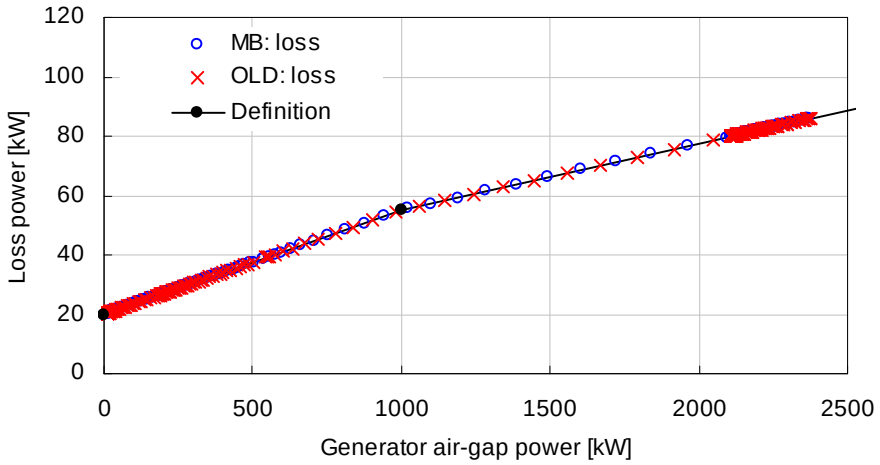

2.5 Tower: monopile

Aerodynamic loading

A very basic test checked the load distribution in the tower due to applied rotor loads.

The tower load distribution due to drag on the tower itself was checked:

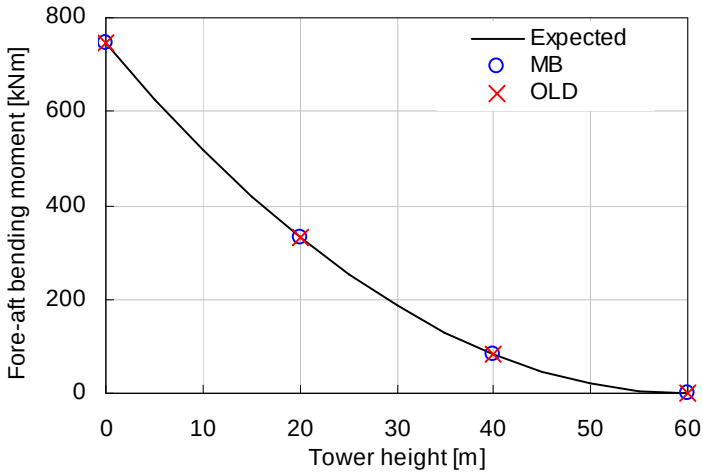

Point masses

Another test looked at the loads in the tower due to point masses, in an analogous manner to testing point masses in the blade.

Foundations

Testing on the simple monopile foundation models were carried out. Here are the results for a translational foundation, with steady loading at a range of levels:

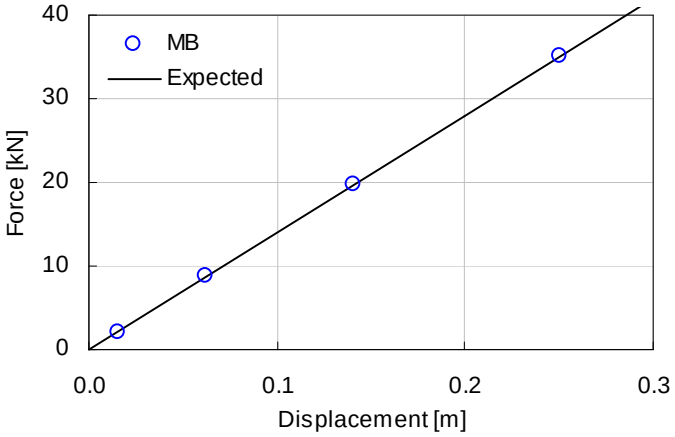

Here is the equivalent plot for a linear rotational foundation:

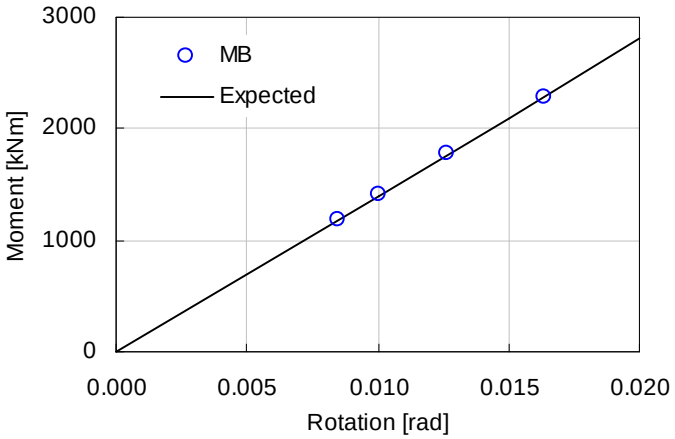

2.6 Tower: multi-member

Hydrodynamic drag

Water velocities and tower loads due to uniform currents were checked. This shows a bug in old Bladed in the calculation of hydrodynamic forces on partially-submerged tower members.

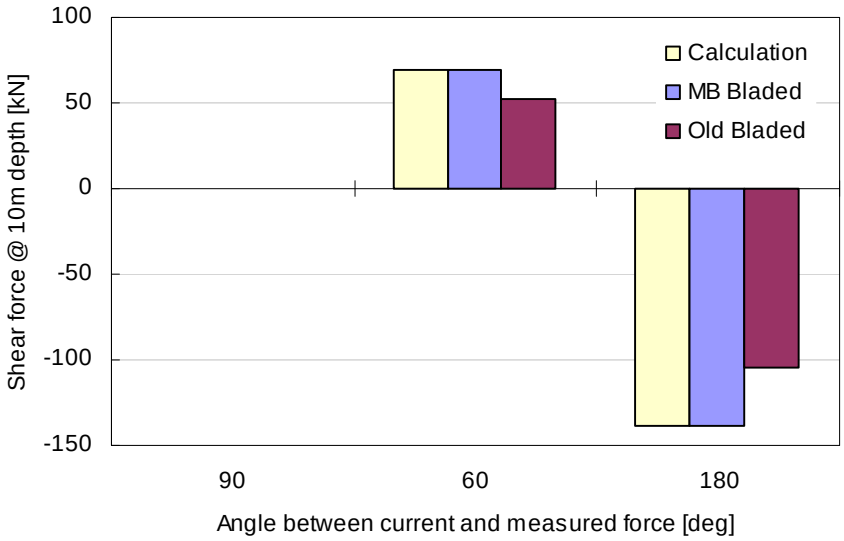

Point masses

Point masses were tested in a similar manner to the monopile tower.

Tower vibration damper

Tests including tower vibration dampers were carried out.

Foundations

Testing on linear and non-linear foundation models were carried out.

2.7 Pitch system

Pitch angle error

The change in angle of attack, and in blade loads in local coordinates, was checked when applying a pitch angle error (imbalance) to each of 3 blades in turn. It was confirmed that the pitch angle error affects the part of the blade outboard of the pitch bearing, but not the part inboard.

Pitch control

The relationship between demanded and measured pitch angle was checked by applying a step change in demand, for the following configurations:

- position-/rate-demand,

- 1st-/2nd-order.

Pitching inertia

Bladed calculates and outputs the blade pitching inertia, which depends on blade properties and geometry. The inertia due to the following factors was checked:

- distributed blade inertia
- extra blade pitching inertia (blade screen)
- blade deflection
- an offset mass axis
- prebend
- precone
- sweep
- cone

It was also checked that the inertia has the same effect on each blade.

The inertial loads during a pitching movement were also checked.

Pitch bearing friction

The pitch bearing friction model includes the variation in friction with axial loads, radial loads and bending moments. These relationships were tested. The MB Bladed results differ from the Old Bladed results due to a change in the assumption of the effect of a reversing of the axial force on the friction.

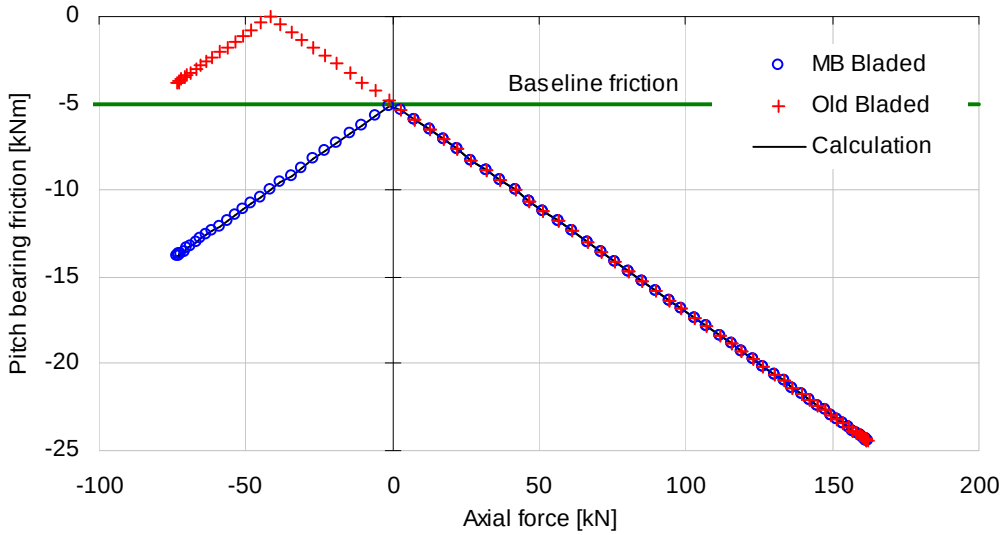

Pitch actuator

The pitch actuator gear ratio and gearbox efficiency were tested by applying an external pitching moment to the blade, and checking the actuator torque.

The inertia of the pitch actuator was also tested by observing the various torques during a change in pitch rate.

2.8 Environment

Tide height

The tide height was tested by setting up a simulation with a uniform current loading the tower. The change in loading as the tide height was varied was checked.

Wind

The wind direction was checked for consistency against the angle of attack of a parked blade, the output yaw misalignment, and the resultant angle of drag on the tower.

The turbulent wind output was checked; the results are slightly different between MB Bladed and Old Bladed due to the point on the structure at which the time series is output. MB Bladed outputs at the hub centre, whereas Old Bladed output at the hub height on the tower centre line.

The tower shadow models were checked at a radius of 2m, at all yaw angles around a tower of radius 1m. The relative wind speed is shown below for the 3 available tower shadow models:

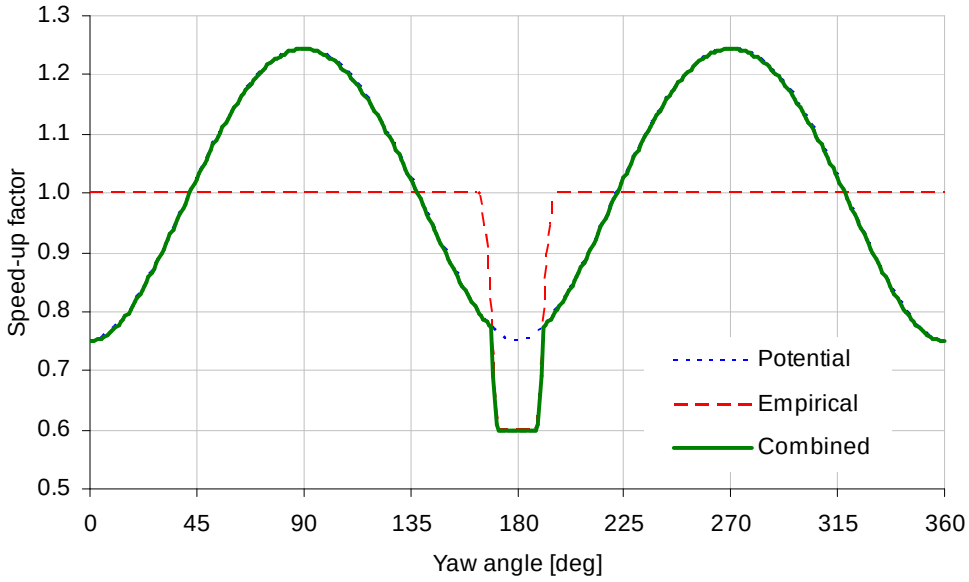

2.9 Faults

The behaviour when the various fault conditions are enabled is checked in the tests described in this section.

Yaw fault

A test on the constant rate yaw fault showed similar results between Old and MB versions.

2.10 Simulation type

The general function of the different simulation types, both the steady calculations, and the dynamic simulations representing particular situations (normal stop, idling etc) was tested by the tests in this section.

Steady operational loads

Comparisons were carried out for:

- fixed speed & pitch
- variable speed & pitch

Steady parked loads

Comparisons were carried out varying: azimuth, yaw, pitch, wind inclination.

Stops

Comparisons of normal and emergency stops were carried out.

3 COMPARISON AGAINST ANSYS

3.1 Methods and tools

The functional test is carried out by running a number of test cases using the Multibody framework of Bladed, and the results are then compared to the corresponding results from a similar structural model elaborated by the general purpose FEM package ANSYS (Vers. 10.0). All ANSYS structural models are defined using the tapered Timoshenko beam element called BEAM44 that is almost identical to the beam element derived for use in the Multibody framework. One exception is, however, that the BEAM44 element does not allow a specification of the cross-section centre of mass, which is an important parameter of the beam model applied in the Multibody framework.

The functional test of the modal frame components is carried out using a test stub for the Multibody framework, while the more elaborated test with a compound structure is carried out using the new Bladed Multibody.

3.2 Description of the Data for the test examples

The functional test of the modal frame is performed using a typical 3 bladed multi-megawatt upwind turbine. The tests were performed with a separate blade fixed at the root as well as with a complete wind turbine structure. In addition a number of relatively simple test cases were initially performed in order to ensure correct input for the ANSYS model.

The local blade coordinate system is defined according the definition used by Bladed, i.e. origin at the root, the *Z*-axis in the longitudinal direction coinciding with the pitch axis and the *Y*-axis perpendicular to the *Z*-axis and parallel to the chord for cross-section with zero twist.

The ratio of the cross-section is taken as the square root of the ratio of the flapwise stiffness to the edgewise stiffness in order to take into account that ANSYS assumes homogeneous material for this element.

3.3 Description of the test cases

Test case 1. A beam modelled by separate prismatic beam elements

This set of test cases is mainly defined in order to calibrate the methods, which is done by testing that an ANSYS structural model and a similar structural model in the Bladed Multibody Framework model give identical results in a set of elementary test cases.

As indicated in Figure 3.1 the structure used for the test case consists of a blade like cantilever beam that is fixed at the left end (root) and free at the right end (tip). The beam is pre-curved at the middle with a transversal offset characterised by the geometrical parameters *a* and *b*. Four prismatic and straight elements (1-4) are used, and the properties are assumed. In case that includes shear deformations, the edgewise and flapwise shear constant is taken is 0.5 and 0.5 times the relative profile thickness, respectively.

The beam is described in a global coordinate system XYZ with the *X*-axis pointing in the longitudinal direction as indicated Figure 3.1. The beam elements are described in local coordinate systems xyz, where the *x*-axis is the elastic beam axis (centroid). In all cases it is assumed that the element *z*-axis is parallel to the global XZ-plane.

Gravity is generally neglected in this case.

The test case generally assumes that external forces are applied in the initial configuration of the beam, which means that second order effects of the external loads are neglected. Geometric stiffening (stress stiffening) is considered only if explicitly specified.

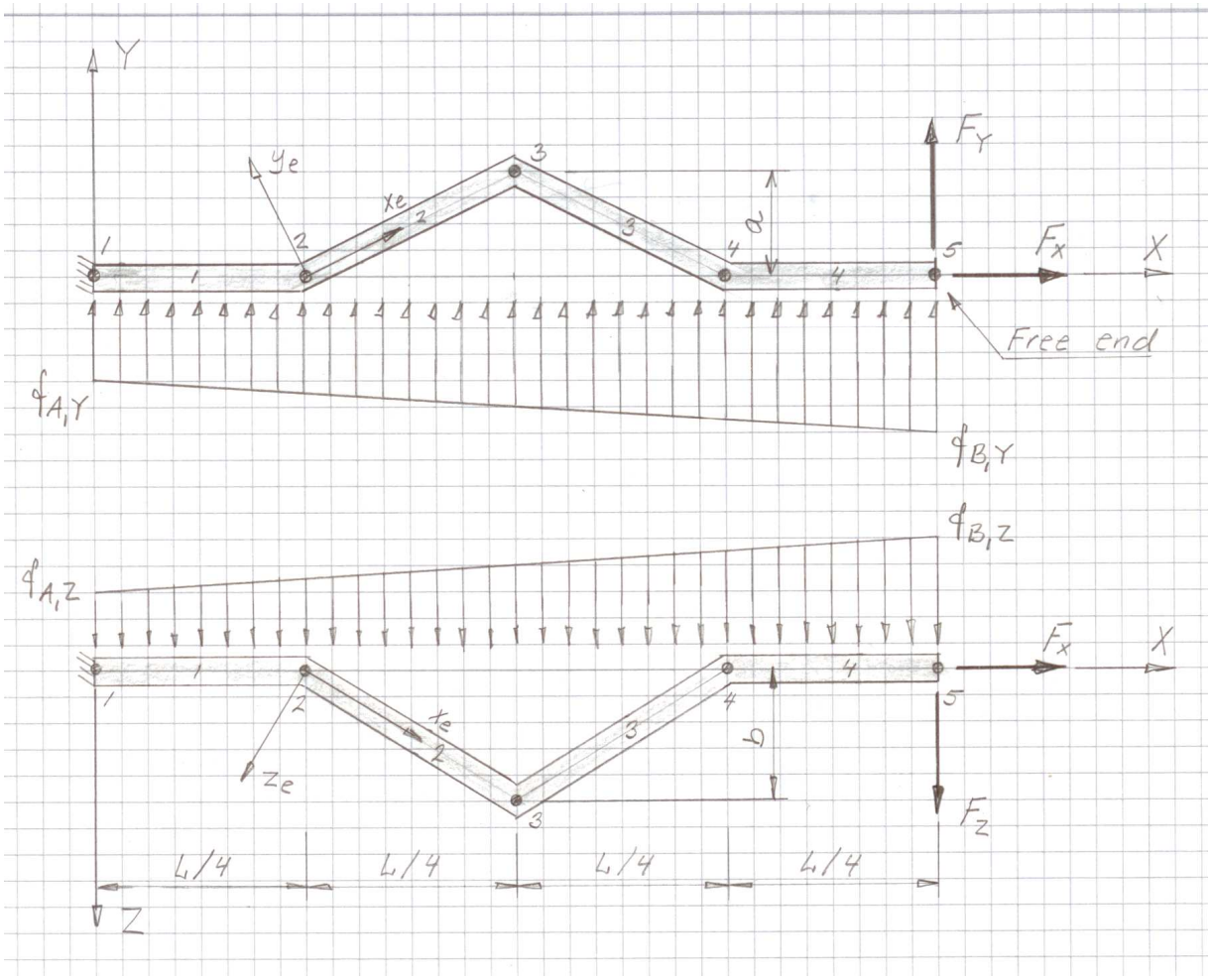

Figure 3.1: Basic geometry of test case 1

Test case 1 consists of the following sub-cases:

a) $a = b = 0$. Shear deformation neglected. A distributed load in the global *Y* direction having an intensity of 2 kN/m at the fixed end and 3 kN/m at the free end.
b) $a = 1.0$, $b = 2.0$. Shear deformation neglected. A distributed load in the global *Y* direction having an intensity of 2 kN/m at the fixed end and 3 kN/m at the free end, together with a distributed load in the global *Z* direction having an intensity of 2 kN/m at the fixed end and 1 kN/m at the free end.
c) Similar to a), but with the two elements closest to the free end rotated 30 deg around the element *x*-axis.
d) Similar to a), but with shear deformations included.
e) Similar to d), but with an offset of the shear centre.
f) $a = b = 0$. Shear deformation included. Stress stiffening included. A concentrated axial load of 1 MN at the free end together with a distributed load in the global *Y* direction having an intensity of 2 kN/m at the fixed end and 3 kN/m at the free end.

In all cases the following results are calculated and compared:

- The frequency of the ten (10) lowest natural vibration modes
- The displacement (translation and rotation) of station 3 and 5 in global coordinates
- The section force and moment (stress resultants) at node 1 and node 3 in element coordinates

Test case 2. A separate blade

This test considers the blade separately assuming that the blade is fixed at the root and free at the tip. It is assumed that the centre of mass and shear centre coincides with the neutral axis.

It is noted that the ANSYS model does not completely constrain the axial displacements in the same way that is done in the Bladed MB model. This is due to the fact that in Bladed MB, the element axis is not necessarily parallel to the pitch axis and hence the local z-axis of the blade structure is not parallel to the global z-axis. This difference could have a minor effect on the calculated mode shapes of the blades, particular for the higher order modes.

The lowest modes shapes are calculated and compared with respect to frequency and shape defined in terms of the displacements and rotations at the tip and the blade middle. In Bladed Multibody the modes are calculated via a Campbell diagram at very low rotor speed and the corresponding mode shapes are calculated. In ANSYS the mode shapes are calculated by a linear modal analysis.

Test case 3. A complete wind turbine structure

This test case considers a complete wind turbine structure consisting of a three bladed rotor supported by a tubular steal tower.

The lowest modes shapes are calculated and compared with respect to frequency and shape defined in terms of the displacements and rotations at characteristic points, i.e. the tower top, the rotor centre and the three the tips.

3.4 Results

Test case 1. A beam modelled by separate prismatic beam elements

The results of this test case showed that the results from the Bladed Multibody framework and ANSYS is identical in this initial case, which verifies the method for defining the ANSYS input parameters. The only exception is test case 1f that is considered to be geometrically non-linear in ANSYS, while the Bladed Multibody framework applies a linear approach with an explicitly modelled geometric stiffness matrix.

Test case 2. A separate blade

The main results for test case 2 is given in the table below in terms of five characteristic modes calculated by ANSYS and Bladed Multibody.

From the table it appears that the relative differences between the calculated frequencies of the lowest four modes are smaller than 0.2%, which indicates a close agreement between the modes calculated by ANSYS and Bladed Multibody. For mode 7, i.e. the torsional mode, the relative difference between the calculated frequencies is 0.5%, which still indicates a close agreement between the calculated modes.

From the table it also appears that the relative differences between the calculated mode shapes are generally small for the most significant displacement components. An important exception is that a very large relative difference appears for the axial displacement (elongation) and the axial rotation (torsion). It is believed that this discrepancy is mainly caused by the fact that the axial displacement is not completely constrained in the ANSYS model.

Mode		1: 1st flapwise	2: 1st edgewise	3: 2nd flapwise	4: 3rd flapwise	7: Torsion
Diff		**Δ%**	**Δ%**	**Δ%**	**Δ%**	**Δ%**
Freq		0.2	0	0.2	0	0.5
Blade middle	**Disp**	-0.5	-0.1	-0.1	-0.3	12
		0.4	0	-0.7	0.2	-20.5
		193	0	157	84.4	0
	Rot	0.4	1.6	1.6	21.3	-81.1
		-0.1	-4.4	-0.9	-0.6	5.3
		0	-11.4	-8.6	-3.3	-2.3
Blade tip	**Disp**	**0**	0.3	**0**	**0**	3.6
		0.5	**0**	-1.2	0.1	3.8
		-111	-55.8	-48.3	-46.2	-34.3
	Rot	0	1.9	-1.9	3.1	4670
		-0.1	0	-0.2	-0.3	3.2
		0	-8.8	2.1	-5.4	**0**

Test case 3. A complete wind turbine structure

The main results of test case 3 are given in the table below in terms of the 15 lowest modes calculated by ANSYS and Bladed Multibody. In addition the shapes of mode 1 and mode 14 are shown in the figures.

Mode		0: Rotor rotation	1: 1st long tower	2: 1st lat tower	3: 1st asym flap	4: 1st asym flap
Diff		Δ%	Δ%	Δ%	Δ%	Δ%
Freq			0.2	0.2	0.2	0.2
Tower top	Disp	0	**0**	1.2	0	0.7
		0	1.2	**0**	-0.3	0.6
		0	0	0	0	0
	Rot	0	1.2	0.1	0	0
		0	0.1	0	0	0.8
		0	0.5	-0.6	-0.6	1.4
Rotor centre	Disp	0	0	1.1	0	0.4
		0	1.2	0	-0.9	0.6
		0	0.2	0	0	0.9
	Rot	0	0	0	0	0
		0	0.1	0	0	0.8
		0	1	-0.2	-0.6	0
Blade 1 tip	Disp	0	0	0	0.5	**0**
		0	0.4	0	-0.5	0.5
		0	0.2	0	0	0.2
	Rot	0	0	0.1	0	0
		0	0.2	0	0	0.1
		0	0	-0.2	-0.6	0
Blade 2 tip	Disp	0.1	-0.1	-0.2	0	-0.2
		0	0.3	0	0	-0.3
		0.1	0.2	1.2	0.1	-0.1
	Rot	0	0.3	0.3	0.2	0
		0	0.1	-0.1	0.1	0
		0	0.2	-0.2	0.1	-0.1
Blade 3 tip	Disp	0	-0.8	-0.1	**0**	-0.2
		0.1	-0.2	0	0	-0.1
		0	0.3	1.1	-0.1	-0.2
	Rot	0	-0.2	0.3	0.1	-0.1
		0	0	0.2	0.2	-0.1
		0	0.2	0	0.1	-0.1

The results indicate an excellent agreement between the modes calculated by ANSYS and Bladed Multibody. It is, however, surprising that the stated differences between the mode shapes of the separate blade does not appear for the 1st symmetric flapwise modes, i.e. mode 3, 4 and 5.

Mode		5: 1st sym flap	6: 1st sym edge	7: 1st asym edge	8: 2nd asym flap	9: 2nd asym flap
Diff		Δ%	Δ%	Δ%	Δ%	Δ%
Freq		0.2	0	0	0.2	0.1
Tower top	Disp	0	1.4	0	0	1.4
		0	-13	0	0.9	-0.1
		0	0	0	0	0
	Rot	0	0	0	1	0
		0	1	0	0	0.6
		0	0	-1.5	-0.3	0
Rotor centre	Disp	0	-0.9	0	0	0.3
		0	0	5	-0.2	0
		-0.5	1	0	0	0.6
	Rot	0	0	0	0	0
		0	1	0	0	0.6
		0	0	-1.5	-0.2	3.3
Blade 1 tip	Disp	**0**	3.2	-0.7	-1.1	**0**
		1.5	-13.9	**0**	-1.4	-1.1
		0.1	7	-0.3	-0.8	0.5
	Rot	0.1	-15.1	0.1	-1	1.5
		0.1	3.3	-0.6	-0.9	0.1
		0	-15.1	-1.7	0	-2.2
Blade 2 tip	Disp	0.2	0	-0.7	**0**	0.4
		0.2	1.2	-2	-0.4	-0.7
		0.3	1.5	-1.8	0.7	0
	Rot	0.3	1.7	-1.6	0.6	0.4
		0.3	0	-2.4	0.2	0.1
		0.3	-0.1	2.9	0.1	0.5
Blade 3 tip	Disp	0.2	-3.8	-1.1	0.1	0.1
		0.3	0.2	3.5	-0.2	0
		0.2	**0**	2.1	5.3	0.1
	Rot	0.3	0.1	2	1.2	0.4
		0.3	-1.7	-0.2	0.4	0.1
		0.3	-5.2	-1.2	0.2	0.2

Mode		10: 2nd sym flap	11: 2nd lat tower	12: 2nd flap	13: 3rd asym flap	14: 1st in-plane
Diff		Δ%	Δ%	Δ%	Δ%	Δ%
Freq		0.2	0.2	0.2	0.3	-0.4
Tower top	Disp	0.3	1.1	0.1	0	1
		0	0.7	0.8	-0.2	0
		0	0	0	0	0
	Rot	0	0.1	1.5	-4.1	0
		0	1.1	-0.2	0	0
		0	2.3	0.3	-0.5	0
Rotor centre	Disp	0.3	1.1	-0.1	0	1.1
		0	0.3	1.1	-0.3	0
		0	0.7	-0.1	0	0
	Rot	1.2	0	1.7	-0.4	0.5
		0	1.1	-0.2	0	0
		0	0.8	0.8	-0.5	0.6
Blade 1 tip	Disp	0.1	2.4	**0**	-4.2	5.6
		1	-0.1	9.6	0.1	**0**
		0.2	2	0.2	-0.1	-15.1
	Rot	1	0.5	0.8	0.8	0
		0.3	2.7	0.2	-8	6.8
		0	-2.5	-7	8.8	-2.3
Blade 2 tip	Disp	0	**0**	0.1	**0**	-12.8
		0.3	-0.1	-0.6	0.3	0.1
		-0.4	-0.1	11.8	-0.3	0
	Rot	-0.7	0.4	-0.9	0	0.4
		0.1	-0.1	0.5	0.1	-1.6
		0.2	0.3	0.1	0.3	-3.4
Blade 3 tip	Disp	**0**	0.4	-0.1	0	2.8
		-0.3	0.3	-0.1	-1.1	-0.1
		0.3	0	0.3	0.1	0
	Rot	0.4	0.6	1.5	0.7	0.3
		0.2	0.4	0.4	0.3	-2.6
		0.1	0.6	-0.2	0.3	-0.6

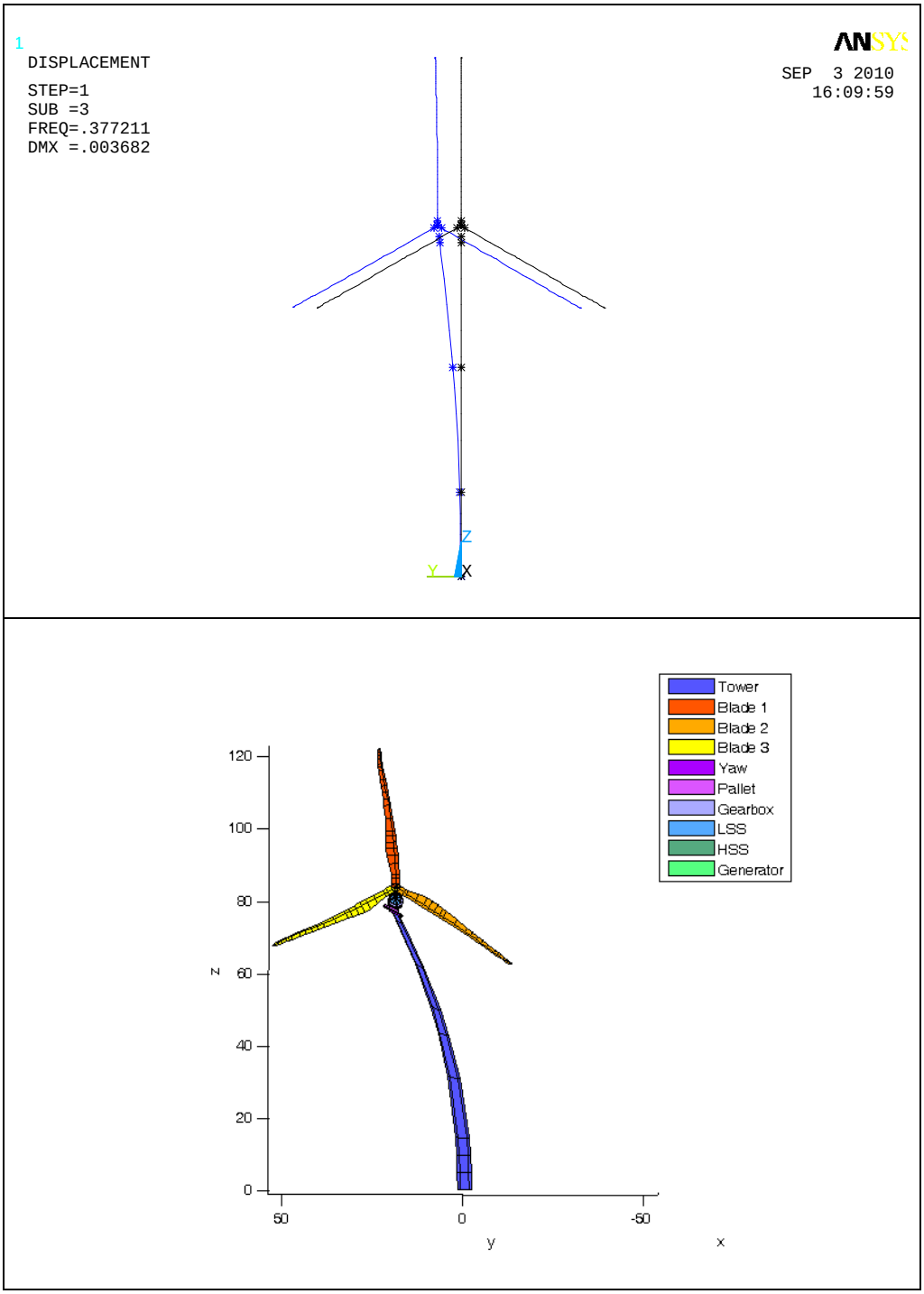

Figure 3.2: Mode shape 2 of the complete wind turbine structure calculated by ANSYS (above) and Bladed (below).

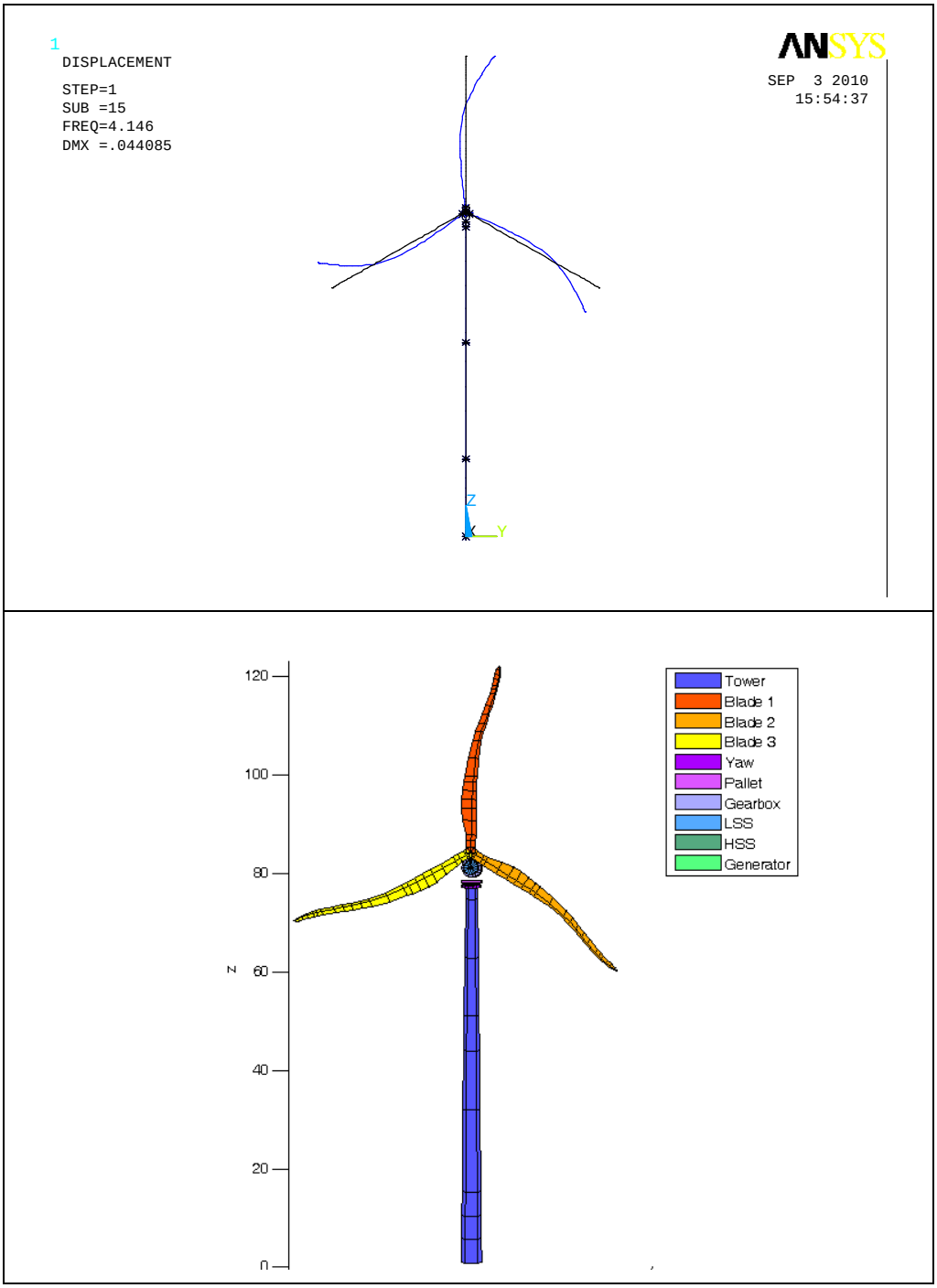

Figure 3.3: Mode shape 14 of the complete wind turbine structure calculated by ANSYS (above) and Bladed (below).

3.5 Conclusion

The modal frame component of Bladed Multibody has been tested using a similar structural model elaborated by the general purpose FEM package ANSYS. The test includes a case with a separate blade fixed at the root as well as a complete wind turbine structure, and it is based on comparing the lowest mode shapes calculated by the two software packages.

The results for the complete wind turbine show an excellent agreement between the 15 lowest modes calculated by Bladed Multibody and ANSYS, both with respect to frequency and shape of the modes.

It is noted that the work does not consider the case, where the centre of mass is offset from the neutral axis due to limitation of the applied ANSYS beam element type.

It is also noted that the work does not include any tests of the non-linear inertia forces that is a significant part of the of the modal frame component in Bladed Multibody

4 OC3 COMPARISONS AGAINST OTHER CODES

The Offshore Code Comparison Collaboration (OC3) [2] is an IEA project coordinated by NREL under Wind Task 23 "Offshore Wind Energy Technology and Deployment", Volume II "Technical Research for Deeper Water Applications" and involved a group of international participants from universities, research institutions and industry across the United States of America, Germany, Denmark, the United Kingdom, Spain, the Netherlands, Norway, Sweden and Korea.

The OC3 project is a benchmarking project looking at the aero-hydro-servo-elastic codes which have been developed for modelling the dynamic response of offshore wind turbines.

Before the completion of the OC3 project, GH performed simulations with a version of Bladed Multibody for phase I, modelling a 5MW offshore wind turbine mounted on a monopile support structure.

Having built the turbine model in the chosen simulation code, the comparison exercise involved carrying out a number of load cases involving increasing complexity. The cases ranged from considering the applied hydrodynamic and aerodynamic loads separately on a rigid version of the structure to a fully coupled simulation involving flexibility of the blades, tower and drive-train; the influence of the controller; as well as dynamic loading from wind and waves.

4.1 Turbine model

The turbine used in this comparison exercise was the NREL offshore 5-MW baseline turbine [3] mounted on a monopile support structure cantilevered at the mud line in water depth of 20m. The turbine is a three-bladed, variable speed, pitch regulated turbine with a rotor diameter of 126m and a tower height of 90m above mean sea level. Figure 4.1 describes the location of the sensors used for the comparison.

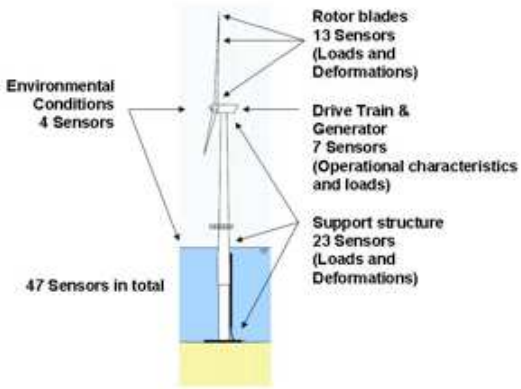

Figure 4.1 – Location of sensors on the NREL 5MW turbine

4.2 Modelling situations

The full list of simulations performed as part of the project is shown in Table 4.1. The simulations vary in complexity: phase 1 consists of a linear model of the structure; phase 2 considers, separately, applied aerodynamic and hydrodynamic loads on a rigid structure; phases 3 and 4 add structural flexibility to the simulations of phase 2; and phase 5 considers a fully coupled simulation involving aerodynamic and hydrodynamic loads, rotor, drive train and support structure motion and the action of the controller.

Phase.Run	Simulation Type	External conditions
1.1	Non-rotating full-system natural frequencies	Structural flexibility only, without damping; no applied loads
1.2		Structural flexibility only, gravitational loads only
2.1a	Rigid turbine with constant rotor speed and fixed blade pitch	Steady wind 8m/s
2.1b	Rigid turbine with rotor speed and blade pitch via controller	
2.2		Turbulent wind 11.4m/s
2.3		Turbulent wind 18m/s
2.4	Rigid turbine in standby	Normal Sea State: Regular Airy, H = 6m, T = 10s
2.5		Normal Sea State: Irregular Airy, Hs = 6m, Tp = 10s
2.6		Normal Wave Height: Stream Function (Dean), H = 6m, T = 10s
3.1	Flexible Onshore Wind Turbine	Steady wind 8m/s
3.2		Turbulent wind 11.4m/s
3.3		Turbulent wind 18m/s
4.1	Parked turbine with rigid rotor but flexible support structure	Normal Sea State: Regular Airy, H = 6m, T = 10s
4.2		Normal Sea State: Irregular Airy, Hs = 6m, Tp = 10s
4.3		Normal Wave Height: Stream Function (Dean), H = 6m, T = 10s
5.1	Flexible offshore wind turbine	Steady wind 8m/s with Normal Sea State: Regular Airy, H = 6m, T = 10s
5.2		Turbulent wind 11.4m/s with Normal Sea State: Irregular Airy, Hs = 6m, Tp = 10s
5.3		Turbulent wind 18m/s with Normal Sea State: Irregular Airy, Hs = 6m, Tp = 10s

Table 4.1 Load cases simulated for Phase I of the OC3 project

4.3 Results comparison

A selection of results is presented here; a wider sample of results is displayed in [2]. The legend for the time-series results is given in Figure 4.2. The Bladed Multibody results have been emboldened.

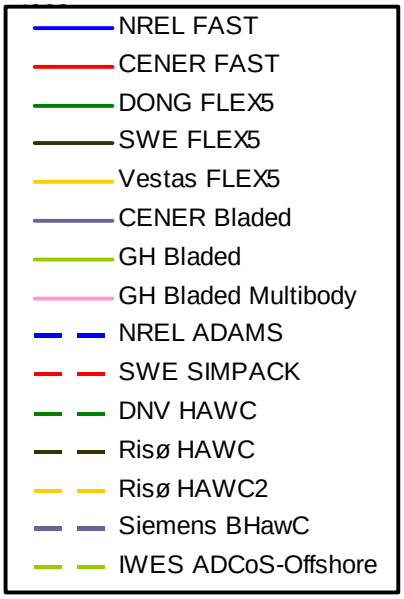

Figure 4.2 – Legend for time-series results

Natural frequencies

Load case 1.2 of the comparison was an analysis of the linearised turbine model, incorporating flexibility of the substructure, tower, drive-train and blades without the effects of air and water. The coupled natural frequencies of the turbine and support structure were then compared. Figure 4.3 presents the natural frequencies of the complete system. Two series are shown for the natural frequencies because, especially for the 2nd blade asymmetric flapwise yaw mode, the results differ substantially depending on whether the yaw degree of freedom of the support structure has been included in the calculation. For this GH Multibody simulation, good agreement is seen for the both cases, with or without the tower torsion mode included. The error bars show the standard deviation in frequency between the different codes. The full data-set of natural frequencies can be seen in [2] although this only includes the GH Multibody results without tower torsion.

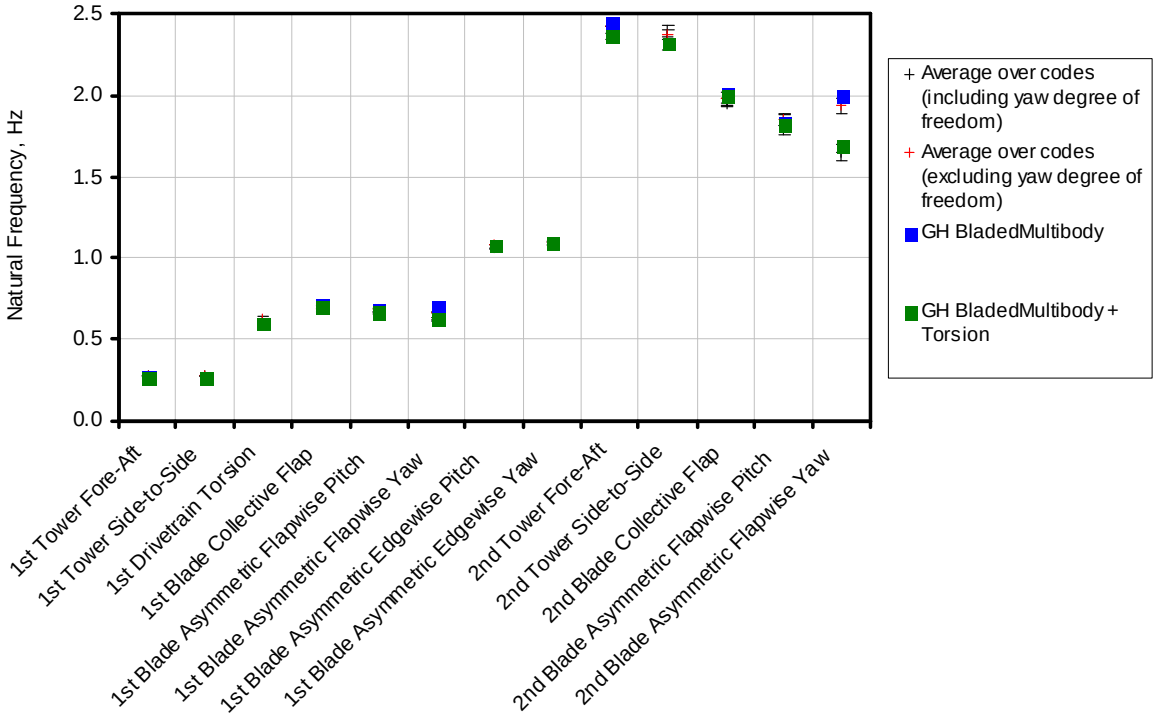

Figure 4.3 – Comparison of natural frequencies

Time-series

The aerodynamic loads under steady conditions are presented in Figure 4.4. The variation in load over time includes effects from wind shear, upflow, rotor tilt and tower shadow. Although there are differences between the codes, the overall variation is approximately 5%. Different aerodynamic models are employed by the various codes and this is assumed to be the source of the difference.

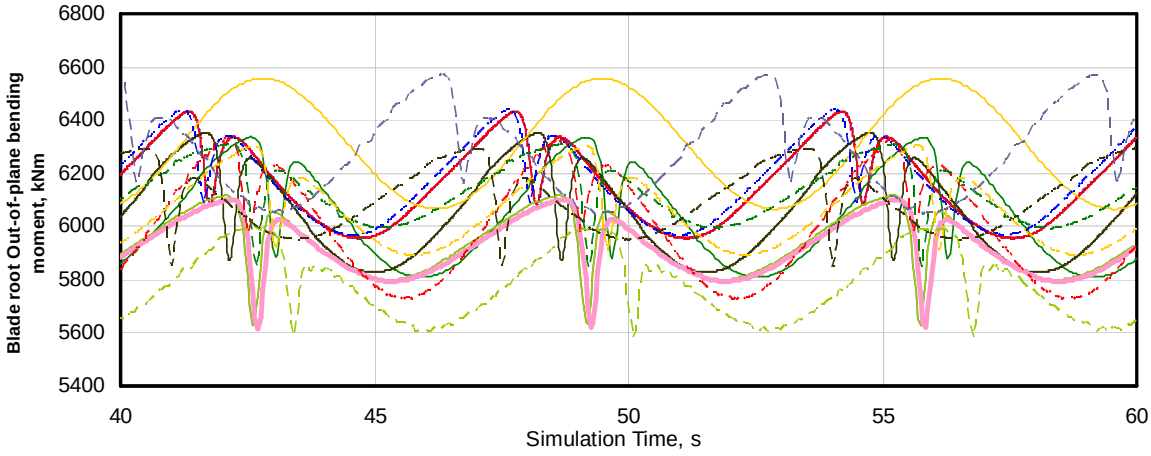

Figure 4.4 – Out-of-plane bending moment, 8 m/s steady wind (load case 2.1a)

The amplitude of tower loads due to wave loads varies much less (Figure 4.5) and this is due to the Morison's equation being used by all the codes to apply the hydrodynamic loads. Differences in higher frequency may be due to differences in damping of transient structural vibrations.

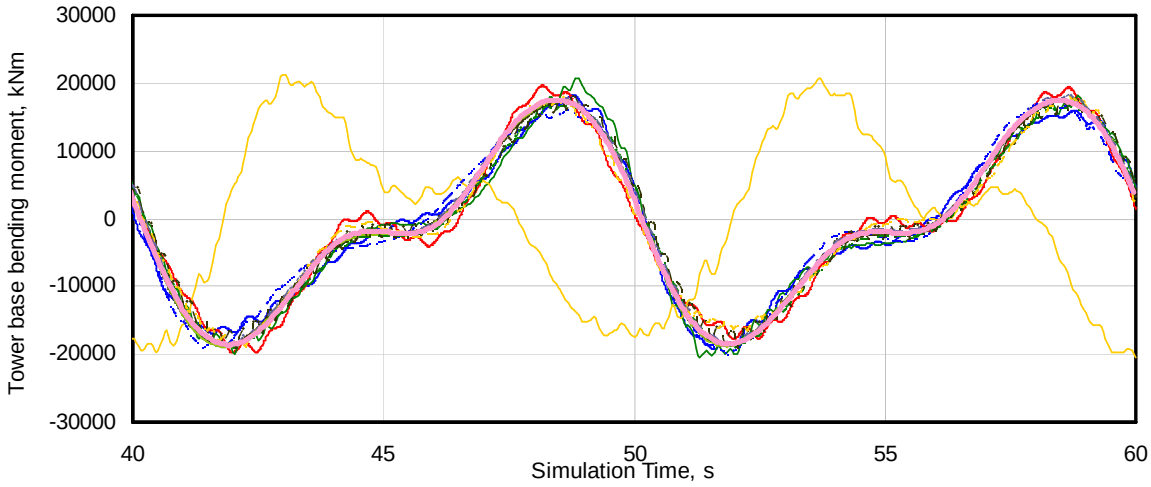

Figure 4.5 – Tower base bending moment, regular waves (load case 4.3)

Load spectra

Analysis of coupled simulations was performed in the frequency domain. In general, Bladed agrees well with most of the codes which submitted results although there is a fairly large amount of scatter.

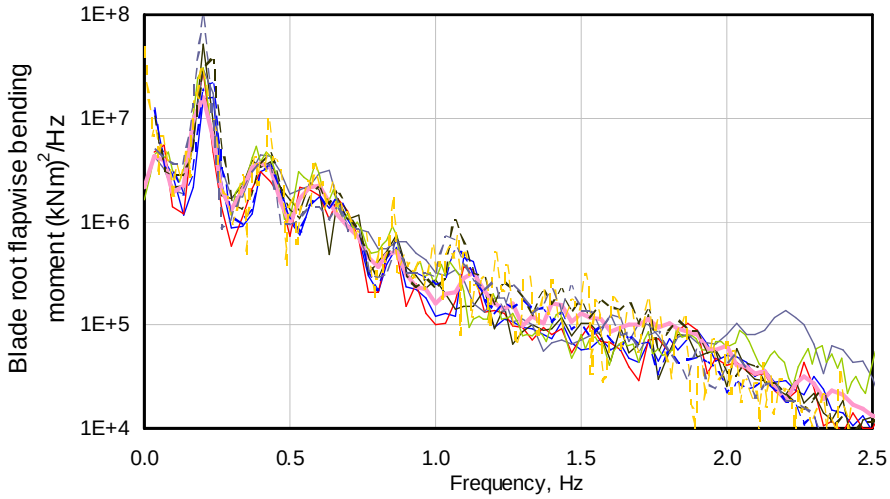

Figure 4.6 – power spectrum of blade root flapwise bending moment, turbulent wind and stochastic waves (load case 5.2)

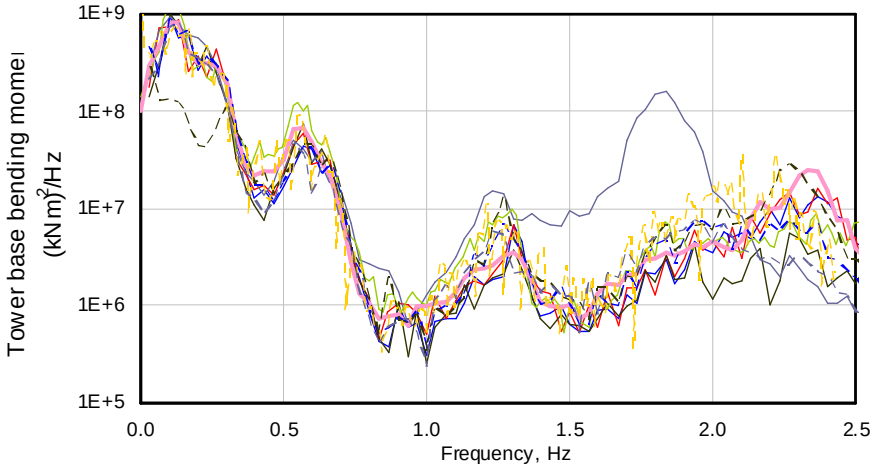

Figure 4.7 – power spectrum of tower base bending moment, turbulent wind and stochastic waves (load case 5.2)

4.4 Conclusion

Bladed Multibody has been used to create a model of the NREL 5MW turbine with which to perform simulations for the IEA's Offshore Code Comparison Collaboration.

The results for the complete wind turbine show good agreement with other simulation codes which include modal, multibody and finite element structural models.

The Offshore Code Comparison Collaboration has recently been extended to include phases looking at a jacket support structure and a tension leg platform for the same turbine. GH is continuing its participation in the code comparison and will shortly submit preliminary results for the jacket support structure.

5 COMPLETE LOADSETS

Complete fatigue and extreme loadsets were carried out in the new multibody version of Bladed and compared against loadsets from previous versions of Bladed. In total, five complete loadsets were compared, covering a range of different turbine types and configurations:

- Multi-megawatt, offshore, 3-blade, multi-member support structure, upwind, variable speed, pitch regulated
- Multi-megawatt, onshore, 3-blade, monopile tower, upwind, variable speed, pitch regulated
- Multi-megawatt, offshore, 3-blade, monopile tower, downwind, variable speed, pitch regulated
- < 500kW, onshore, 3-blade, monopile tower, upwind, fixed speed, stall regulated
- ~1 Megawatt, onshore, 2-blade, tethered tower, upwind, variable speed, pitch regulated

One set of results is presented below.

5.1 Extreme results

The following graphs plot a comparison of MB Bladed extreme loads against old Bladed, for the various Design Load Cases.

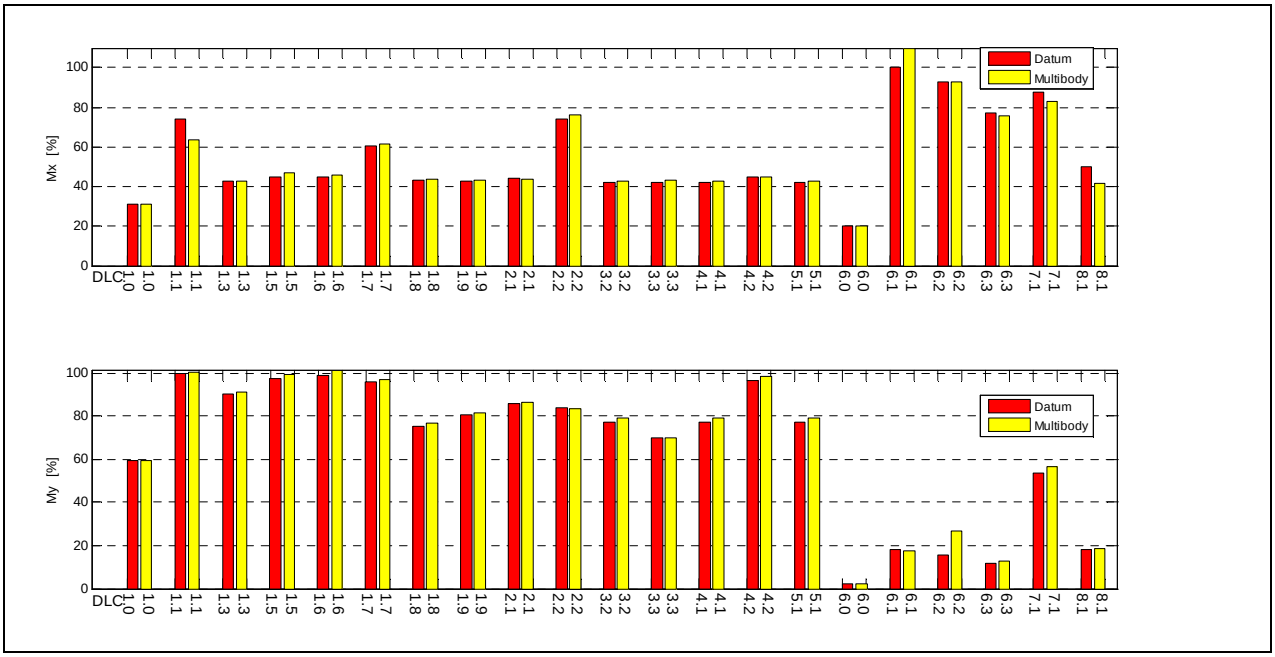

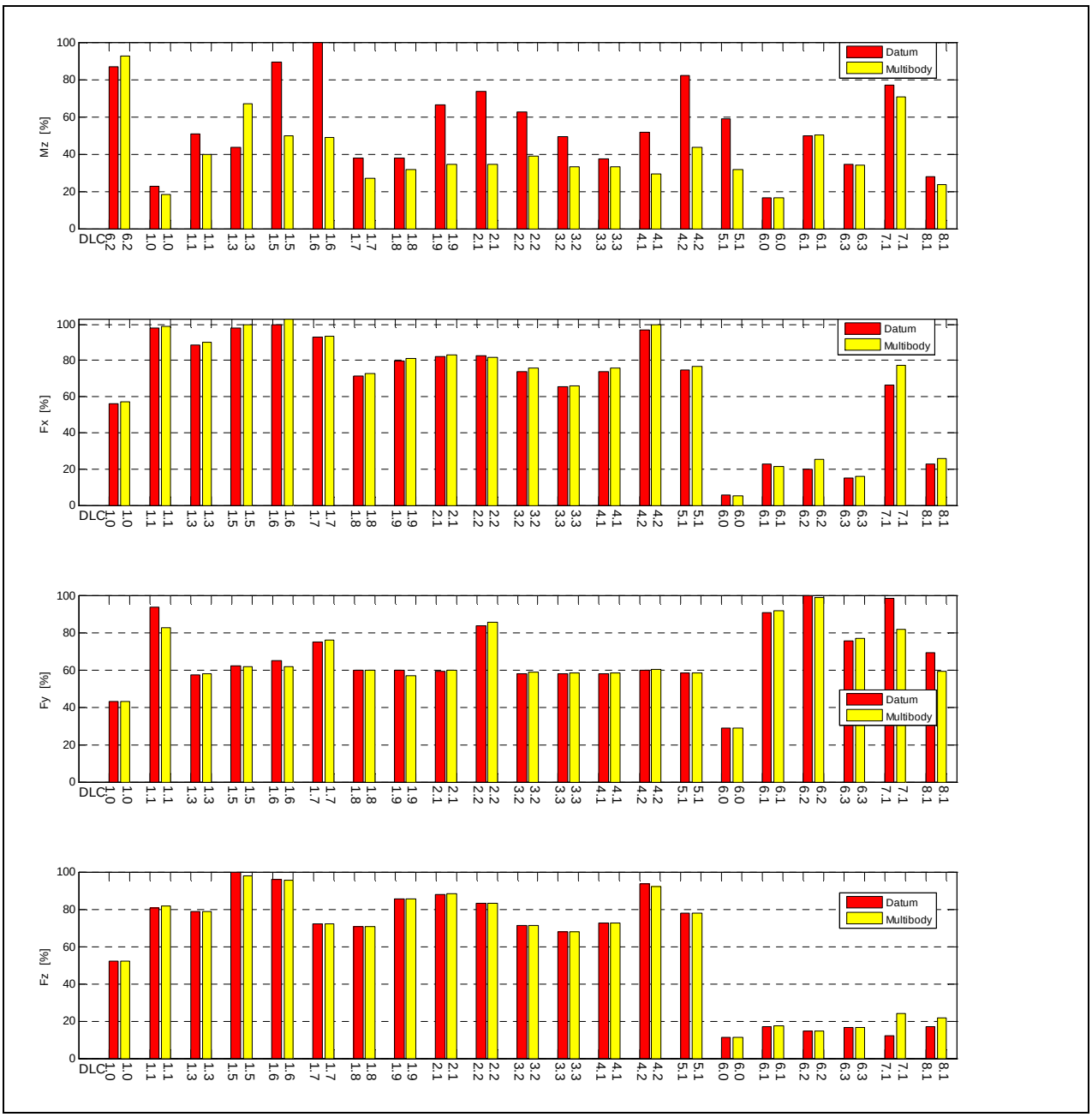

Figure 5.1 – Combined Blade root loads (GL coordinates)

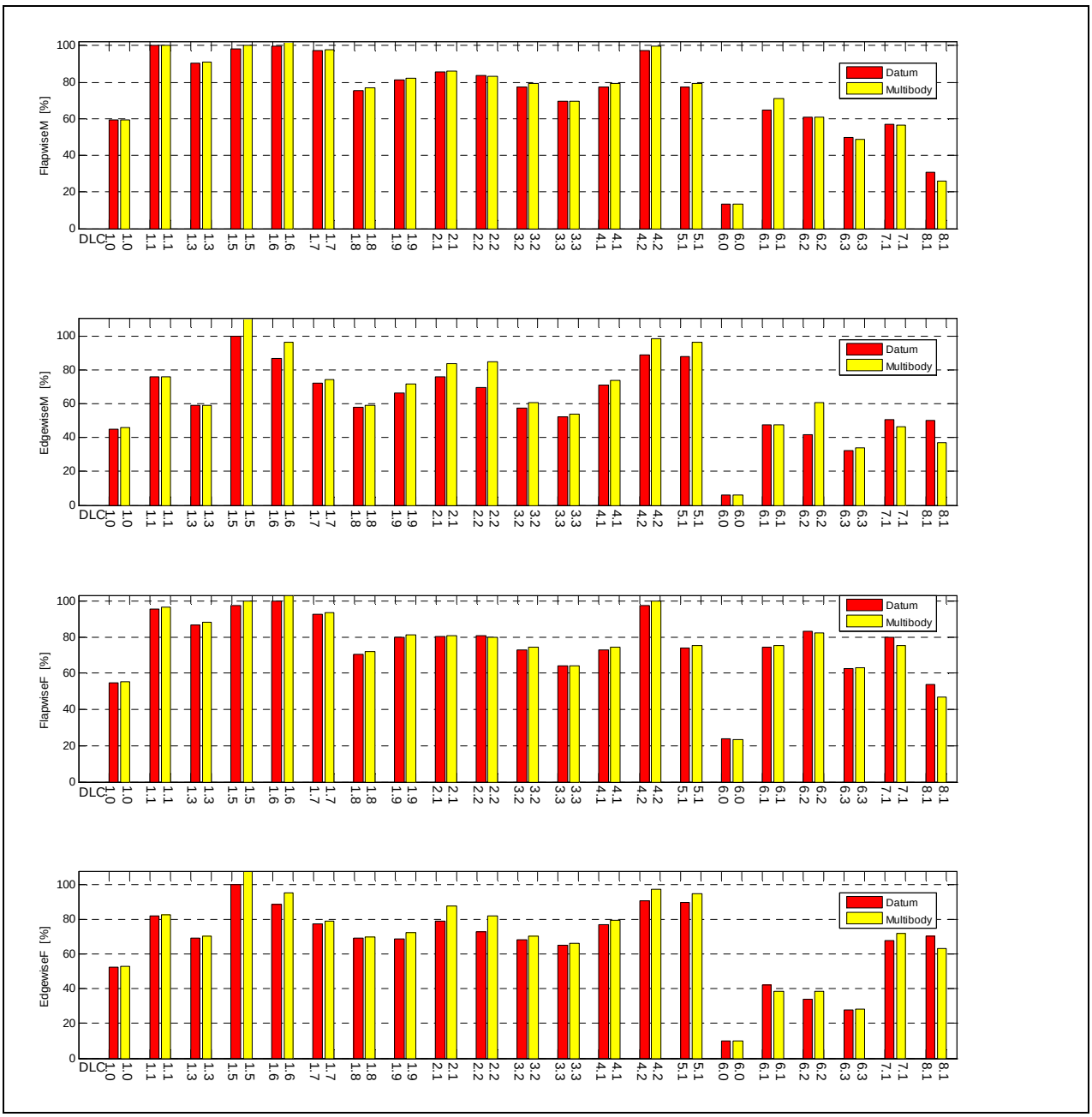

Figure 5.2 – Combined blade root loads (Local coordinates)

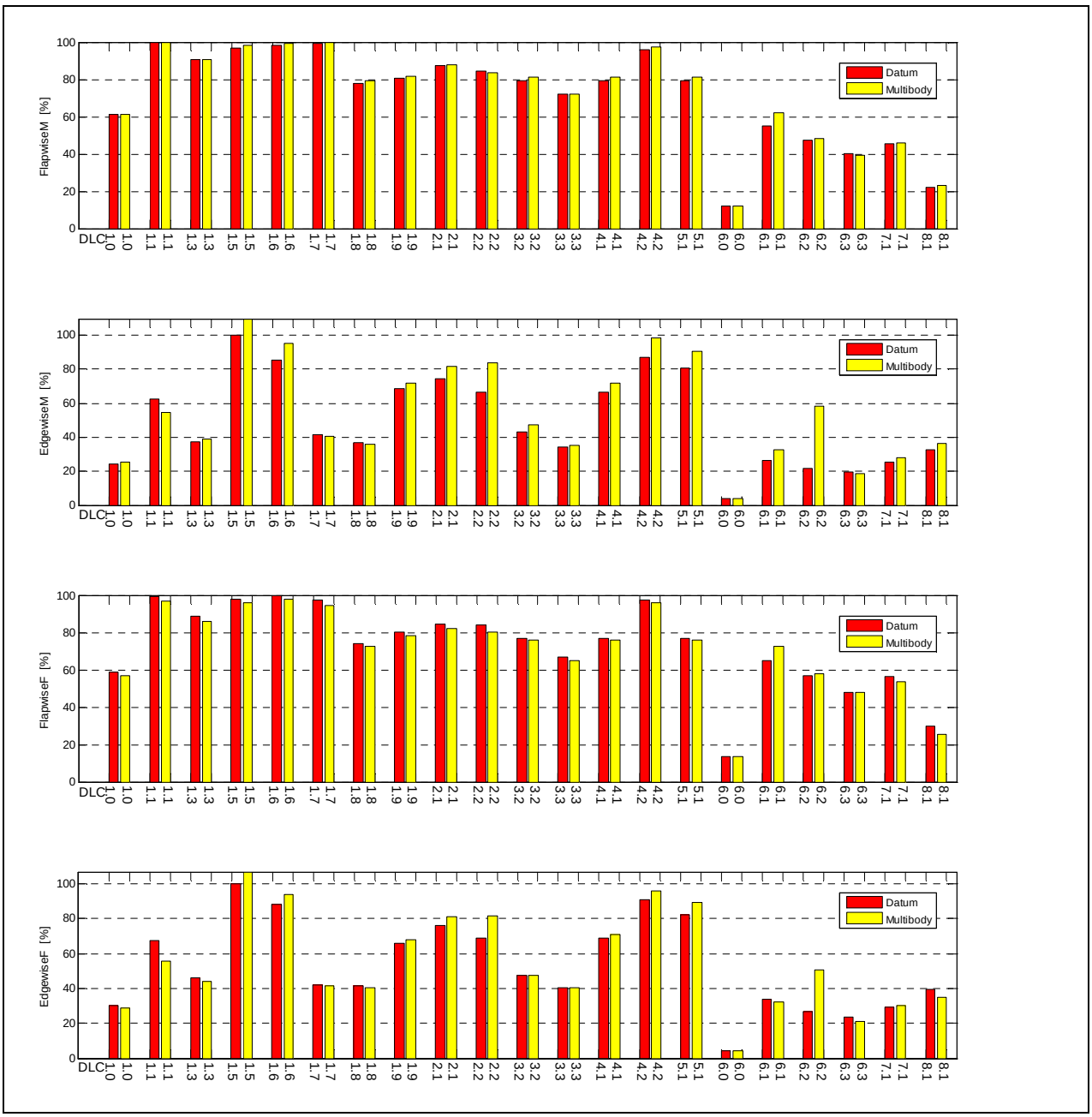

Figure 5.3 – Blade mid-span loads

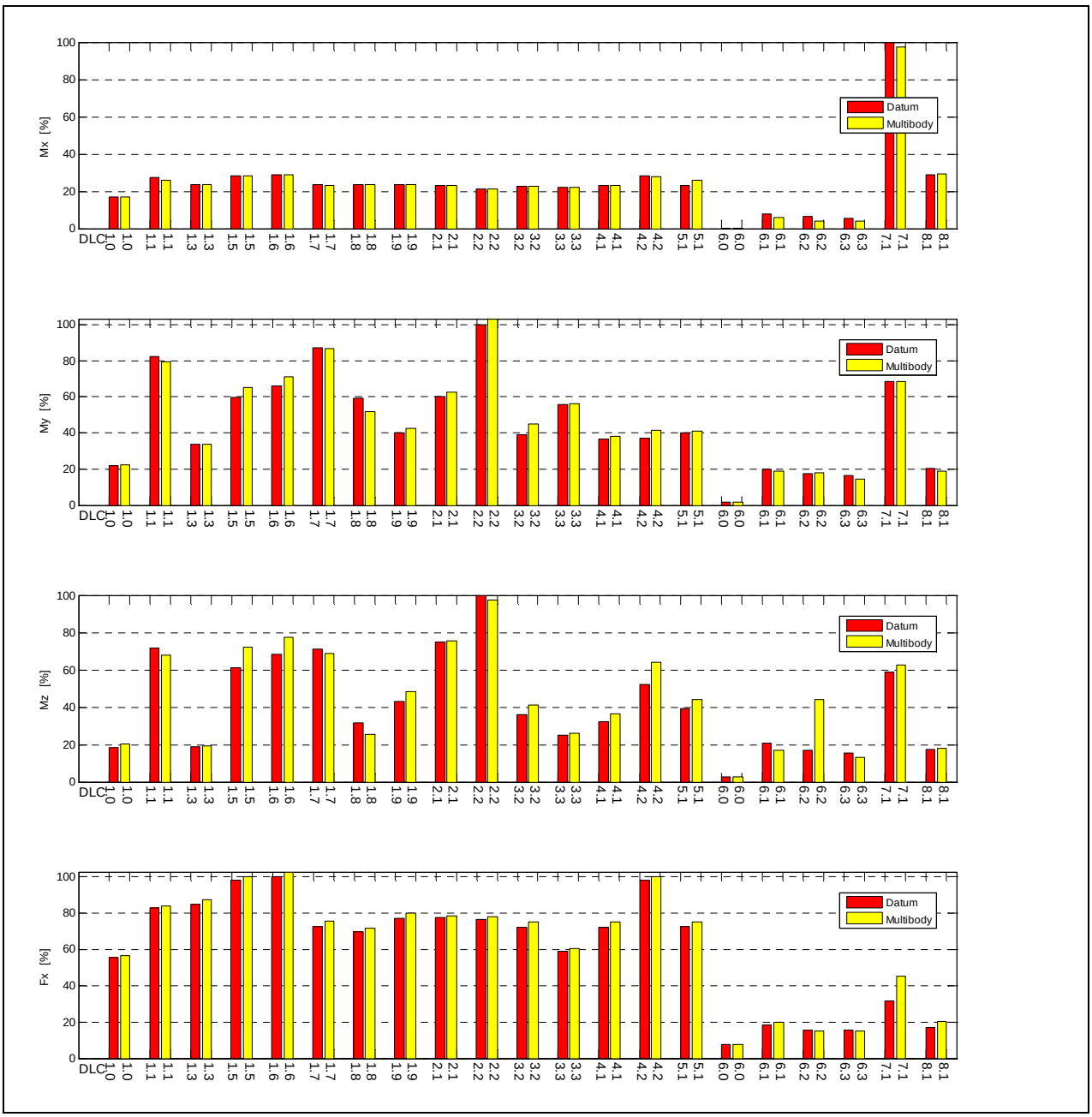
Mx [%]
My [%]
Mz [%]
Fx [%]
Datum
Multibody
DLC
1.0 1.0 1.1 1.1 1.3 1.3 1.5 1.5 1.6 1.6 1.7 1.7 1.8 1.8 1.9 1.9 2.1 2.1 2.2 2.2 3.2 3.2 3.3 3.3 4.1 4.1 4.2 4.2 5.1 5.1 6.0 6.0 6.1 6.1 6.2 6.2 6.3 6.3 7.1 7.1 8.1 8.1

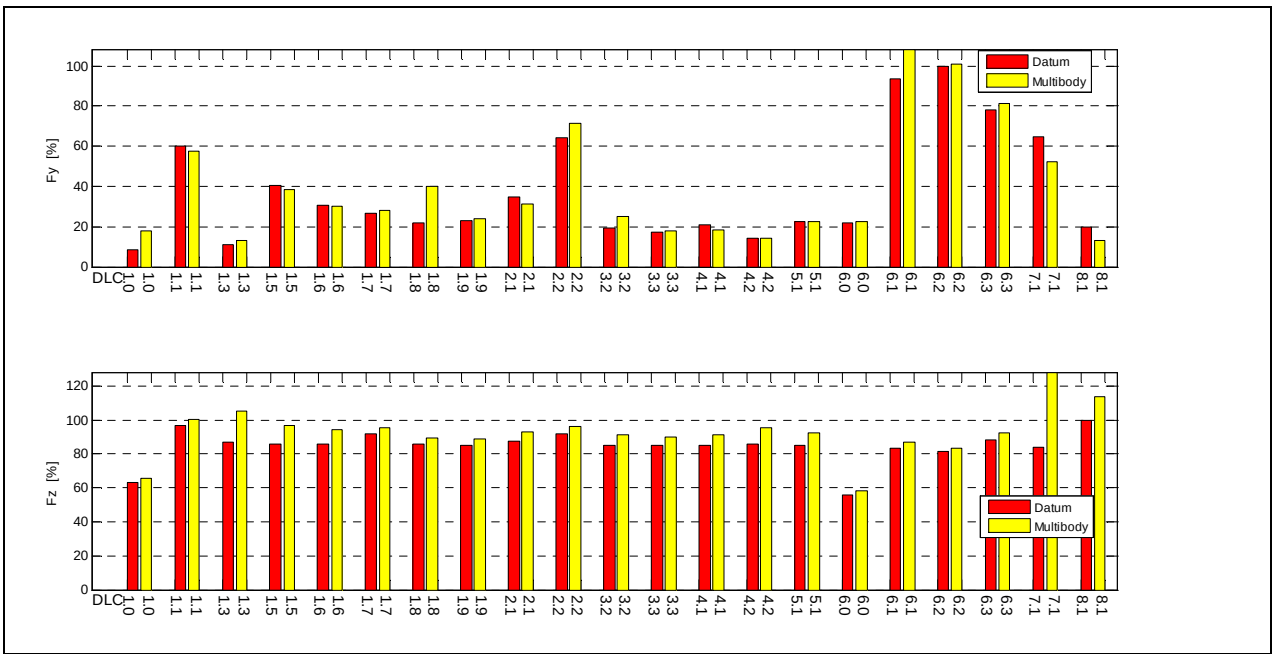

Figure 5.4 – Hub fixed loads

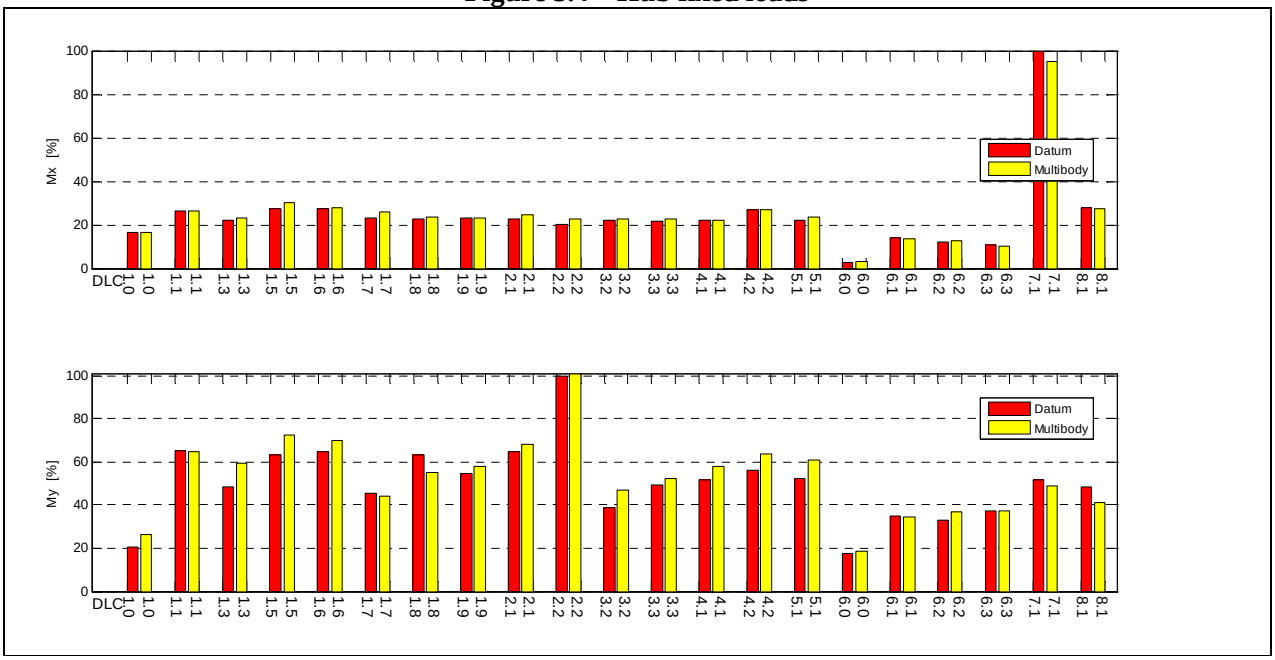

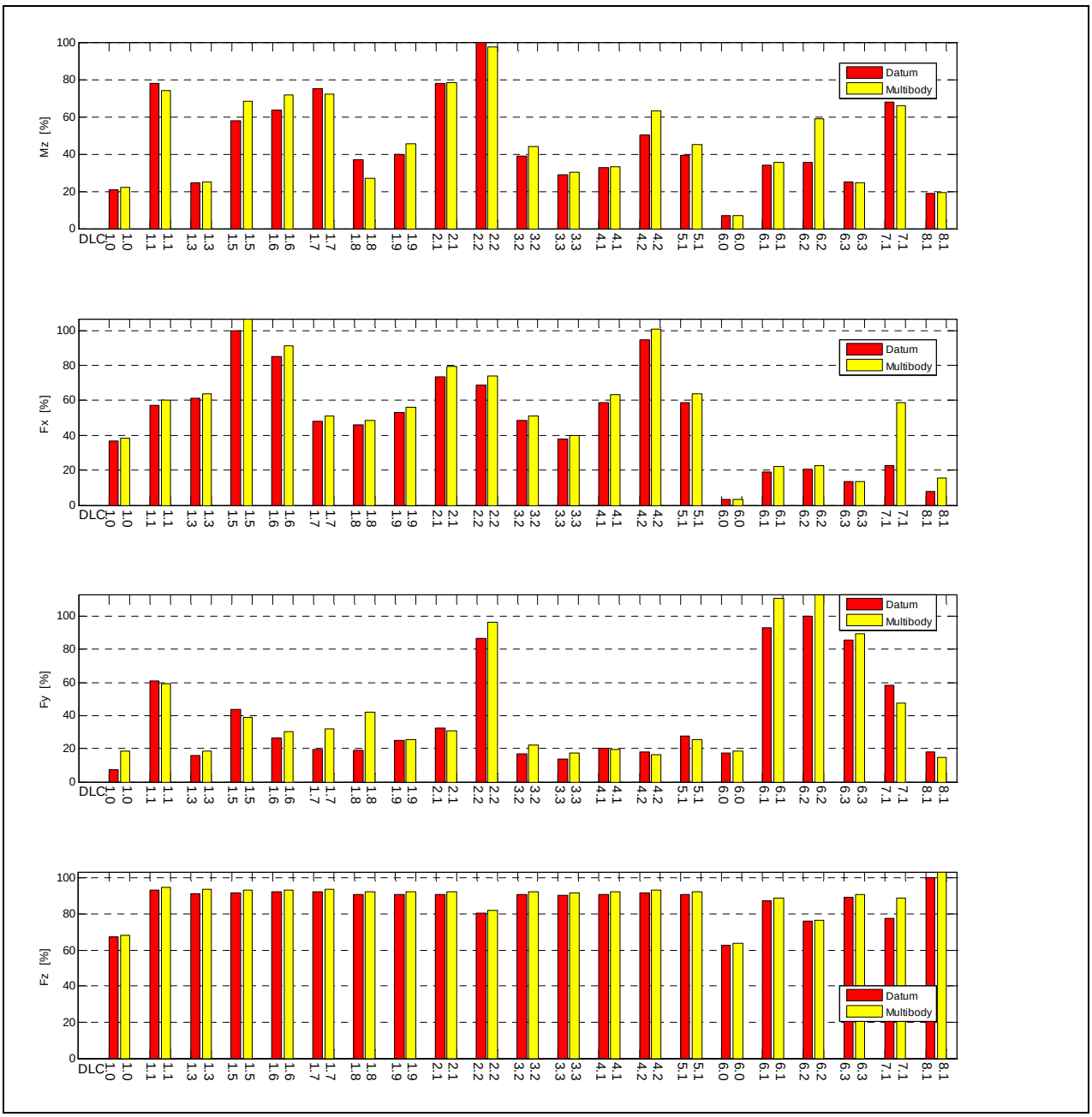

Figure 5.5 – Yaw bearing loads

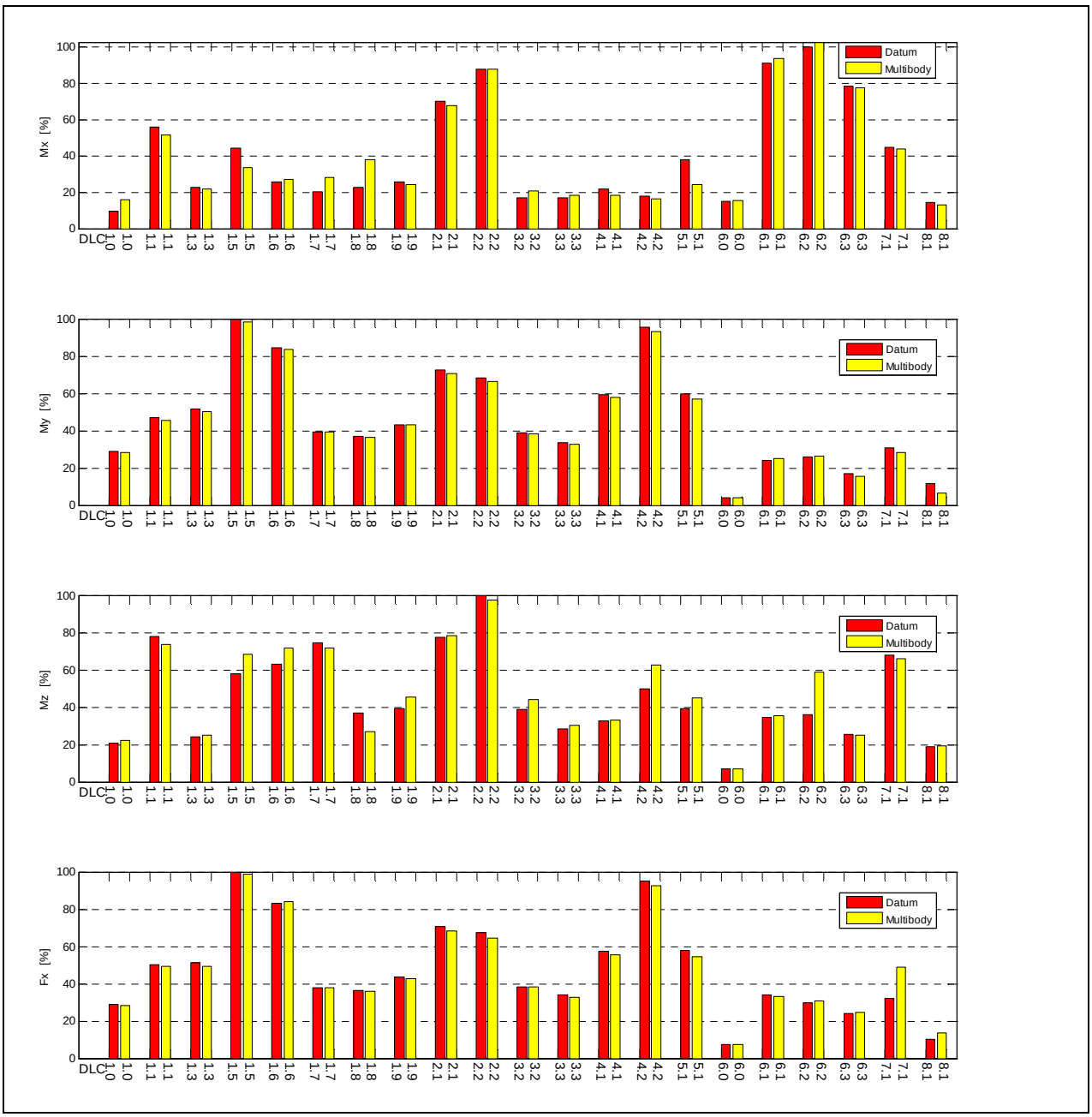
Mx [%]
My [%]
Mz [%]
Fx [%]
Datum
Multibody
DLC

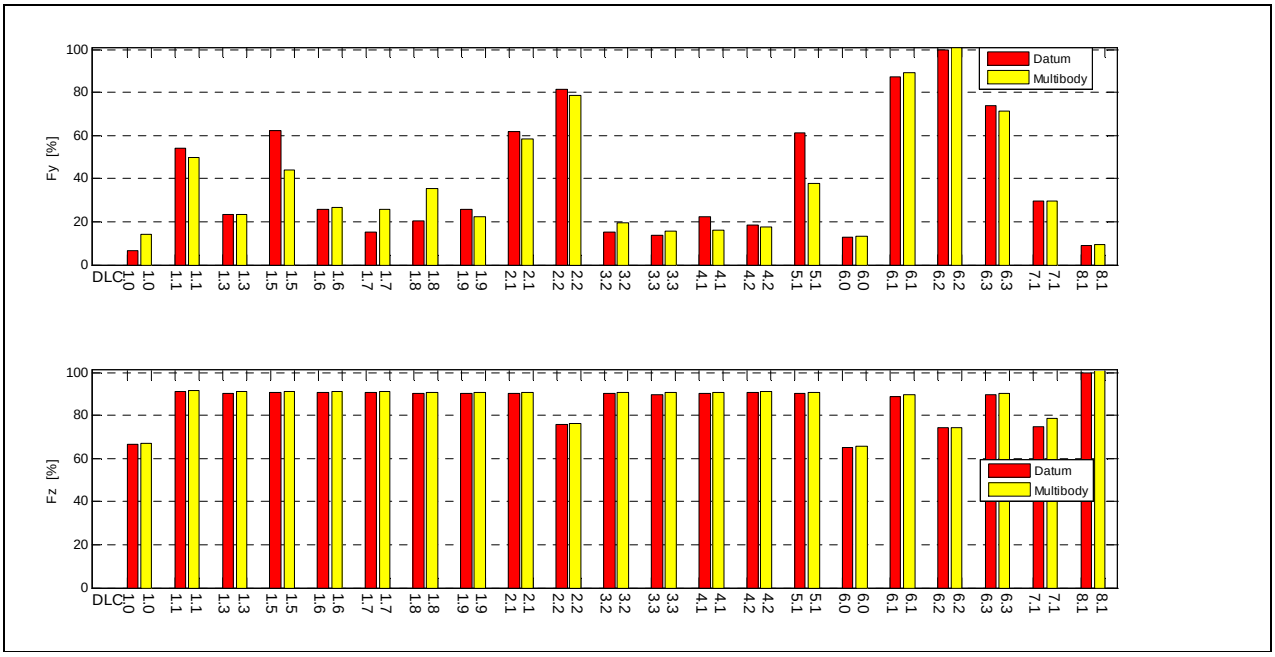

Figure 5.6 – Tower base loads

5.2 Fatigue loads

The table below presents the 1 Hz damage equivalent load comparison.

	SN	Mx (flap)	My (edge)	Mz (span)	Fx (flap)	Fy (edge)	Fz (span)
Blade root	4	-1.9%	-4.6%	-5.0%	0.0%	-1.4%	0.1%
Blade root	10	-1.9%	-5.5%	-3.8%	-1.3%	-1.6%	0.0%
Hub Rot	4	0.0%	-2.1%	-2.8%	-2.1%	0.4%	0.4%
Hub Fixed	4	0.0%	-2.1%	-3.3%	-2.1%	-24.2%	-3.5%
Yaw bearing	4	13.8%	0.3%	-3.3%	-4.4%	-10.3%	-10.4%
Tower base	4	-17.2%	-9.6%	-3.5%	-4.7%	-15.3%	-10.1%

In addition, normalised example time history, cycle distribution and auto-spectrum plots are shown below.

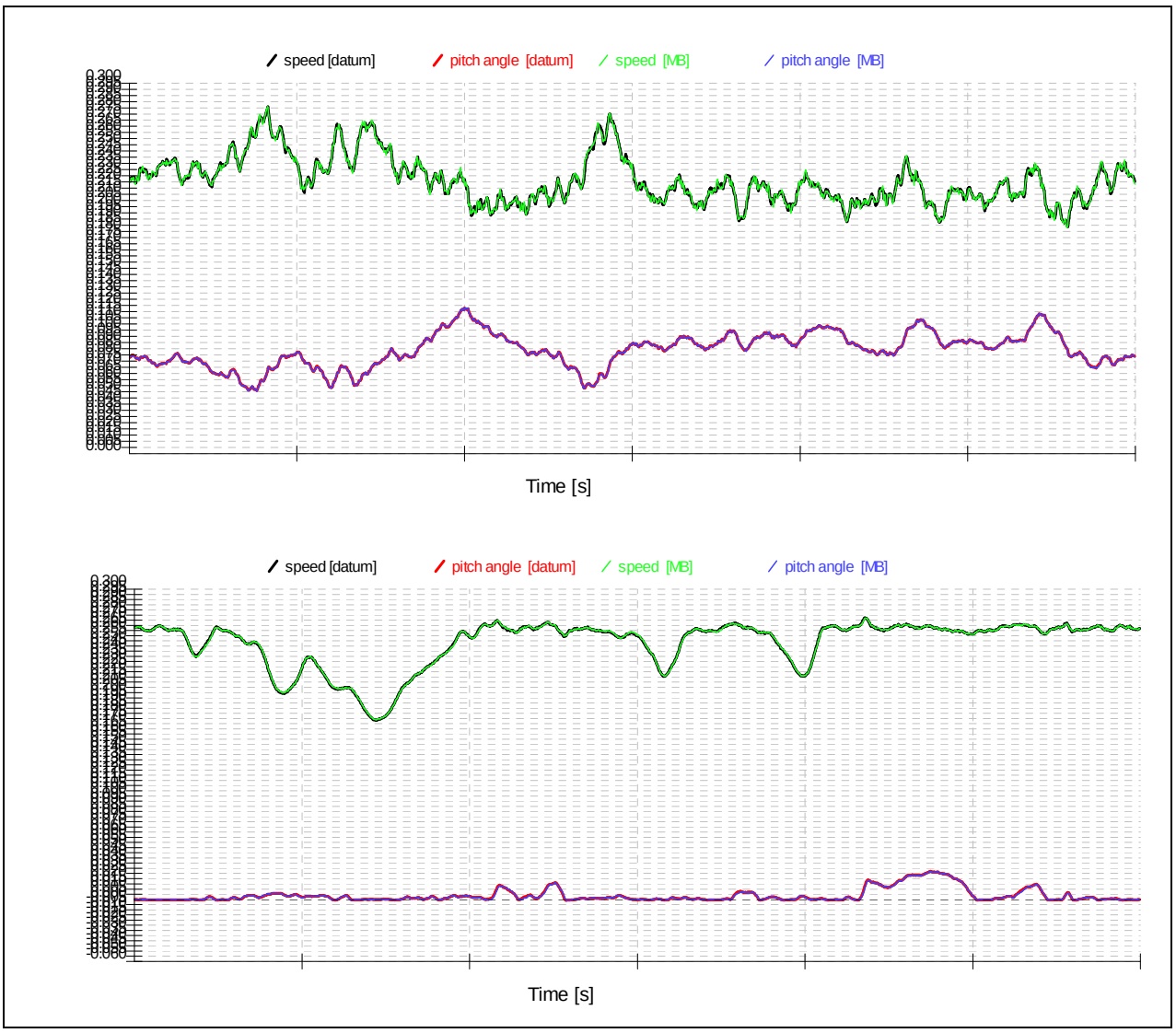

Figure 5.7 – Example time history of speed and pitch angle

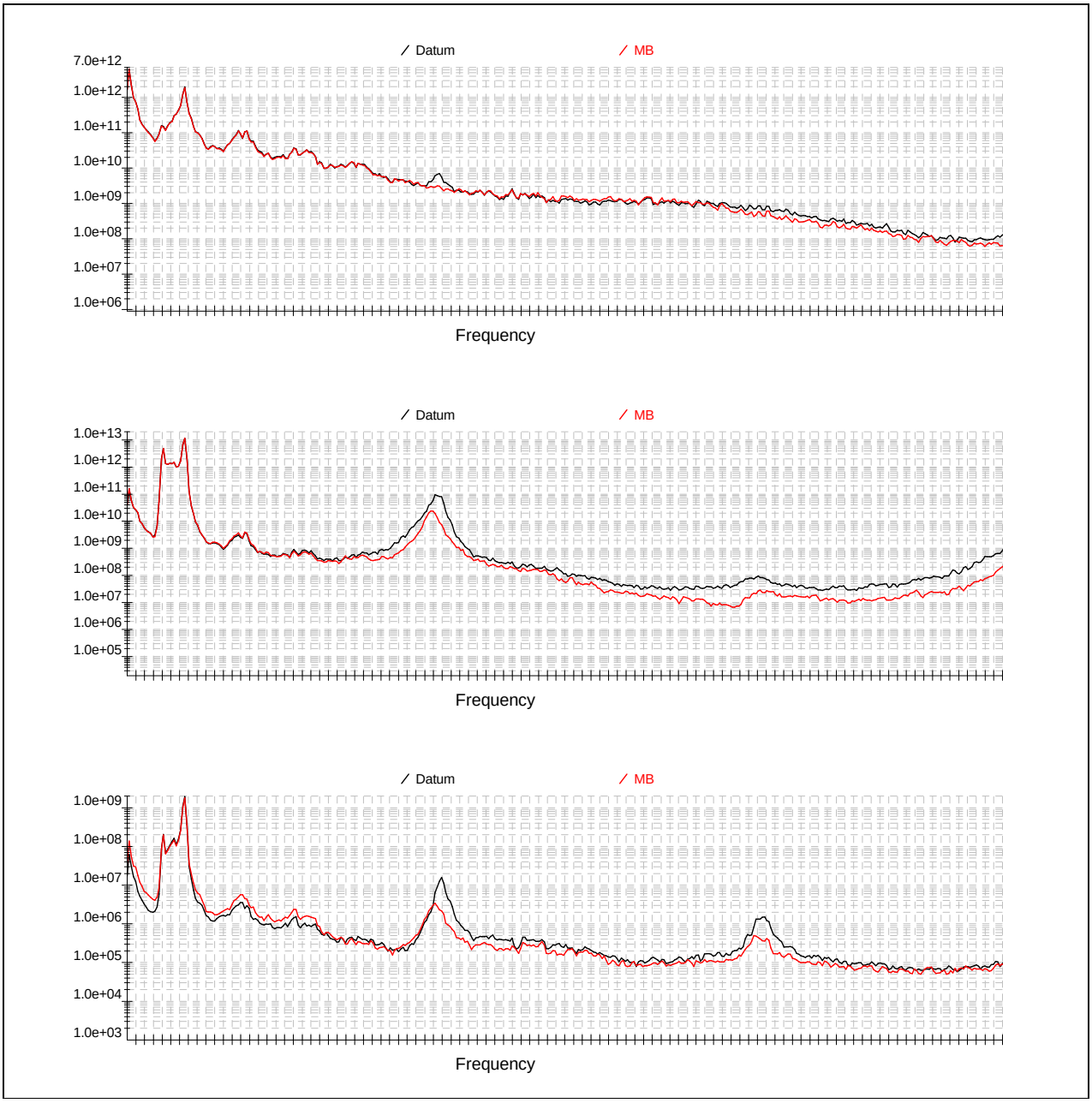

Figure 5.8 – Auto spectra for Blade root flap, edge and spanwise bending moment

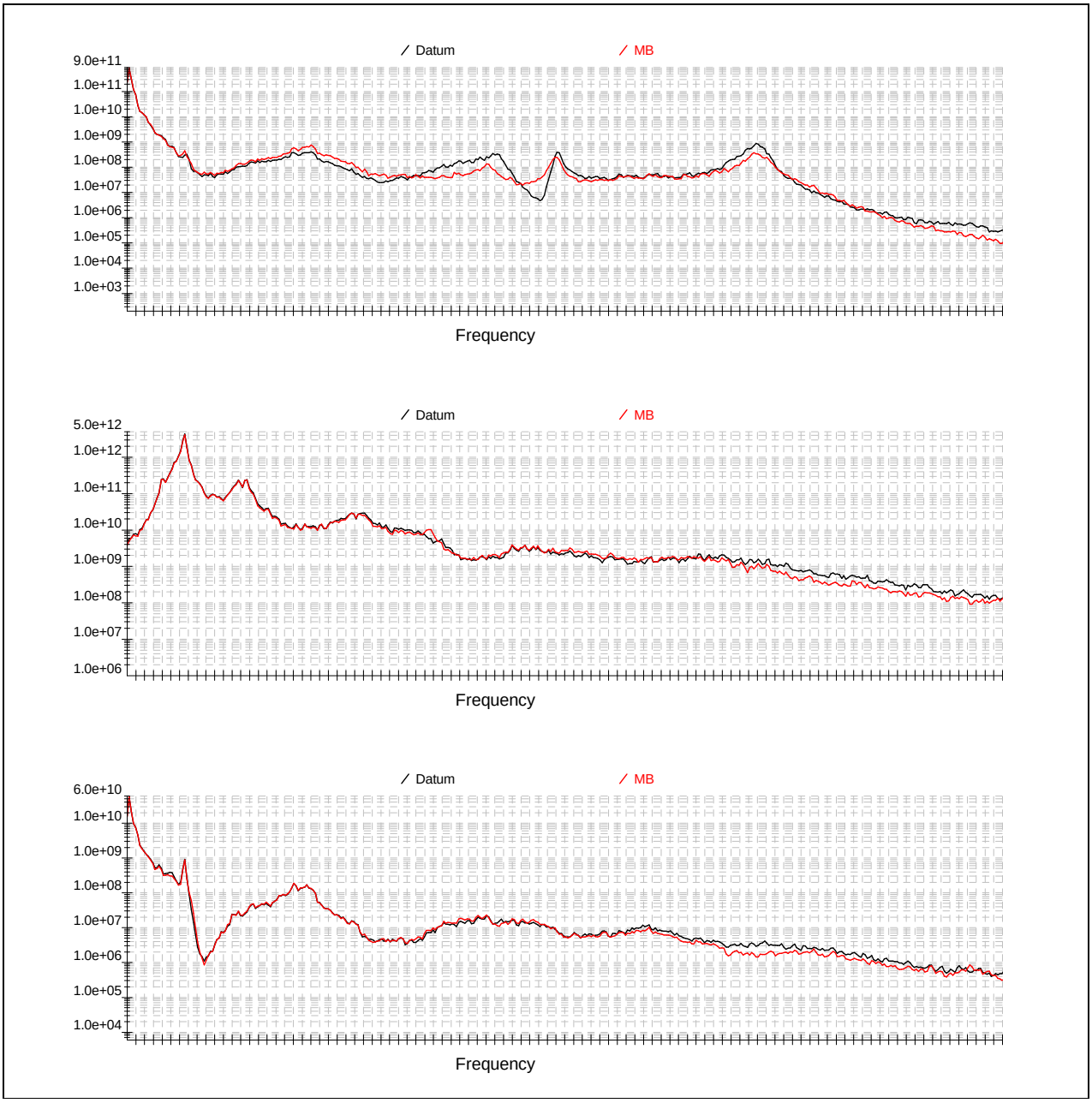

Figure 5.9 – Auto spectra for Hub rotating Mx, My, Fx

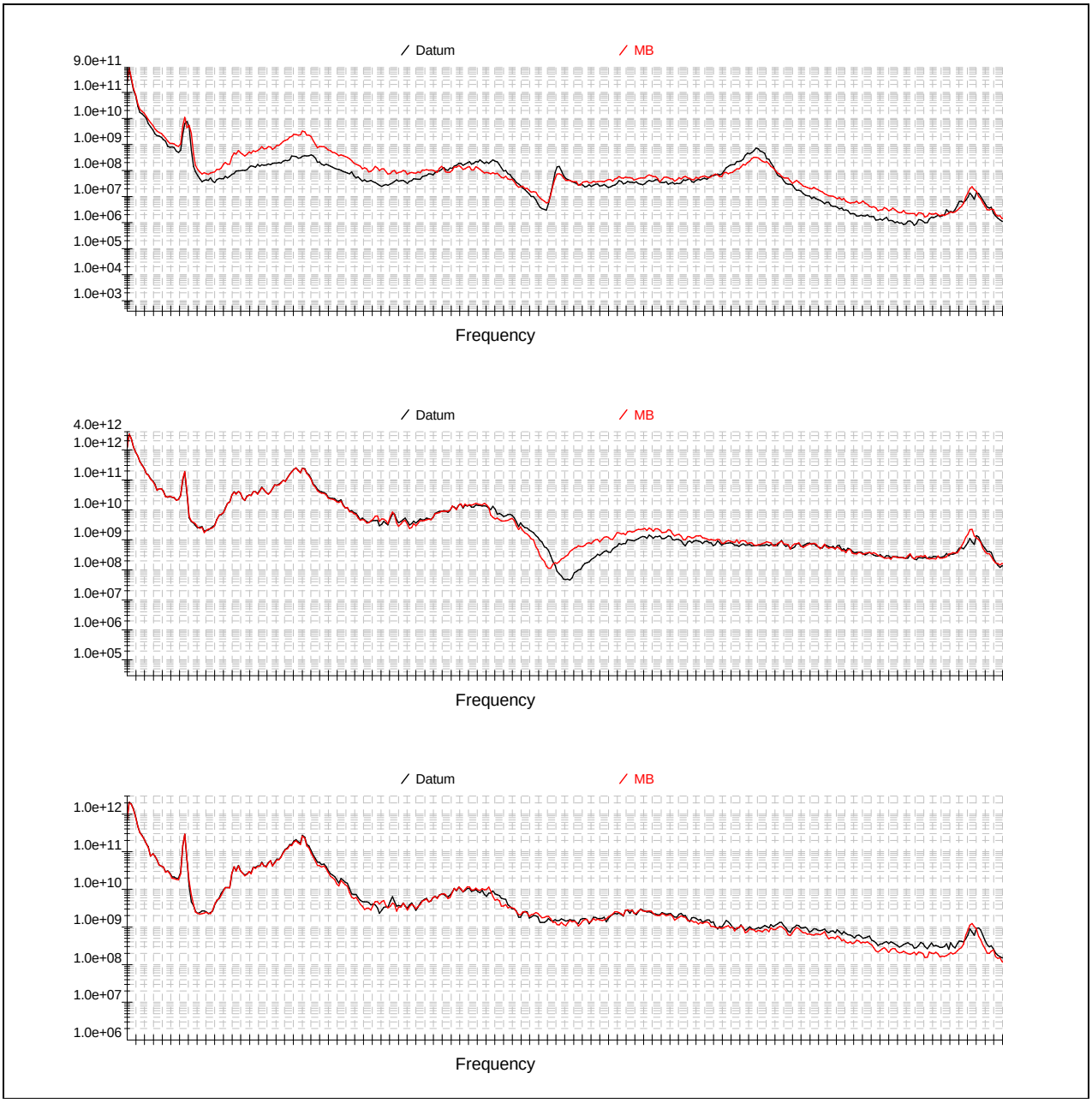

Figure 5.10 – Auto spectra for Yaw bearing Mx, My, Mz

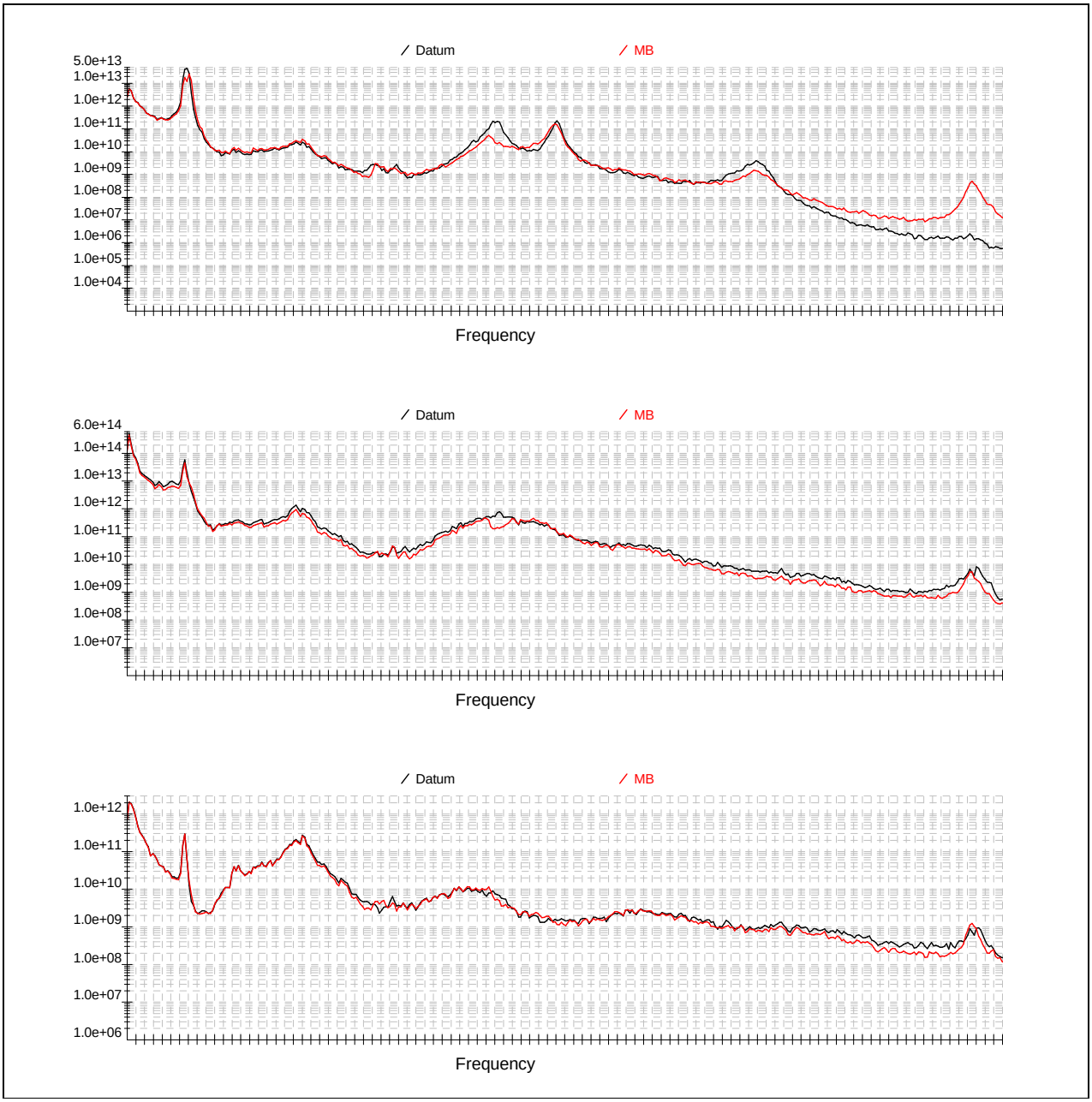

Figure 5.11 – Auto spectra for Tower base Mx, My, Mz

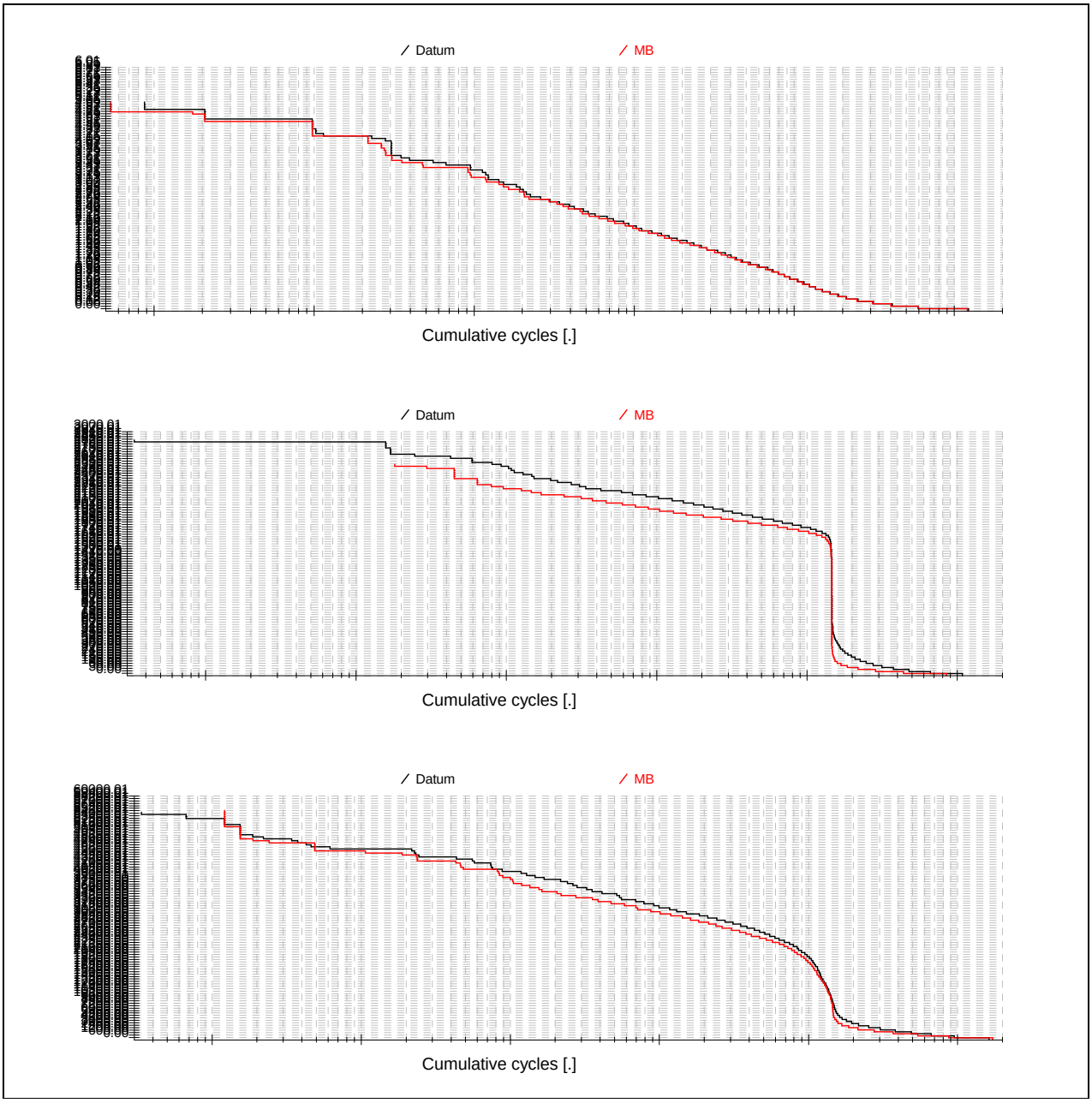

Figure 5.12 – Cumulative cycles for Blade root flap, edge and spanwise bending moment

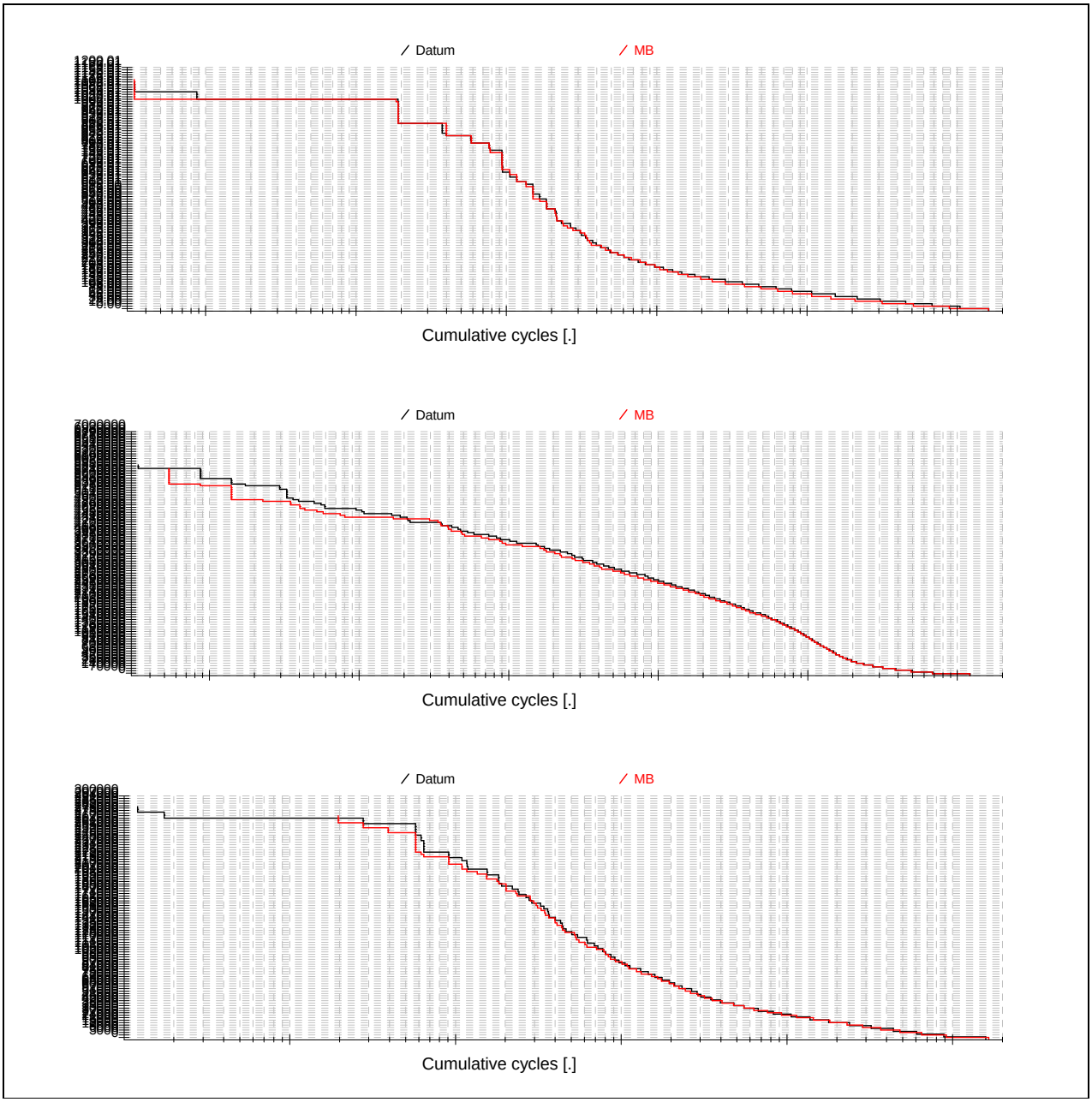

Figure 5.13 – Cumulative cycles for Hub Mx, My, Fx

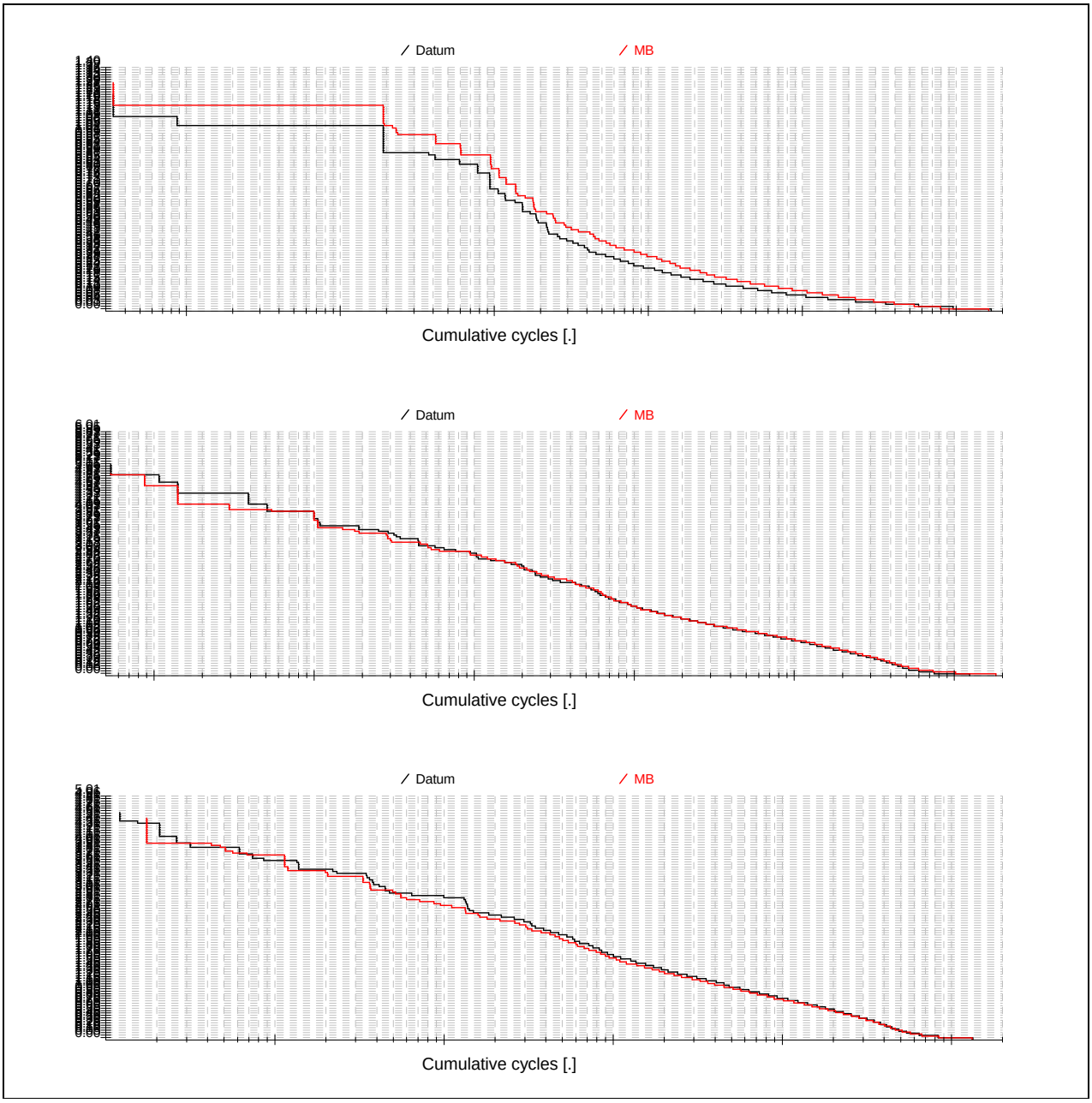

Figure 5.14 – Cumulative cycles for Yaw bearing Mx, My, Mz

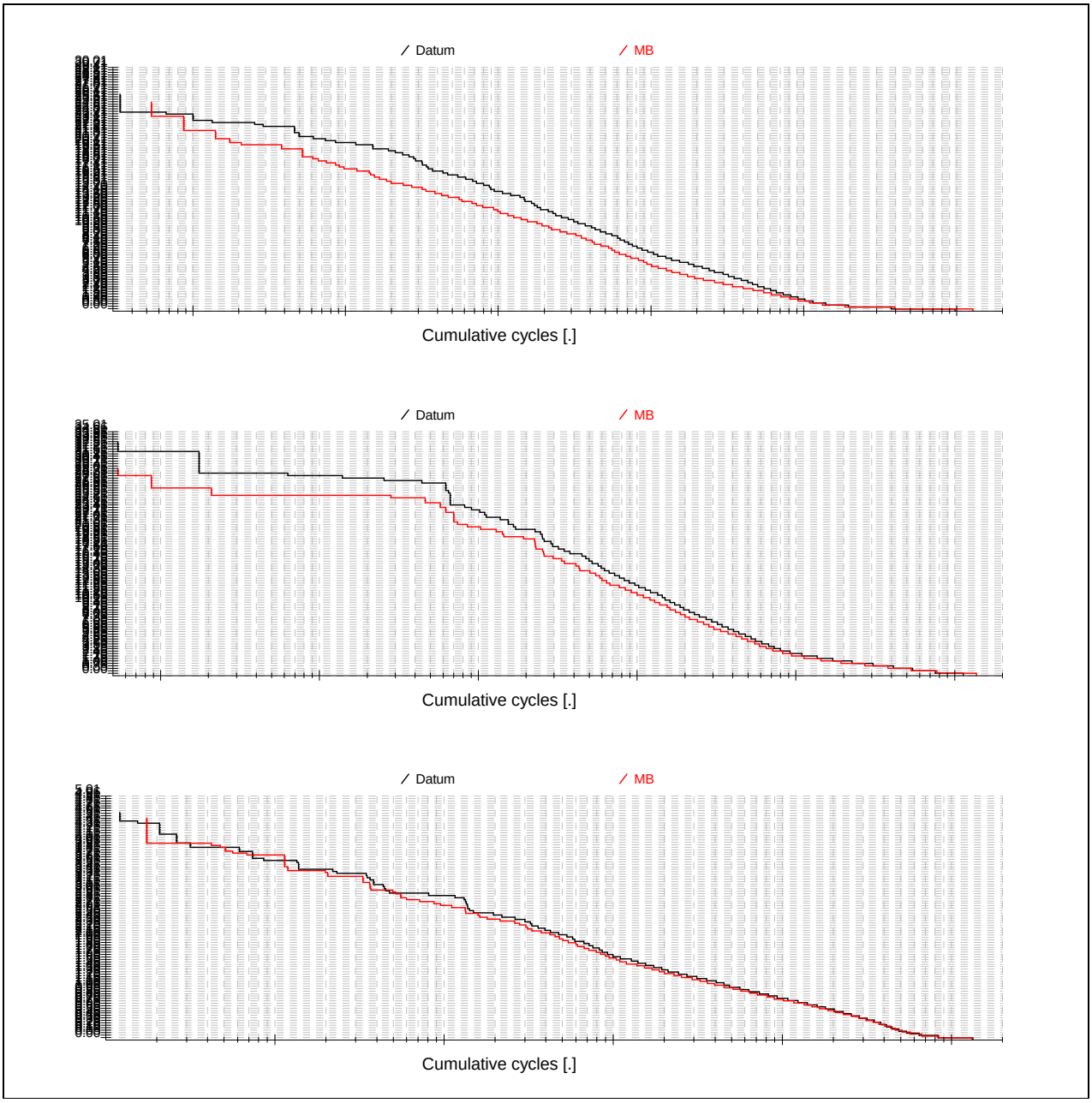

Figure 5.15 – Cumulative cycles for Tower base Mx, My, Mz

5.3 Conclusion

The comparisons carried out have shown in general good agreement between the previous version of Bladed and the new multibody version. There are a number of differences including:

- Coupled flap and edgewise blade modes tend to increase the damping in the edgewise direction and reduce edgewise fatigue loads, particularly towards the outer part of the blade. The change from rotor modes to blade modes is one of the major advantages of the new structural model. This not only allows for the correct multi-directional mode shape but also means individual blade modes are modelled correctly for start up and shut down cases as well as cases where the blade pitch angle is different for different blades, for example in individual pitch control or fault cases.

- Full modelling of the inertial effects of the blade pitching motion has made a change to the pitching moment loads. Along with the more detailed description of the blade comes a rigorous modelling of the effects of various axis offsets defined in the blade. Previous versions of Bladed did not include the contribution of the mass offset from the pitch axis to the inertial loading, and for certain pitch actuator models did not include the effect of pitching acceleration on the output loads.

- Modified coordinate system for blade output loads. In previous versions of Bladed, the z-axis was always parallel to the pitch axis, irrespective of the local bending of the blade. In the new multibody version, the z-axis runs along the local blade element, so the output coordinate system rotates with the bending of the blade.

- Small changes in dynamics can have a large effect for lightly damped modes such as the drive train system. The change in structural dynamics model has inevitably caused some changes to the overall system frequencies as the coupling model between different turbine components has changed. In some cases where the exact system frequency is important, such as the drive train frequency which is damped out by a drive train damper in the controller, this frequency may move sufficiently to produce significantly different loads. In this case a slight re-tune of the turbine controller may be required.

6 COMPARISON AGAINST MEASUREMENTS

An important way to validate the code is by comparing simulation results against measured data from a real turbine. While this can be seen as the 'ultimate test' of validity, it is difficult to achieve for two main reasons. Firstly, it is virtually impossible to measure the incident wind flow over the whole rotor in sufficient detail to be able to input it into a simulation, and secondly there are always uncertainties about the real physical characteristics of the turbine.

This section presents an attempt to validate the model against real measurements from the CART2 research turbine at NREL in Colorado [4]. The measurements were obtained for the purpose of testing two advanced control features, individual pitch control and fore-aft tower damping [5].

6.1 The CART2 turbine

The CART2 is a 600 kW variable speed, pitch regulated, two-bladed, teetered hub turbine with a rotor diameter of 42.67m and 36.85m hub height. For the purposes of the controller tests, the teetered hub was locked by a friction brake; however some slipping of the teeter brake was observed during the measurements.

A Bladed model was set up based on data supplied by NREL. Four blade modes and ten tower modes were modelled, which is sufficient to include the main fore-aft, side-side and torsional modes of the tower, and flapwise and edgewise blade modes up to over 12 Hz. Blade torsional dynamics were not included, and some of the blade structural details were omitted in this comparison, such as the distributed moments of inertia, shear stiffness, and the small difference between aerodynamic and structural twist. A teetered hub was modelled, complete with stick-slip friction for the teeter brake.

The mass and stiffness parameters were provided by NREL. It should be noted however that many of these parameters were not well known and have been "tuned" by NREL following analysis of site measurements of modal frequencies and comparison against their own structural dynamics codes.

A few assumptions were required because limited information was available *a priori*:

- Shaft torsional damping: originally an assumed value of 0.5% of critical damping for this mode was assumed, since the actual damping of the transmission system is notoriously difficult to estimate. However the measurements indicated that the actual damping is lower – see below.
- Teeter brake friction: the friction was not known, so it was roughly estimated from the maximum values of measured blade root bending moments: a value of 140 kNm was assumed.
- In the absence of detailed information, a simple passive pitch actuator model was used, consisting of a 0.0167s first order lag on pitch rate demand with $\pm$18°/s pitch rate limits. The time constant was provided by NREL based on their own observations.
- No information about rotor imbalance was available; some different kinds of imbalance effects were investigated.

The external controller DLL was carefully configured to match the actual controller which was running on the turbine during the tests.

Figure 6.1 shows a Campbell diagram for the turbine, calculated at 45 degrees azimuth angle with the teeter hinge locked. The descriptions of the coupled modes are of limited value, but attempt to show the main degrees of freedom involved. The modal frequencies listed are at the nominal rotational speed of 41.7 rpm.

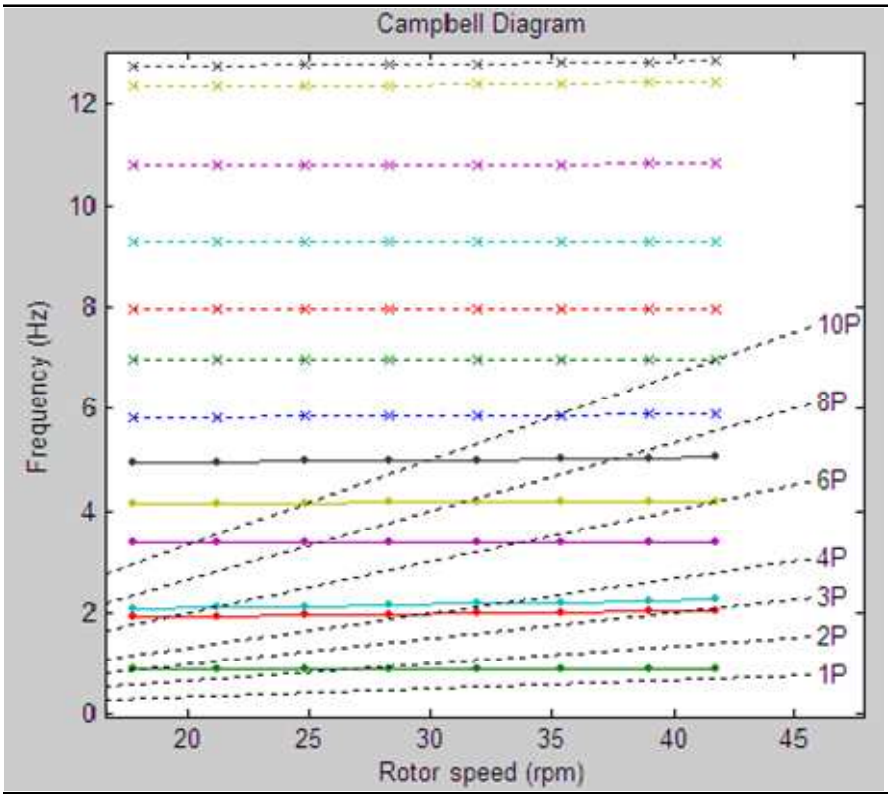

Flap: 12.44 & 12.84 Hz

Edge a/s: 10.82 Hz

Tower s/s / flap: 9.31 Hz

Tower f/a / flap: 7.96 Hz

Tower torsion / flap: 6.98 Hz

Flap sym: 5.91 Hz

Flap a/s: 5.05 Hz

Edge a/s: 4.18 Hz

Shaft torsion / edge sym: 3.36

Flap: 2.06 & 2.27 Hz

Tower f/a & s/s: 0.88 Hz

Modal descriptions attempt to give principal contributions but others are also important. Abbreviations: a/s: antisymmetric, sym: symmetric, f/a: fore-aft, s/s: side to side.

Figure 6.1: Campbell diagram

Also at 41.7 rpm the blade passing frequency and multiples are:

1P	0.695	Hz
2P	1.390	Hz
3P	2.085	Hz
4P	2.780	Hz
5P	3.475	Hz
6P	4.170	Hz

6.2 The NREL site

The NREL test site is located north of Denver, Colorado, very close to the front range of the Rocky Mountains. During the tests the winds blew from the West, i.e. coming from the mountains. Because of the proximity of the mountains, the wind regime is known to be somewhat untypical.

6.3 Selection of measured datasets

Four measured datasets were used to compare against simulations. For simplicity, the same four datasets were selected as were described for the controller tests reported in [5]. The datasets are listed in Table 6.1: the dataset name indicates the date and time of capture and whether the advanced controller features were ON or OFF. The wind speed, direction and turbulence intensity are as measured at hub height (36.6m) on the meteorological mast situated two diameters from the turbine in the direction 292º, i.e. almost exactly upwind of the turbine during these tests.

Dataset	Mean wind direction (deg)	Mean wind speed (m/s)	Turbulence intensity (%)
02050253OFF	276.698	16.3807	15.95
02050340OFF	284.246	12.4217	21.55
02020007ON	277.872	12.0926	20.70
02050317ON	289.563	15.481	18.47

Table 6.1: Measured datasets used for comparison against simulations

The datasets were 10 minutes in length, and sampled at 100 Hz.

6.4 Assumptions about wind conditions

For each measured dataset, a simulation was carried out in which the wind conditions were matched as closely as possible to the measured conditions. This was done as follows.

Bladed includes the facility to generate 3-D turbulence files which are matched to the measured conditions at one point. The measured met mast wind speed and direction at 36.6m height was used to define the longitudinal and lateral components of wind speed at the rotor centre. Bladed than calculated a wind field having the same longitudinal and lateral components at the hub position, by synthesising these two components at all other points, and the vertical component at every point, in accordance with the selected turbulence model. This means that the wind speed variations at each point are correlated with each other as a function of separation distance and frequency in accordance with the coherence model, and the vertical component additionally is consistent with the defined spectrum of vertical turbulence. The spectrum of the longitudinal and lateral components is defined by the measured hub height time histories. No correction was made for rotor induction, because two diameters upstream this should be small.

The Kaimal spectral model adjusted for IEC edition 3 was used initially, using the following parameters:

$\Lambda = 0.7 * \text{hub height} = 25.795\text{m}$

${}^{x}L_u = 8.1\Lambda = 208.94\text{m}$

${}^{x}L_v = 2.7 = 69.65\text{m}$

${}^{x}L_w = 0.66\Lambda = 17.025\text{m}$

Coherency scale parameter = ${}^{x}L_u$

Coherence decay constant, H = 12.

The mast had anemometers at four heights: 3, 15, 36.6 and 58.2m. No attempt was made to estimate the vertical coherence from the time histories at the four heights. In any case no information was available about lateral coherence. Although ${}^{x}L_u$ and ${}^{x}L_v$ are not important because the measured data was used to define the longitudinal and lateral component spectra, the value of Λ defines the vertical spectrum; but again no attempt was made to estimate this from the data.

As explained below, the coherence decay constant H was subsequently adjusted.

For each dataset, the 10-minute mean wind speeds from all four met mast anemometers were used to define the shear profile for the simulations as a user-defined look-up table.

Height (m)	02050253OFF	02050340OFF	02020007ON	02050317ON
58.2	1.0426	1.0622	1.0378	1.0671
36.6	1	1	1	1
15	0.9229	0.8905	0.9311	0.8826
3	0.7984	0.7224	0.8186	0.7045

Table 6.2: Shear profiles for the four datasets

6.5 Initial comparisons and adjustments

Using the above assumptions, some initial simulations were carried out, as a result of which certain changes to the assumptions were made before the final runs. Figure 6.2 shows a comparison of measured and simulated spectra of low speed shaft torque spectra for dataset 02050340OFF. Two significant differences are immediately observed: firstly the peak corresponding to the drive train torsional resonance at 3.4 Hz is higher in the measured data, suggesting that the damping of this mode has been over-estimated, which is quite possible as this is a very difficult quantity to estimate; and secondly that the 2P excitation peak at 1.39 Hz and harmonics at multiples of this frequency are higher than measured, suggesting that the simulated wind field contains higher variations in wind speed across the rotor plane than were present in the field.

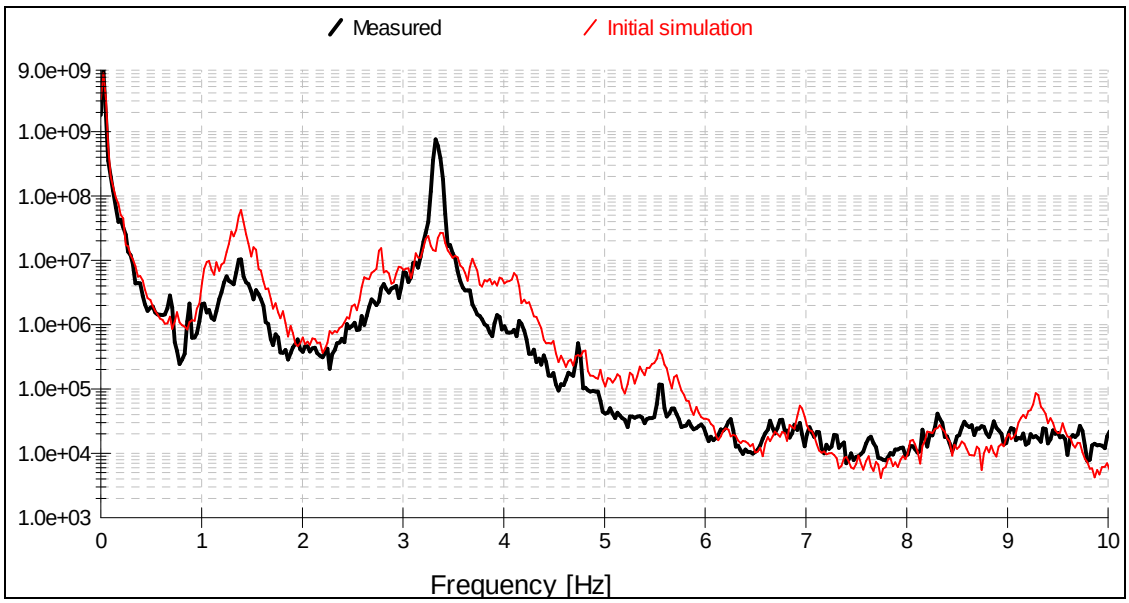

Figure 6.2: Initial comparison of shaft torque spectra (dataset 02050340OFF)

These discrepancies were tackled firstly by adjusting the assumed torsional damping of the drive train, and secondly by modifying the coherence properties of the simulated wind field. A reduction in torsional damping from 0.5% to 0.35% gave a much better fit to the torsional resonance peak, and an increase in the cross-wind coherence (by reducing the coherence decay constant, H) had the effect of reducing the peaks at multiples of the blade passing frequency. These improvements are shown in Figure 6.3, where H was reduced from 12 down to 2.5, and then further to 1.0. The peaks fit best with the highest coherence (H=1.0), but the figure also shows that as the coherence increases there is a reduction of energy at the high frequencies and an increase at the low frequencies, leading to a poorer match to the measured data in these regions. This suggests that still better agreement could probably be achieved by further adjustment of the wind coherence model. The final case in Figure 6.3 uses the 'improved von Karman' or ESDU model, calculated for latitude 40º as appropriate for Denver, with a surface roughness of 0.2m which gives approximately the correct turbulence intensity (20.5%). In all cases the agreement is much better than in Figure 6.2. The von Karman model still overestimates the blade passing effect a little but provides better agreement elsewhere. No doubt the agreement could be improved further by further adjustments to the coherence model, but for the remainder of the simulations the von Karman model as defined above was used. The same surface roughness was used for all cases, with no attempt to tune this to the precise turbulence intensity of each measured dataset.

Note that the calculation of fatigue loading is particularly sensitive to the turbulence model adopted. Figure 6.4 shows the significant variations which can occur purely as a result of changing the turbulence model. While the von Karman model fits best for the tower base My, the Kaimal (H=2.5) model fits the yaw moment spectrum better.

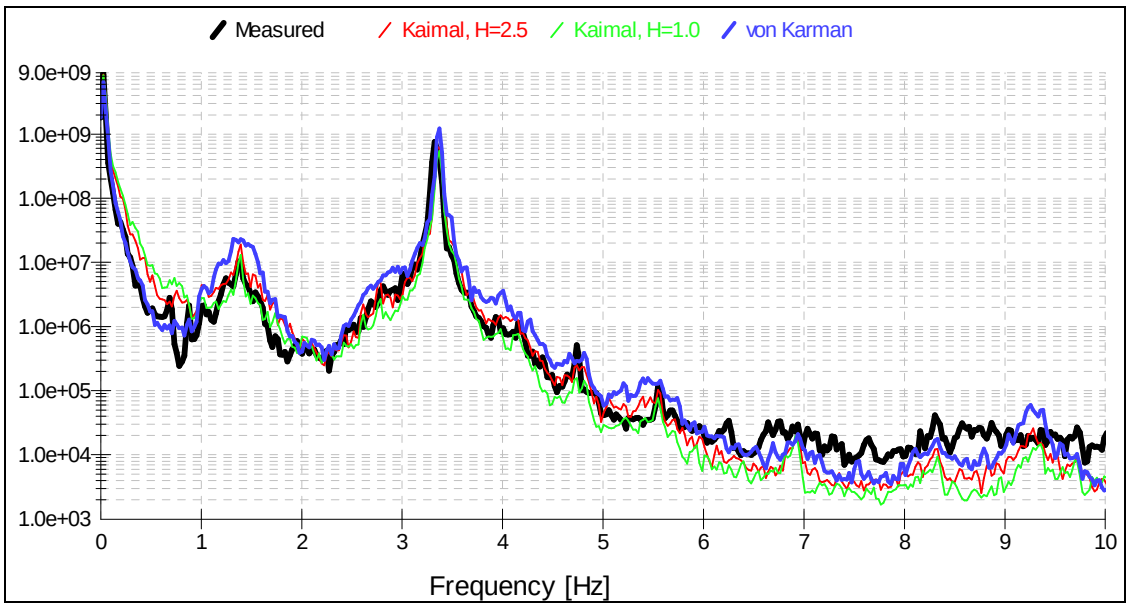

Figure 6.3: Effect of coherence model on torque spectrum (dataset 02050340OFF)

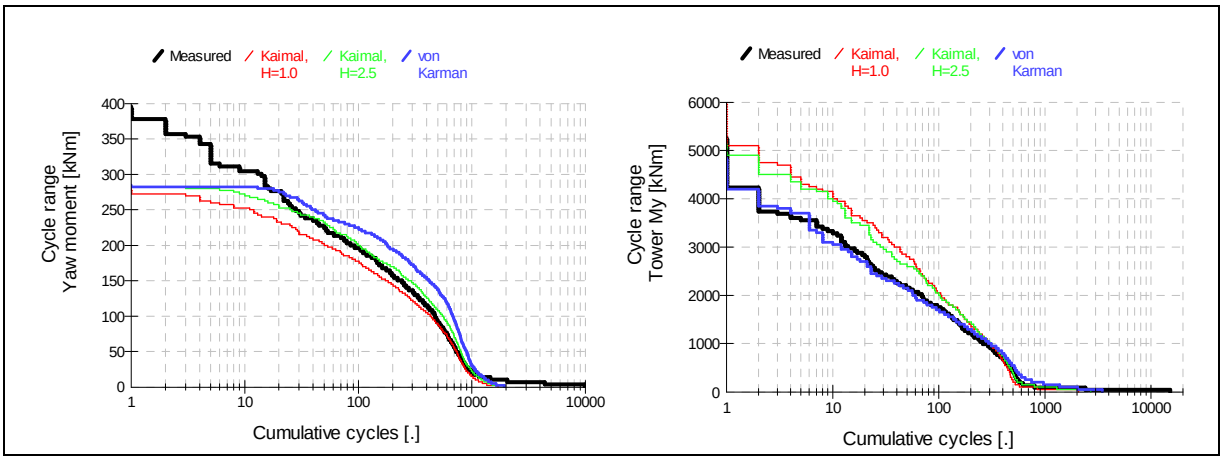

Figure 6.4: Effect of coherence model on rainflow cycle exceedance (dataset 02050340OFF)

Two other major differences are observed between some of the measured and simulated results. One is inevitably the presence of noise on the measured signals, and the other is the effect of a degree of imbalance which is clearly present on the real turbine. The signal noise is easily identified in the spectrum of the signal, which flattens off to a constant level at high frequency in the presence of white noise. Two obvious examples are shown in Figure 6.5, which are the generator speed and electrical power signals from run

02050340OFF (the generator speed signal must have been faulty at this time because the noise level is much lower in the other three datasets).

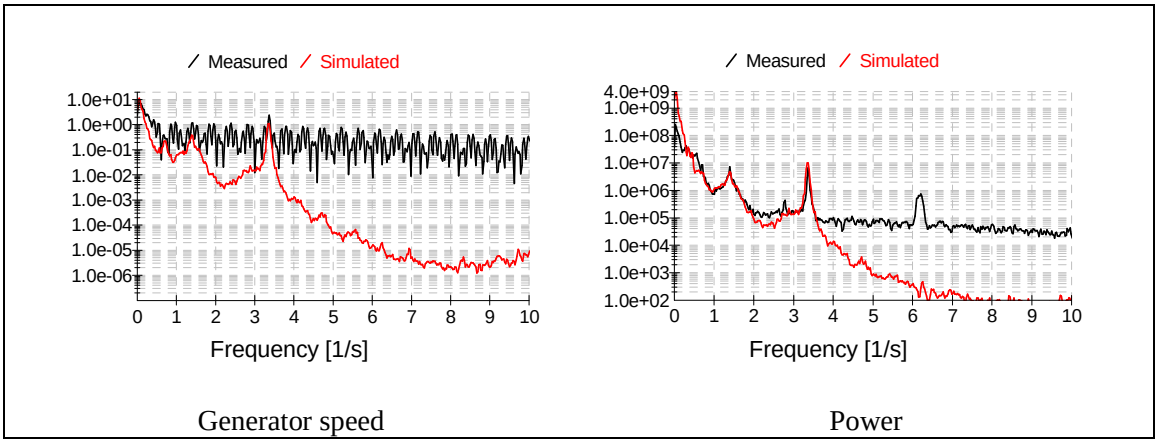

Figure 6.5: Effect of signal noise (dataset 02050340OFF)

Imbalance is demonstrated by the presence of a 1P peak in certain loads, notably the non-rotating shaft loads (estimated by transformation of the blade root loads) and the tower base side-side bending moment. This was noticed in the controller evaluation reported in [5], and tentatively blamed on slippage of the teeter brake: this causes the teeter to stick at non-zero angles from time to time, causing a 1P imbalance effect. However, the simulations now include teeter brake slippage as demonstrated below, and this does not appear sufficient to explain the extent of the observed imbalance effect. Other possible causes of imbalance might be:

- Differences in mass properties between the two blades
- Differences in structural properties between the two blades
- Differences in aerodynamic properties between the two blades
- Other mass imbalance (e.g. in the hub)
- An offset in the pitch angle of one blade
- An azimuthal offset, such that the two blades are not exactly 180º apart.

Calibration errors in blade root load sensors might lead to an apparent 1P effect in the derived non-rotating hub loads, but this could not explain the large 1P peak in the tower base side-side bending moment, which must be a real effect.

Any of these effects could in principle be modelled using Bladed multibody. There could be almost unlimited scope for postulating differences in the distributed blade mass, structural and aerodynamic properties. The overall mass imbalance and the pitch and azimuth imbalances are much more straightforward to investigate. Simulations showed that a pitch imbalance could explain the 1P peak in tower Mx, while an azimuthal imbalance could explain the 1P peak non-rotating hub loads. However the azimuthal imbalance also has the effect of causing a mass imbalance, so an opposing mass imbalance had to

be added to compensate this otherwise new 1P peaks would appear in other loads such as the shaft torque which were not observed in the measurements.

As shown in Figure 6.6, the following combination of postulated imbalance effects was found to match the observed imbalance effects reasonably well, although they are rather large:

Out of balance mass	425.2	kg
Radius of out of balance mass	2.519	m
Azimuthal position of out of balance mass	-88	deg

	Error in Blade Set Angle (deg)	Error in Pitch Angle (deg)	Error in Blade Azimuth (deg)
Blade 1	4	0	4
Blade 2	0	0	0

This does not constitute any proof that these particular imbalances are in fact present. Nevertheless they have been included in the subsequent simulations, as they do appear to explain the observations reasonably well.

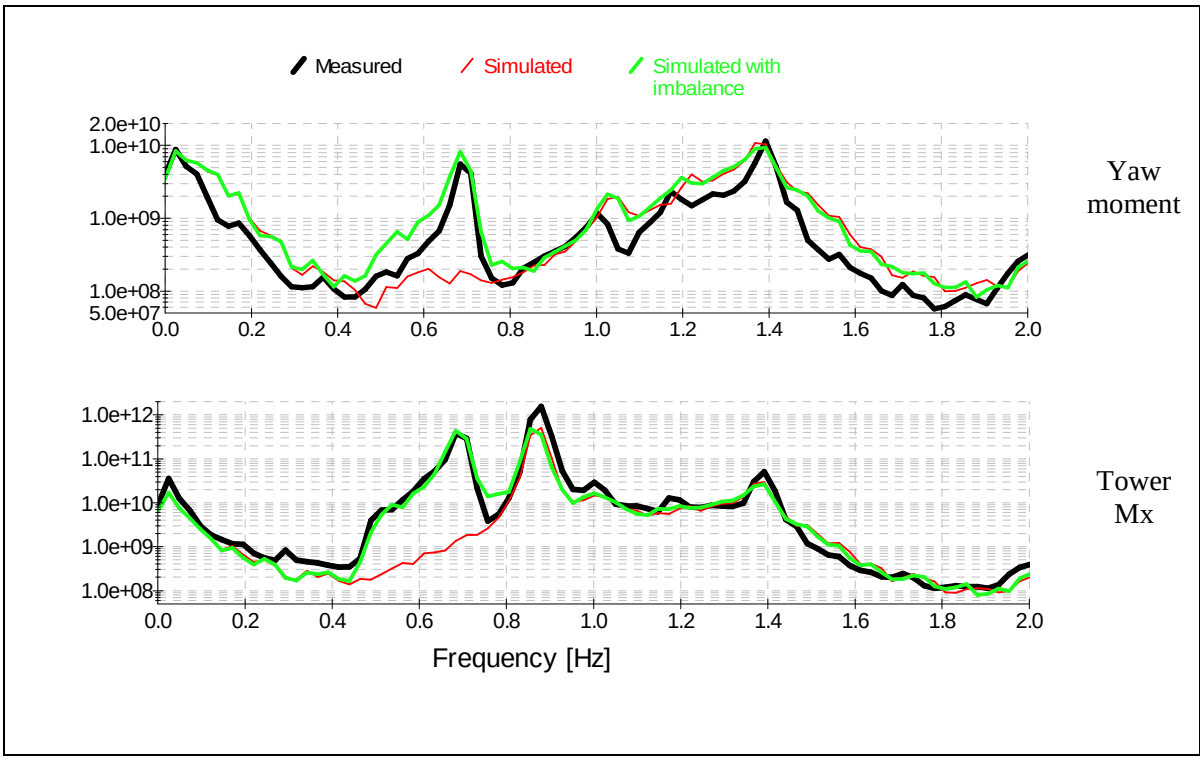

Figure 6.6: Effect of imbalance (dataset 02050340OFF)

Figure 6.7 compares teeter angle time histories for dataset 02050340OFF, to demonstrate that the stick-slip behaviour of the teeter hinge is realistically modelled. As with all the asymmetrical loads, the time histories cannot be expected to match in detail because although the hub wind speeds are matched between measurement and simulation, the teeter behaviour is driven by the differential turbulence across the rotor, for which measured time history information is not available. Also there is a mean offset in the simulation due to the effect of the pitch imbalance described above, which is likely to have been calibrated out in the measured data. Otherwise the characteristics are similar between measured and simulated traces: both show the teeter sticking at a small angle and occasionally slipping to a different angle, punctuated by the occasional burst of actual teetering against the brake friction (incidentally the latter effect does not occur in the two 'ON' cases where the individual pitch control reduces the teeter moment to such an extent that the brake hardly ever slips).

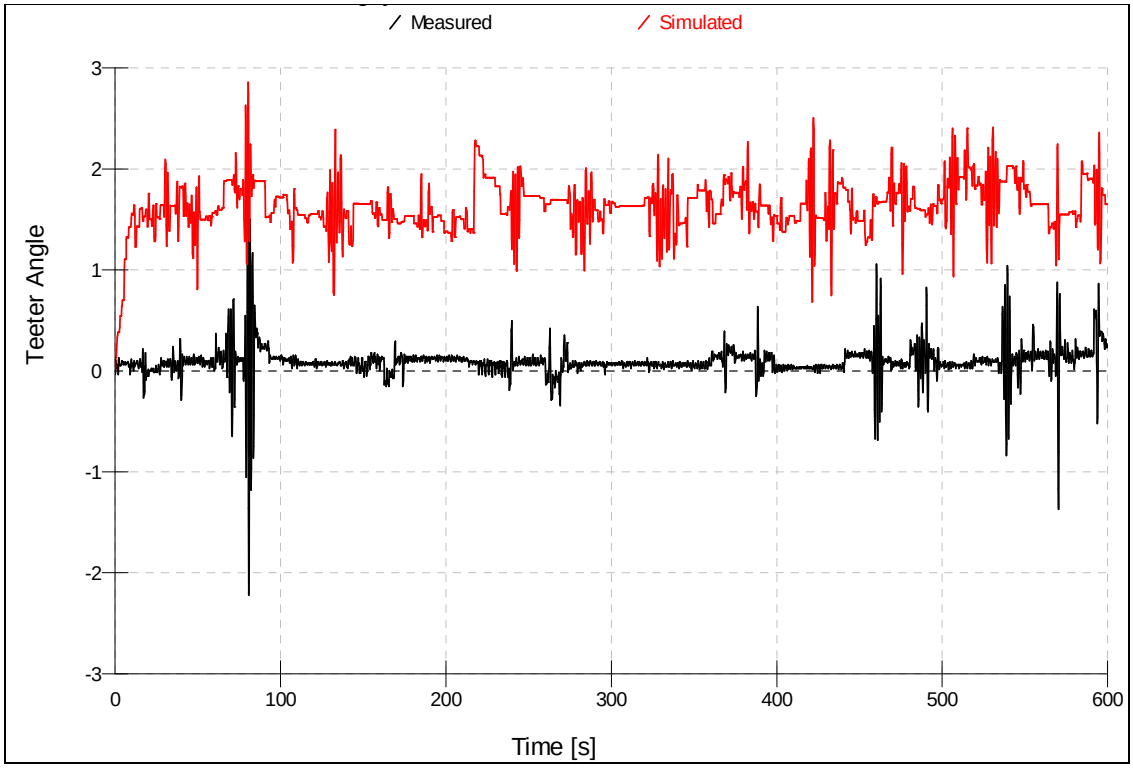

Figure 6.7: Teeter behaviour – dataset 02050340OFF

6.6 Analysis of results

Some example time history plots are shown in Figure 6.8. These are for dataset 02050340OFF, and show (at least for those variables which are more affected by the average wind speed over the rotor than by wind speed differences across the rotor) that the general agreement is very good. A time shift is clearly visible,

corresponding to the time taken for the wind speed measured at the met mast, which was used in the simulations, to reach the actual turbine.

Even for these variables however, the actual performance is affected by the wind speeds over the whole rotor, which could not be measured. Other variables such as blade and hub loads (and teeter angle as already shown), are even more affected by the distributed wind field. Therefore the comparison of time histories is of limited value and further comparisons have been done in terms of statistically derived quantities, in particular frequency spectra and rainflow cycle counts.

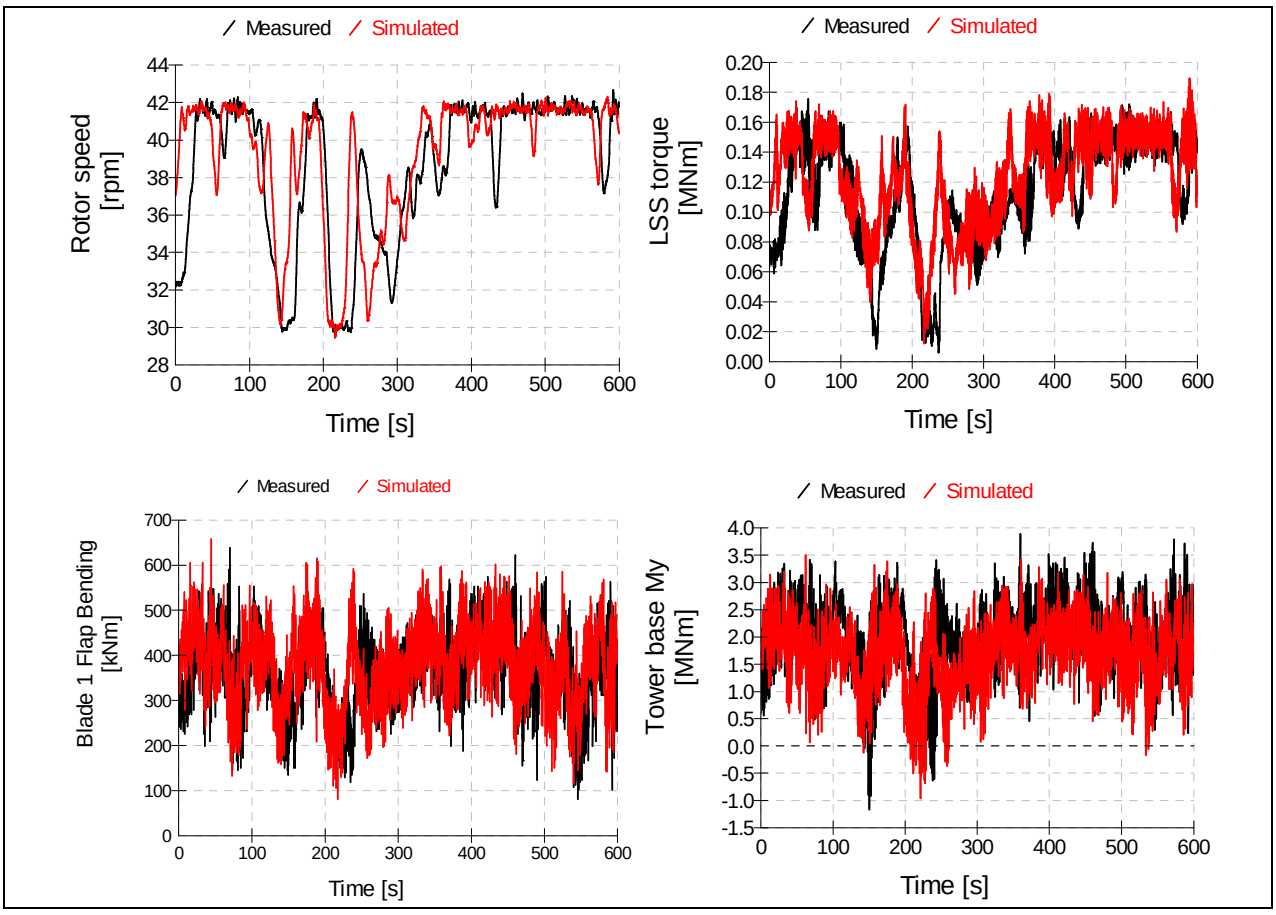

Figure 6.8: Example time histories – dataset 02050340OFF

Spectral comparisons (up to 10 Hz) of the most important loads and other variables are presented in Figure 6.9 to Figure 6.12, and rainflow cycle exceedance plots are given in Figure 6.13 to Figure 6.15.

Note that some of the measured loads were not directly measured, and therefore do not correspond exactly to the simulated loads:

- Rotating hub My: the 'measured' load is obtained from the measured flapwise and edgewise blade root moments on the two blades, resolved into the out of plane direction using the measured pitch angle, to obtain the two blade root My moments which are then combined. This ignores the effect of blade root shear forces and also the inertial forces due to accelerations of the hub mass and inertia (effects which are included in the simulated load).
- Nod and Yaw moments: the same two blade root My moments are resolved into non-rotating co-ordinates using the measured azimuth angle. Again this ignores shear forces and hub inertial forces. For the simulated results the non-rotating hub moments are used.
- Tower base moments: these have been resolved into fore-aft and side-side directions using the measured yaw position (this signal was very noisy with large spikes, and had to be cleaned before use).

In general a very good level of agreement is demonstrated, bearing in mind especially the uncertainties of modelling the wind field. Clearly there are some discrepancies, but in most cases this is likely to be due to the uncertainties about the wind field. The following points can perhaps be highlighted (ignoring the effect of signal noise which has already been mentioned):

- Spectra of rotor and generator speed, shaft torque and power show excellent agreement.
- The 1P individual pitch action is well predicted as shown in the pitch rate spectra for the 'ON' cases. An otherwise noisy response in the measurements may be due to the unmodelled details of the pitch actuation system.
- Teeter rate spectra agree very well (bearing in mind that there was almost no teetering in the 'ON' cases.
- Spectra of blade root flapwise and edgewise moments (only blade 1 is shown) agree very well with some minor differences. The measured flapwise loads show a slight peak around 5.6 Hz, which corresponds to 8P. The simulation shows less response of the edgewise moment at the drive train frequency at 3.4 Hz and more at the antisymmetric edgewise mode frequency at 4.2 Hz. The latter frequency corresponds very closely with the 6P forcing frequency, which will be sensitive to the wind field structure. Note also that no attempt has been made to adjust the modal damping, for which a standard value has been used.
- Good agreement is seen between the spectra of rotating and non-rotating shaft moments, including the effect of individual pitch control on the rotating 1P peak and the non-rotating 2P peak. As the spectra fall off at higher frequencies, the measured data shows more pronounced dips between the peaks.
- The tower base Mx spectra agree very well at low frequency, but the measured spectra fall away more above 4Hz. Simulations also show a bit more response at the drive train frequency.
- The tower base My spectra also agree well at low frequency, although the simulations show more activity at 1P. This is undoubtedly due to the way in which the imbalance was modelled – clearly more work would be required to pinpoint more exactly the actual sources of imbalance. The simulations also show a bit more response around 4.8 Hz and also particularly at the 8 Hz tower mode, which does not seem to be excited at all in the real turbine.

The rainflow cycle exceedance plots indicate how well the fatigue loads would be predicted. The plots are particularly sensitive to details of the wind field. Nevertheless the agreement is generally very good, and any differences can easily be explained by the turbulence model as Figure 6.4 shows. The following points can be highlighted:

- Blade flapwise and edgewise moments mostly show excellent agreement. For the 'ON' cases only, some difference in the edgewise moments appears. This may conceivably suggest the need for some adjustment of the aerodynamic model to account fully for the effects of rapid pitching on the aerodynamic response.
- Shaft and tower moments show very good agreement, sometimes better for some datasets, sometimes for others, further emphasising the sensitivity to turbulence structure. The shaft bending moments show a cut-off around 300 kNm which is due to the assumed teeter hinge friction level – in reality the moments often exceed these values, indicating that the friction characteristic of the teeter brake is rather variable in practice.

	02050253OFF	02050340OFF	02020007ON	02050317ON
Rotor rpm	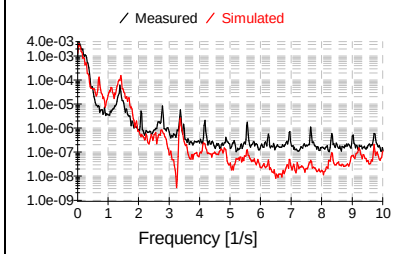	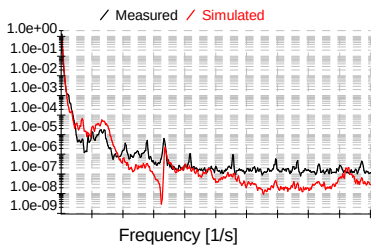	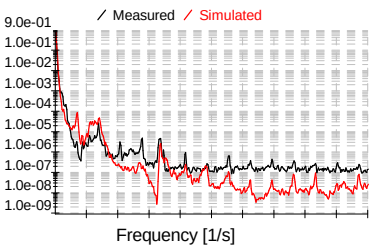	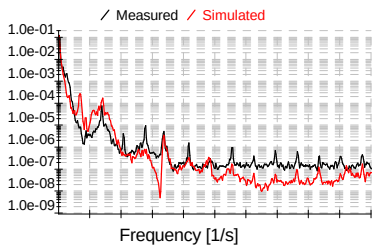
Generator rpm	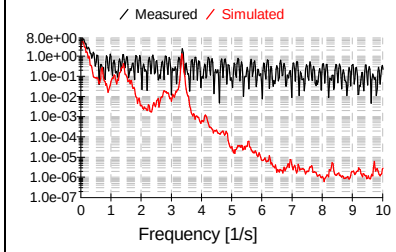	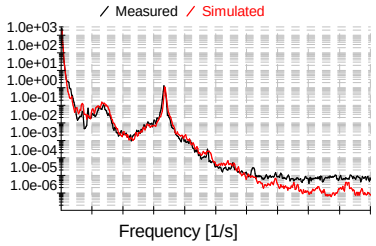	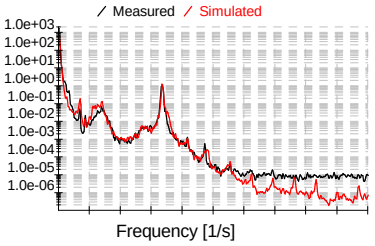	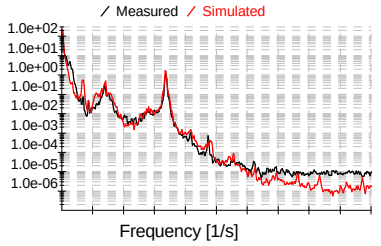
Shaft torque	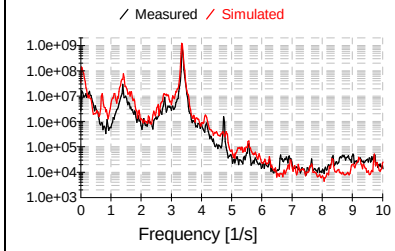	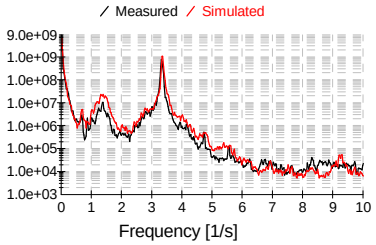	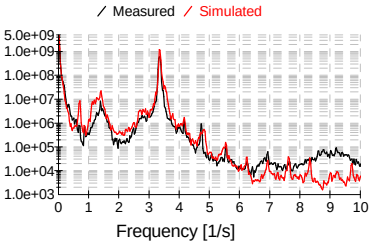	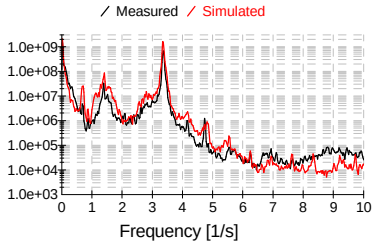
Power	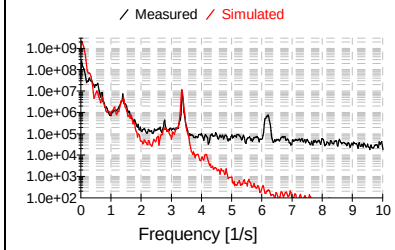	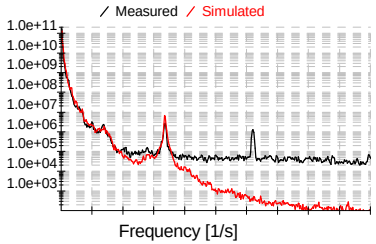	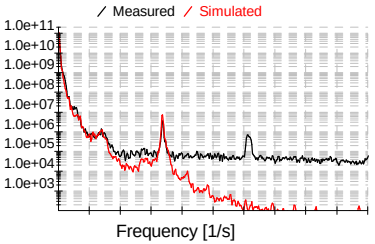	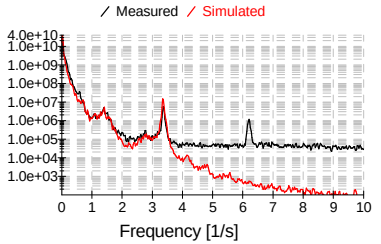

GL Garrad Hassan

Figure 6.9: Comparison of measured and simulated spectra

	02050253OFF	02050340OFF	02020007ON	02050317ON
Pitch rate	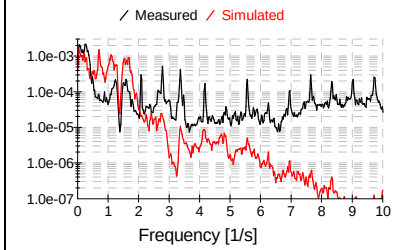	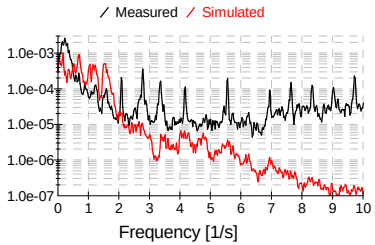	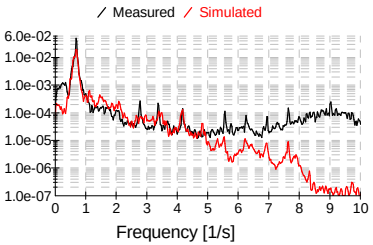	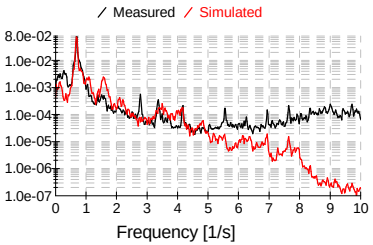
Teeter velocity	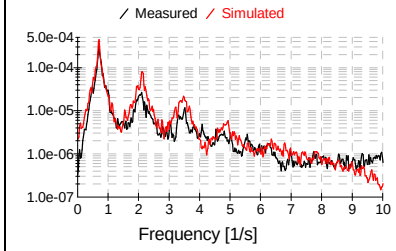	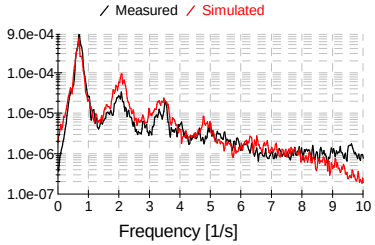	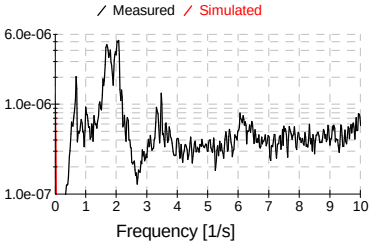	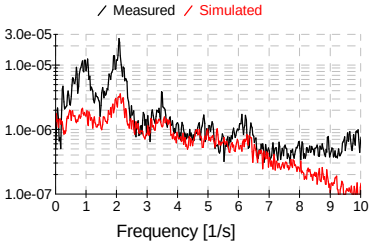
Flap moment	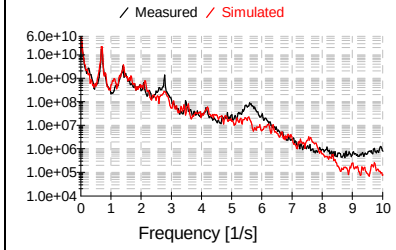	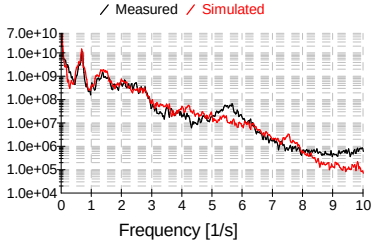	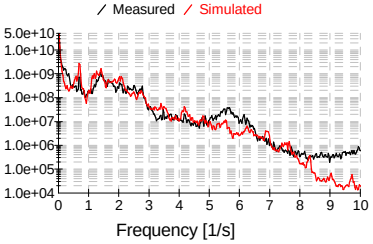	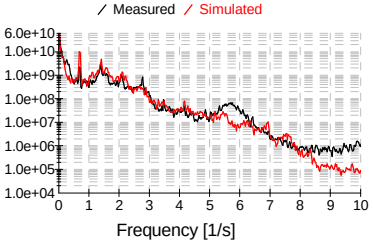
Edge moment	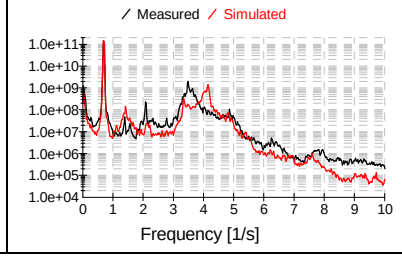	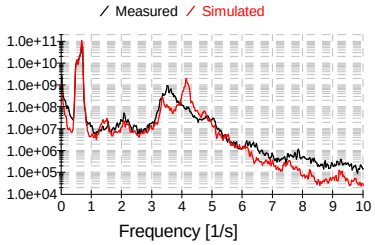	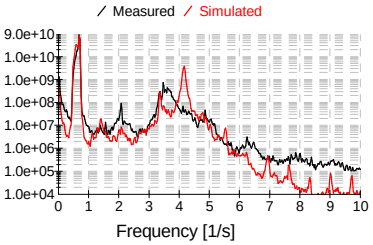	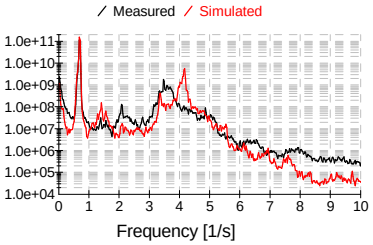

Figure 6.10: Comparison of measured and simulated spectra

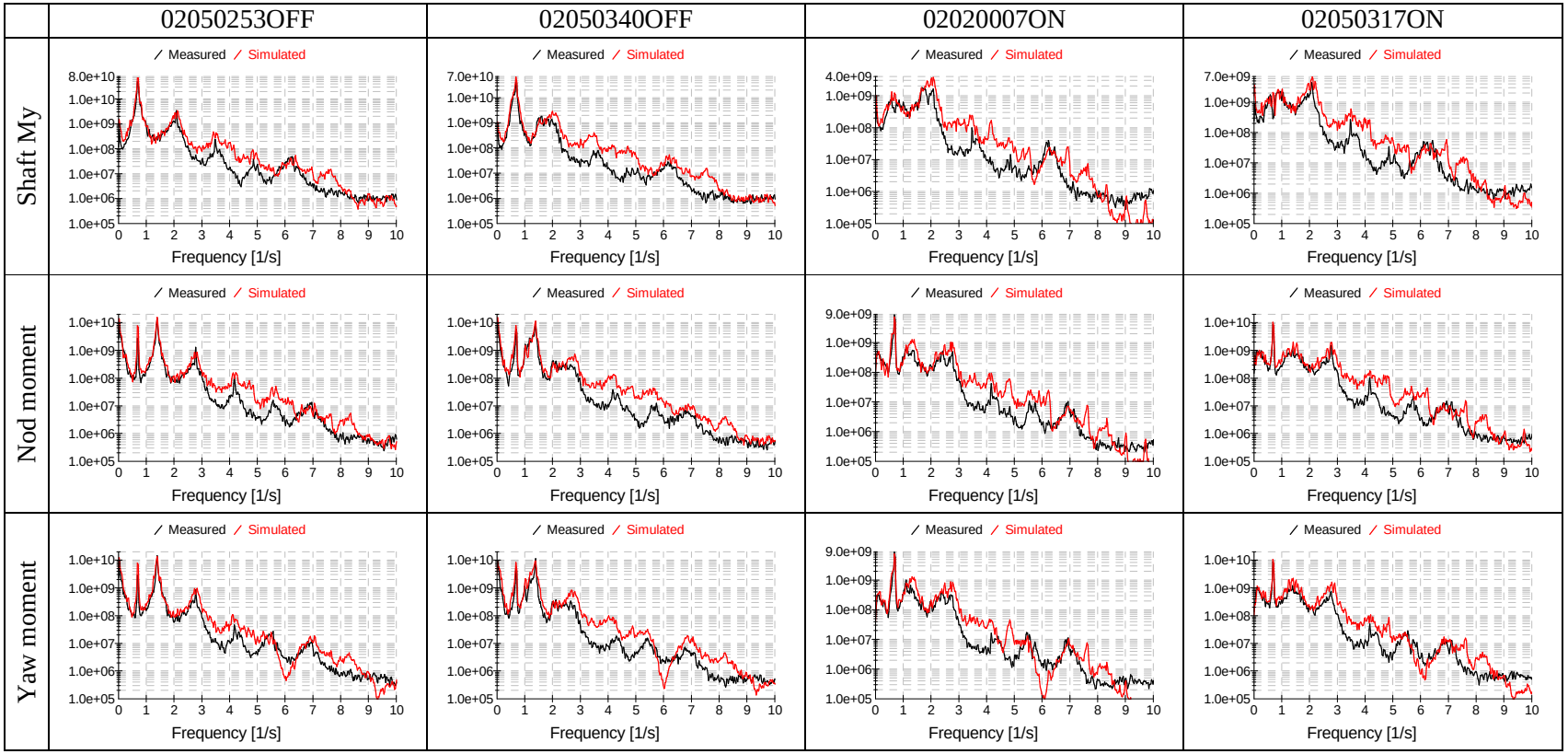

Figure 6.11: Comparison of measured and simulated spectra

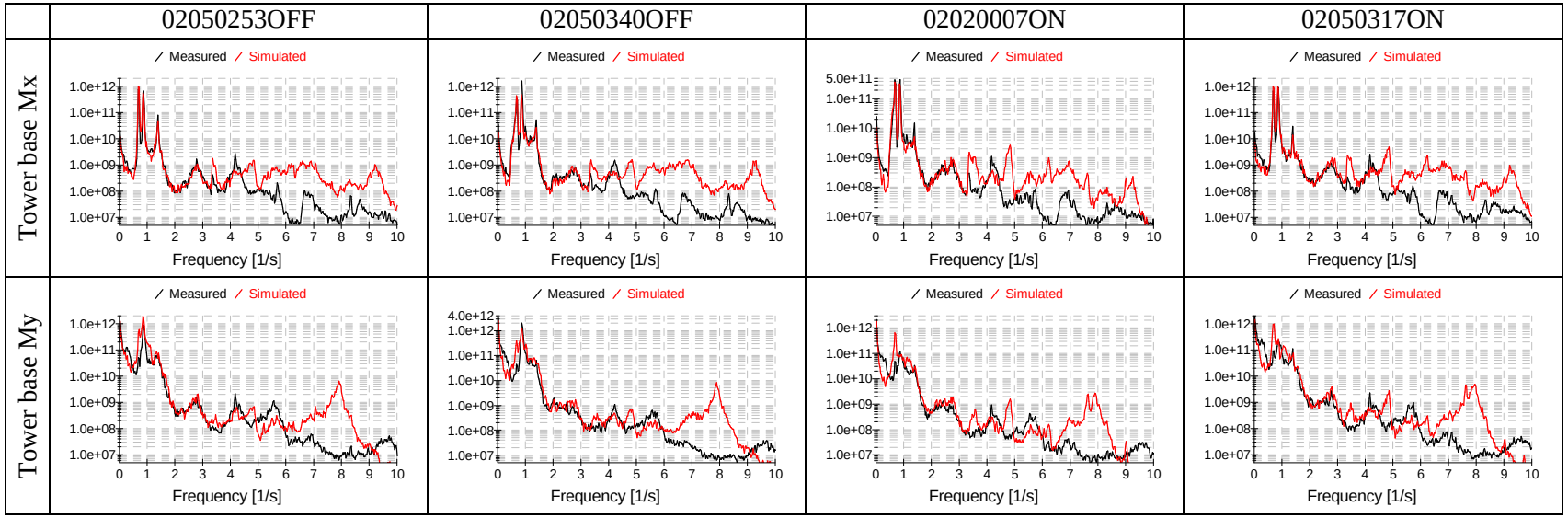

Figure 6.12: Comparison of measured and simulated spectra

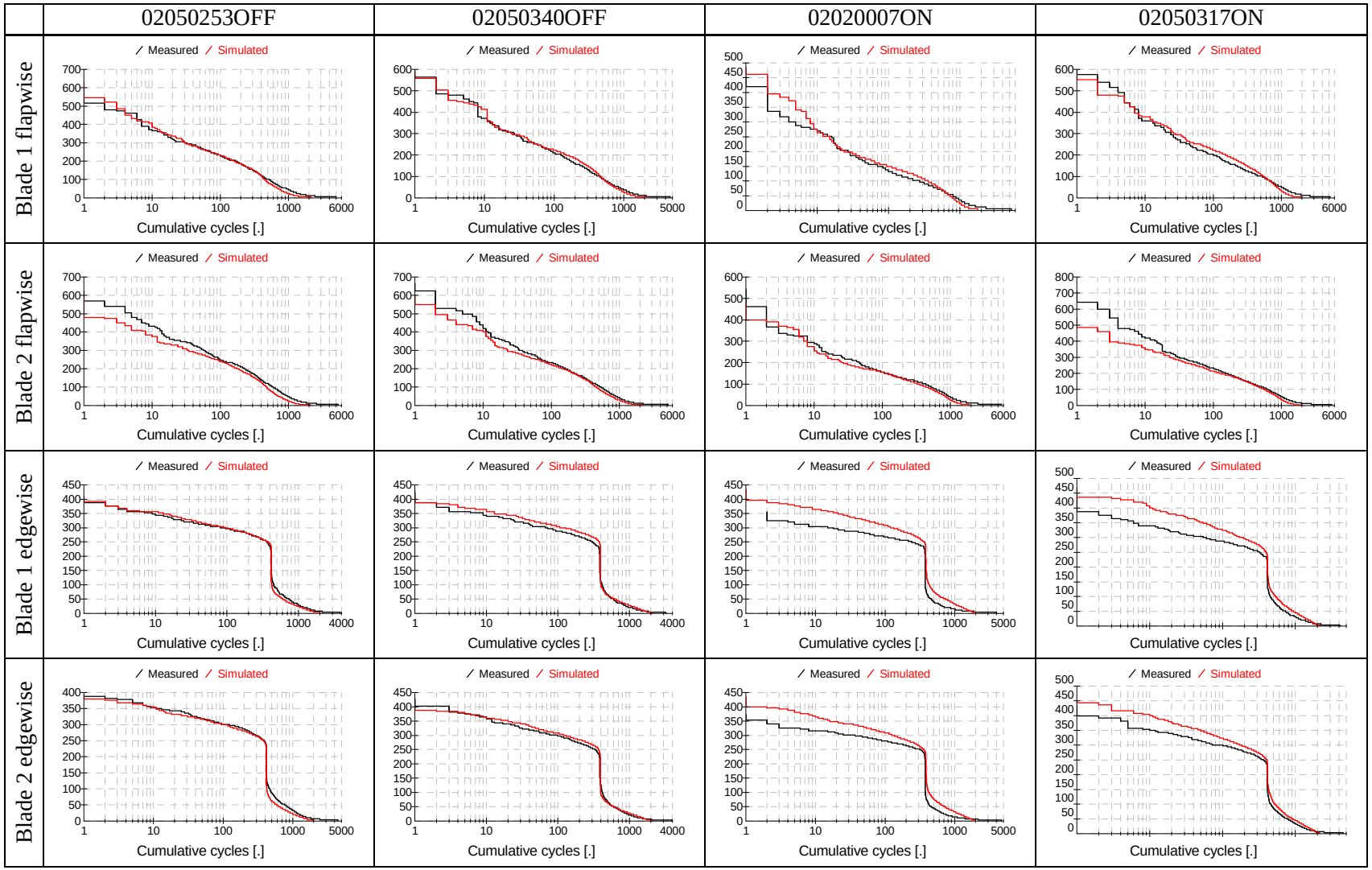

Figure 6.13: Comparison of measured and simulated rainflow cycle exceedance plots

	02050253OFF	02050340OFF	02020007ON	02050317ON
Shaft torque	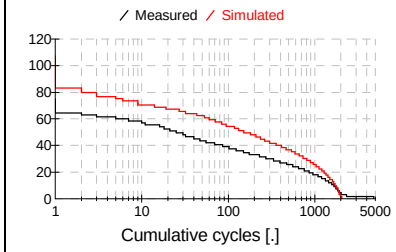	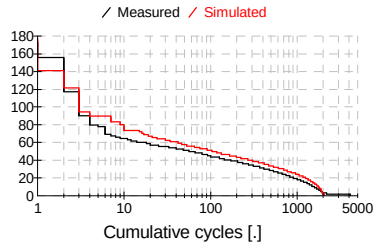	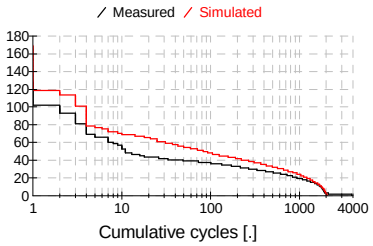	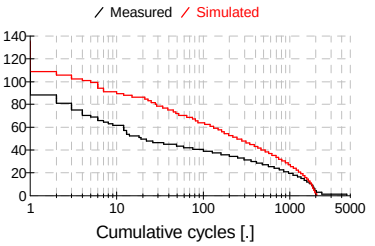
Rotating hub My	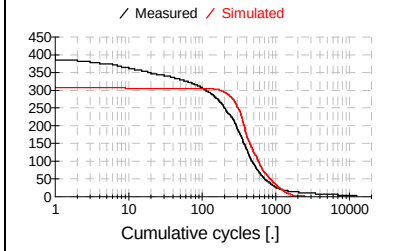	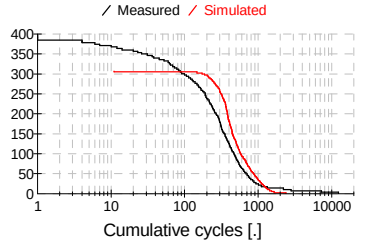	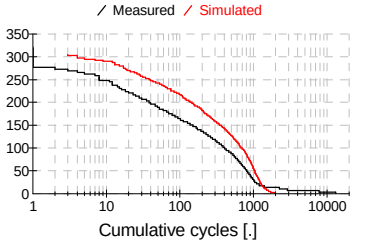	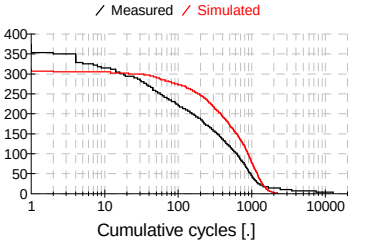
Nod moment	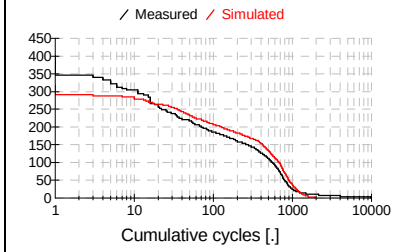	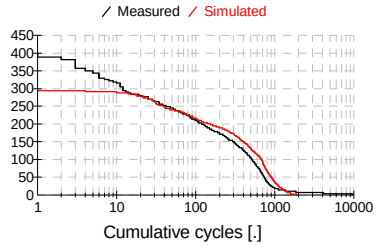	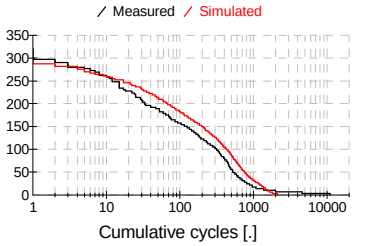	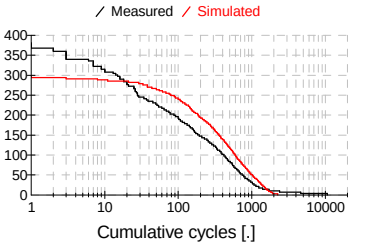
Yaw moment	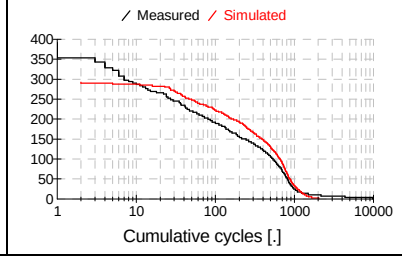	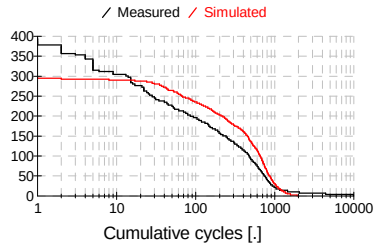	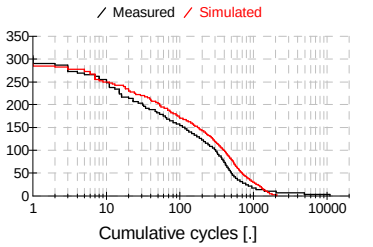	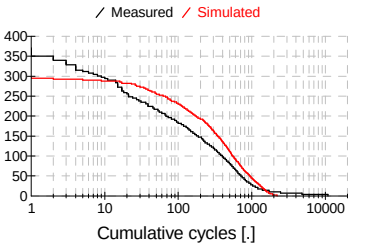

Figure 6.14: Comparison of measured and simulated rainflow cycle exceedance plots

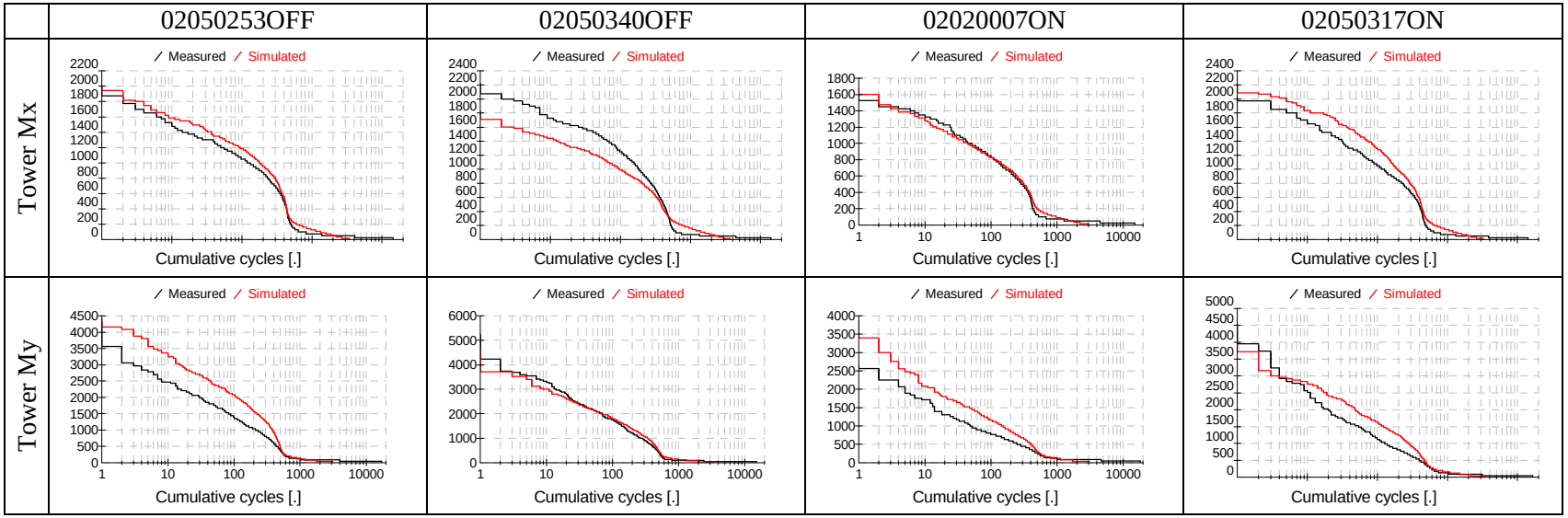

Figure 6.15: Comparison of measured and simulated rainflow cycle exceedance plots

6.7 Conclusions

Simulations have been carried out for the CART2 wind turbine for comparison against some measured 10-minute datasets which was available from another project. Point-by-point validation is never possible because it is impractical to measure the whole approaching wind field in the detail required. Simulated wind fields were used which matched the measured wind speed and direction at hub height as measured at an anemometer two diameters upstream. The mean shear profile for each dataset was also matched, but the detailed structure and coherence of the wind field could not be known.

The measured and simulated results were compared by means of spectral analysis, and also using rainflow cycle counting to give an indication of fatigue loading. Excellent agreement was obtained overall. The spectral peaks representing structural resonances corresponded very closely with the predicted frequencies of the coupled system modes. The heights of the peaks, representing the amount of excitation, also corresponded well in most cases: this depends on the assumed structural damping, which is never easy to ascertain, and especially for resonances close to forcing frequencies at multiples of the blade passing frequency it is also sensitive to the assumed structure of turbulence. The assumed shaft torsional damping was adjusted to match the measurements, but no attempt was made to match the assumed blade and tower modal damping factors. Several different models were tried to represent the unmeasured details of the turbulence structure, and these gave a range of results which was wide enough to explain any differences between the measured and simulated rainflow cycle exceedance plots.

7 REFERENCES

1. E A Bossanyi, "Bladed Theory Manual", 282/BR/009 – Issue 20, July 2010.

2. J Jonkman and W Musial, “IEA Wind Task 23 Offshore Wind Technology and Deployment: Subtask 2 The Offshore Code Comparison Collaboration (OC3)”, March 31 2010.

3. Jonkman J, Butterfield S, Musial W, and Scott G. “Definition of a 5-MW Reference Wind Turbine for Offshore System Development”, NREL/TP-500-38060. NREL: Golden, CO, 2009.

4. Geometry and Structural Properties for the Controls Advanced Research Turbine (CART) from Model Tuning, August 25, 2003–November 30, 2003, K A Stol, NREL/SR-500-32087, http://www.nrel.gov/docs/fy04osti/32087.pdf.

5. E. Bossanyi, A. Wright and P. Fleming, Progress with field testing of individual pitch control, Proc. Conference on the science of making torque from wind, The European Academy of Wind Energy, June 2010.